THE EFFECTIVE APPLICATION OF DYNAMIC ARC RADIOTHERAPY

A thesis submitted to The University of Manchester for the degree of

PhD

In the Faculty of Medical and Human Sciences

2013

CHRISTOPHER JAMES BOYLAN

SCHOOL OF MEDICINE

(page intentionally blank)

TABLE OF CONTENTS

Word count: 53,000 approx.

LIST OF FIGURES

LIST OF TABLES

LIST OF ABBREVIATIONS

VMAT – volumetric modulated arc therapy

IMAT – intensity modulated arc therapy

IMRT – intensity modulated radiation therapy

CBCT – cone-beam computed tomography

TCP – tumour control probability

NTCP – normal tissue complication probability

OAR – organ at risk

PTV – planning target volume

CTV – clinical target volume

GTV – gross tumour volume

ROI – region of interest

BDR – binned dose rate

CVDR – continuously-variable dose rate

IGRT – image-guided radiation therapy

MLC – multi-leaf collimator

LINAC – linear accelerator

DAO – direct aperture optimisation

BEV – beam's eye view

dMLC – dynamic multi-leaf collimator

DVH – dose-volume histogram

SIB – simultaneous integrated boost

NPC – nasopharyngeal carcinoma

PRV – planning reference volume

ALTERNATIVE FORMAT

Permission has been obtained to submit this thesis in the 'alternative format', whereby sections are included in the form of scientific publications. The rationale for submission in alternative format is given in the introduction (section 1.6). The published and submitted papers are given below.

LIST OF PUBLICATIONS

1. **A VMAT planning solution for prostate patients using a commercial treatment planning system**

Published in Physics in Medicine and Biology, 2010, vol. 55, pp. N395-N404

2. **A bias-free, automated planning tool for technique comparison in radiotherapy – application to nasopharyngeal carcinoma treatments**

Accepted by Journal of Applied Clinical Medical Physics, July 2013

3. **The use of a realistic VMAT delivery emulator to optimize dynamic machine parameters for improved treatment efficiency**

Published in Physics in Medicine and Biology, 2011, vol. 56, pp. 4119-4133

4. **The impact of continuously-variable dose rate VMAT on beam stability, MLC positioning and overall plan dosimetry**

Published in Journal of Applied Clinical Medical Physics, 2012, vol. 13, pp. 254-266

5. **Pre-treatment independent plan verification for VMAT using a treatment delivery emulator and Monte Carlo dose model**

Accepted by Radiotherapy and Oncology, September 2013

6. **A megavoltage scatter correction technique for cone-beam CT images acquired during VMAT delivery**

Published in Physics in Medicine and Biology, 2012, vol. 57, pp. 3727-3739

ABSTRACT

Volumetric modulated arc therapy (VMAT) is a technique for the delivery of intensity modulated radiotherapy (IMRT) whereby the linear accelerator (linac) delivers dose continuously while rotating around the patient. VMAT has gained attention due to its ability to produce complex dose distributions, deliverable in a much shorter treatment time than IMRT. The purpose of this thesis was to investigate the clinical application of VMAT, and to identify any benefits over IMRT in the areas of treatment planning, delivery, and imaging.

A VMAT planning strategy was developed which demonstrates that complex dynamic arc deliveries can be sequenced from static, IMRT-based control points. For prostate patients, the VMAT solution demonstrated superior sparing of critical structures compared to IMRT plans. A further comparison of VMAT and IMRT was performed with the development of an automated planning methodology, which aimed to reduce the impact of planner bias. Applied over a series of nasopharynx patients, the technique showed that VMAT achieved an improvement in parotid sparing compared to IMRT.

To investigate the limitations on the delivery of VMAT plans, a software emulator was produced to accurately simulate linac motion. The emulator was used to determine 'ideal' linac parameters for a range of VMAT plans. Leaf speed was found to be a limiting factor for the achievable plan complexity, along with the availability of continuous variable dose rate (CVDR). For a commercial CVDR system, experiments confirmed the improved delivery efficiency, and an improvement in dosimetric accuracy compared to the binned dose rate (BDR) system.

An independent dose calculation methodology was developed for VMAT, such that accurate pre-treatment plan QC can be performed. It was found that the accuracy of a Monte Carlo simulation was improved when accounting for the effects of realistic linac motion. Finally, the impact of MV scatter on simultaneously-acquired cone beam CT images was investigated, and a scatter correction methodology was developed and validated.

This thesis shows that VMAT can offer an alternative to static-field IMRT, provided that knowledge of the limitations of dynamic linac motion are accounted for within planning. Results suggest that modern linac designs (i.e. faster MLC speed, and a higher, continuously-variable dose rate) are required to achieve robust delivery of complex plans. The workflow benefits of VMAT can also be optimised through the use of independent dose calculations incorporating delivery characteristics, and through the use of image guidance from CBCT scans acquired during treatment.

Christopher James Boylan
The University of Manchester
Doctor of Philosophy
'The effective application of dynamic arc radiotherapy'
June 2013

DECLARATION

No portion of the work referred to in this thesis has been submitted in support of an application for another degree or qualification of this or any other university or other institute of learning.

COPYRIGHT STATEMENT

ACKNOWLEDGEMENTS

I would like to thank my supervisors Carl Rowbottom and Ranald Mackay, for their support, advice and encouragement throughout the past few years. I appreciate the many opportunities they have provided for me to progress with my research and career. I am also indebted to all of my colleagues within Christie Medical Physics and Engineering (CMPE), who have been extremely helpful and understanding. Particular thanks goes to Adam Aitkenhead, who has proven to be a useful sanity-checker and general MATLAB de-mystifier throughout my research. Thanks also to Steve Smith for his frequent programming advice, especially in my earlier projects.

Much of this thesis would not have been possible without the clinical implementation of VMAT within the department. For this, I'd like to acknowledge Elekta, who provided support over the course of my PhD scheme, and also the many clinicians - especially in the urology team - for their interest and enthusiasm in my research. The assistance from Julie Stratford and the R1 radiographers is also greatly appreciated.

Finally, a huge thanks to my mum and dad, who have been supporting and encouraging me for 30 years now (and must be quite tired of it), and to Kaisla for her patience and understanding.

THE AUTHOR

MSc Physics and Computing in Medicine and Biology, University of Manchester, 2006
BSc Physics, University of Warwick, 2005

I am a HPC-registered clinical scientist, and hold corporate membership of IPEM. Following completion of the training scheme in 2009, my employment has been as a Research Physicist in radiotherapy at The Christie NHS Foundation Trust, Manchester. I have presented work at various national and international meetings including ESTRO conferences, UKRO, and the International Lung Cancer Congress.

FUNDING DISCLOSURE

My salary as a Research Physicist during my PhD was partly funded by an unrestricted educational grant from Elekta (Crawley, UK). 50% of my PhD fees came from my employer, Christie Medical Physics and Engineering.

1. INTRODUCTION

1.1. Radiotherapy for the treatment of cancer

Radiotherapy remains a widely-used technique for the treatment of cancer, with approximately 40% of all cancer patients receiving some form of radiotherapy as part of their management [1, 2]. The effectiveness of radiotherapy is well established and, along with surgery and chemotherapy, it has been identified as contributing significantly to improving cure rates and survival in recent decades [3, 4]. In broad terms, radiotherapy exploits the fact that ionising radiation causes damage to cells within the body. Primarily, the mechanism for induced cell death, mutation, or subsequent carcinogenesis, is radiation damage to DNA [5]. A higher dose of radiation generally means a larger number of DNA strand breaks, and sufficient strand breaks increase the probability of cell lethality. For the treatment of cancer, therefore, the intention is to cause sufficient radiation damage to the tumour to break the cycle of abnormal cell proliferation.

Crucially, radiotherapy causes damage to both normal cells and tumour cells. The aim of radical radiotherapy, therefore, is to obtain tumour control while minimising the dose to normal tissue, such that acute and late side-effects can be reduced, and patient quality of life can be preserved [6]. This can be achieved in a number of ways. The linear quadratic (LQ) model for radiation-induced cell death states that:

$$S = \exp\left(-\alpha d - \beta d^2\right) \qquad \text{(eq. 1)}$$

where S is the surviving fraction of cells and d is the radiation dose in Gy [5]. α and β are radiosensitivity parameters, which vary between different tissues. It is these differences - and in particular the different radiosensitivities between normal and tumour cells - which are exploited through the use of treatment fractionation. If d is the fractional dose and n is the total number of fractions, taking the natural logarithm of equation 1 becomes:

$$-\ln S = E = n\left(\alpha d + \beta d^2\right) \qquad \text{(eq. 2)}$$

Here E is the logarithmic cell kill (or 'effect'). The ratio α/β is commonly used as a method of discriminating between different radiosensitivity endpoints in different tissues. Thus, fractionation allows the effects of differences in α/β ratios to be maximised over the course of treatment (Figure 1a). Provided that the tumour α/β ratio is greater than a nearby late-reacting normal tissue α/β, fractionation is a method of eliciting a larger response (cell kill) in the tumour than in the nearby normal tissue.

a)

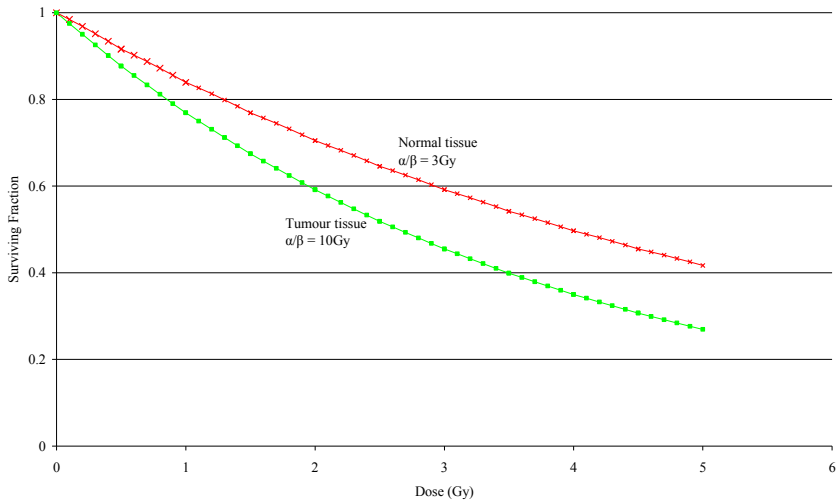

b)

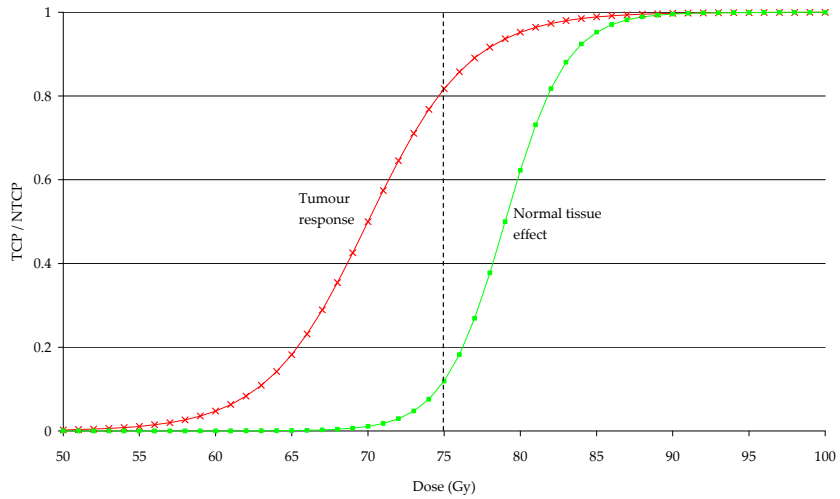

Figure 1. Demonstrating the principle of a) fractionated radiotherapy (in this case the number of fractions n is 10), and b) TCP and NTCP, where in this case an 80% TCP will result in 10% NTCP at 75Gy. By optimising the therapeutic ratio, this gap between the induction of normal tissue complications and tumour control can be increased.

With increasing dose, there is increasing likelihood of tumour response. If cell killing through irradiation is considered a random event, it is possible to consider the dose-response relationship as approximating a Poisson distribution, such that:

$$\mathrm{TCP} = \exp(-\mathrm{E}) \qquad \text{(eq. 3)}$$

where TCP is the tumour control probability and *E* is the 'effect' from equation 2. Here, equation 3 represents a simplification of the true tumour response – improved models have been developed to account for the variations in inter-patient radiosensitivity and for non-uniform irradiation [7], giving the characteristic dose response curves observed in Figure 1b. This figure also shows the normal tissue complication probability (NTCP), where the effect in this case is the onset of some normal tissue endpoint (for example, lung tissue fibrosis). In Figure 1b it can be observed that a dose of 75 Gy delivered will elicit an 80% TCP and 10% NTCP. The 'therapeutic ratio' is essentially the conceptual difference between these two values and fractionation is one way in which this can be optimised.

In Figure 1 the normal and tumour cells are receiving the same dose, albeit with different outcomes due to the differences in radiosensitivity and fractionation. In practice radiotherapy involves the irradiation of large populations of different cells, such that tissue response is a function of the dose distribution in a volume and individual sensitivities. In normal tissues, it is helpful to consider the concept of serial and parallel organ structures. Serial organs consist of components (or 'subunits') which, if damaged through irradiation above some critical level, cause the entire organ to fail. Parallel organs, on the other hand, can tolerate a number of damaged subunits before failure. Practically, most organs exist on a scale of relative seriality – for example, the spinal cord is considered a highly serial organ, whereas the liver is considered highly parallel. For external beam radiotherapy, delivered with linear accelerators (linacs), many technological advances have been made to improve dose conformity to the tumour. Figure 2 shows the dose distribution for a typical head and neck patient. The plan is optimised in such a way that the planning target volume

(PTV, as defined by [8]) is receiving almost a complete prescription dose (in this case 51.3 Gy), whereas high dose to the spinal cord is avoided, and the nearby parotid gland (a mainly parallel organ) is receiving a lower volume of high dose. This is achieved through the choice of entrance beam angles, and the use of conformal beam shaping defined by multi-leaf collimators (MLCs).

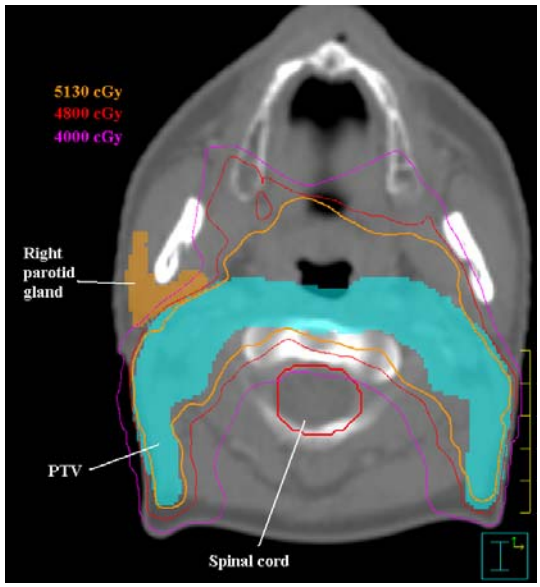

Figure 2. Typical conformal dose distribution for a head and neck (oropharynx) radiotherapy patient.

The use of MLCs, alongside developments in imaging and computerised planning, enables the therapeutic ratio to be optimised [9]. However, while conformal shaping of the treatment beams reduces the dose to normal tissue, it does not avoid it entirely due to the impact of scattered and leakage radiation. As well as contributing to relatively short-term toxicity, scatter and leakage dose from the treatment beam can lead to longer-term radiation induced secondary malignancies, further emphasising the requirement for careful characterisation of planned dose to the patient [10].

In this introduction, the concept of intensity modulated radiotherapy (IMRT) as a 'gold standard' treatment technique will be discussed, and then volumetric modulated arc therapy (VMAT) - a dynamic technique for the rotational delivery of IMRT - will be introduced. The context of the thesis will then be set out with respect to the literature, and finally the aims and hypothesis will be described.

1.2. From IMRT to VMAT

1.2.1. Principles of IMRT

Intensity modulated radiotherapy (IMRT) is now an established paradigm for the treatment of cancer [11]. Previously, conformal radiotherapy has involved the delivery of multiple static beams that often conform to the shape of the target while blocking nearby organs at risk (Figure 3a). Each conformal beam nominally has a uniform radiation fluence profile, although this can be modified with the use of wedges or compensators to achieve intensity modulation. IMRT is an extension of this, in that the in-plane radiation fluence can be modulated almost arbitrarily, often using MLCs (Figure 3b). Through the delivery of multiple IMRT beams, it is therefore possible to build a highly conformal dose distribution within the patient. The technique has allowed for an expansion of the therapeutic ratio in the clinic, in that target doses may be escalated while maintaining an acceptable level of toxicity to surrounding tissue [12]. Conversely, IMRT can be used to spare specific organs at risk (OARs), while maintaining an iso-effective homogenous dose distribution in the target [13]. IMRT has also been used to deliver different dose prescriptions to multiple target volumes simultaneously [14]. This concept of a simultaneous integrated boost (SIB), usually in the context of head and neck radiotherapy, has been applied effectively through the use of IMRT.

a) Conformal plan b) IMRT plan

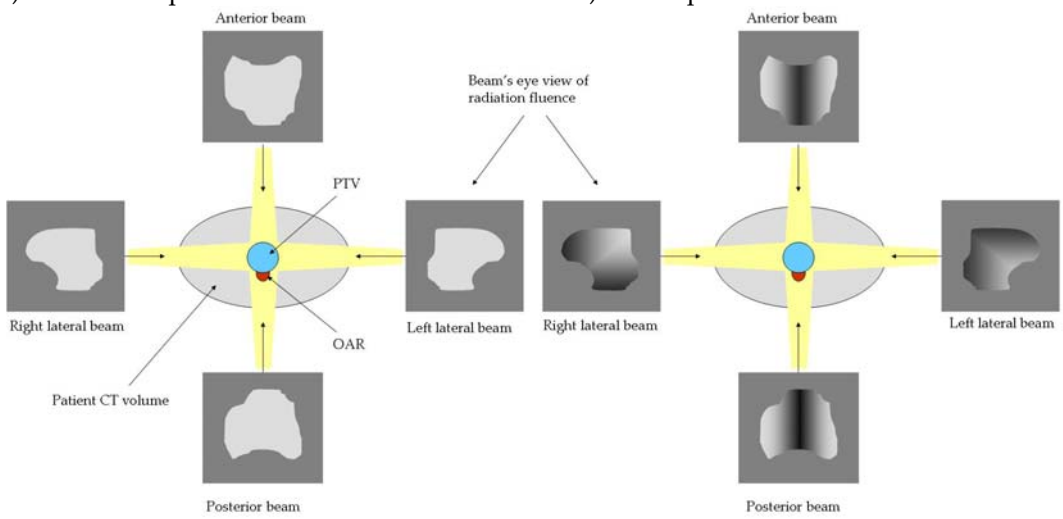

Figure 3. For an example radiotherapy plan with a target volume (PTV) and nearby organ at risk (OAR), a four beam arrangement can be delivered with a) conformal radiotherapy, whereby the shape of the aperture can be adjusted, but with uniform in-plane intensity, or b) IMRT, where the in-plane fluence can be modulated to produce improved conformity.

Figure 3b demonstrates how multiple idealised radiation fluence profiles can be summed to produce the desired dose distribution within the patient. In practice, these ideal fluences are usually delivered through the use of MLCs on the linac. Whereas previously MLCs were used only to define a field shape, often conforming to the beam's eye view (BEV) of the tumour outline, in IMRT the beam-shaping and movement capabilities of the MLCs are exploited to build up an approximation to the ideal fluence. This can be done in two ways: the 'step-and-shoot' method, and the 'dynamic MLC' (dMLC) method. The step-and-shoot method (Figure 4a) is based on the principle that the ideal fluence can be approximated by summing a sequence of static, MLC-defined fields. The level of approximation to the ideal fluence depends on physical constraints such as the leaf width, minimum leaf gap and the allowed number of segments. For the dMLC delivery method (Figure 4b), there are no individual segments - instead, the radiation beam remains on while the MLCs move across the field with varying velocities. Some method of interpretation is required to convert the ideal fluence into a series of instructions for the MLCs [9]. While both of these techniques are very different in practice they remain equally valid mechanisms for the delivery of IMRT. Furthermore, it is possible to recognise aspects of both the step-and-shoot and dMLC techniques in the planning and delivery of arc radiotherapy.

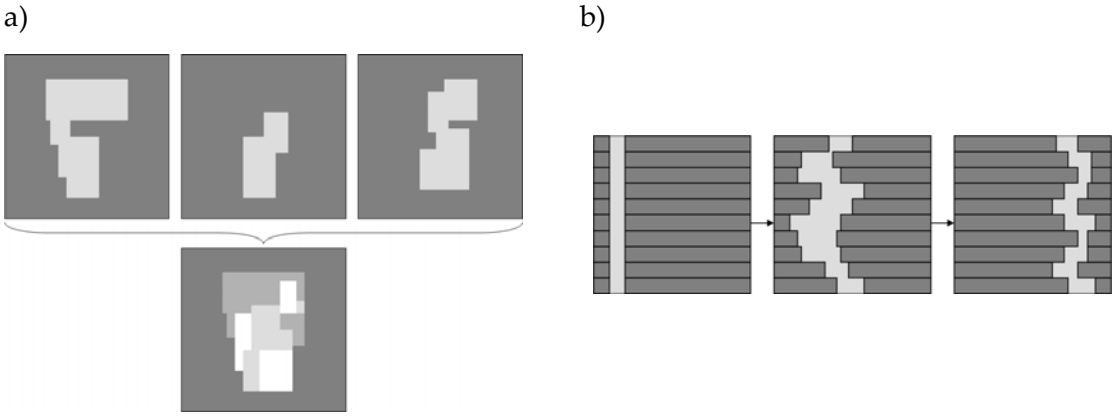

Figure 4. a) Step-and-shoot IMRT delivery involves the summing of static, individual MLC segment to produce an approximation to the ideal fluence. b) Dynamic MLC delivery uses a continuous beam delivery while sweeping the MLCs across the field at different velocities to produce the desired fluence.

1.2.2. Inverse planning

The complexity of IMRT means that inverse planning is commonly used to generate the treatment plans. The concept of inverse planning is that the desired dose distribution is first described through the definition of plan objectives and constraints. The treatment planning system then searches for a set of delivery parameters that best meet the objectives. The inverse optimisation problem can be described in general terms (from Webb [15]): if D is the desired 3D dose distribution and b is the vector of the beam radiation fluence, then they are linked by $D=A.b$, where A is the matrix linking the dose element to the beam element (in treatment planning systems, this constitutes the dose deposition algorithm or kernel). The optimisation problem posed is to find:

$$b = \frac{D}{A} \qquad \text{(eq. 4)}$$

This problem is 'ill-conditioned', in that there are a number of possible fluences b that when operated on by A give the desired distribution D [15]. Furthermore, this generalisation requires both positive and negative values for b, which are not possible. As negative fluences are not allowed, only an approximation to the desired dose distribution is ever possible [16].

To reduce the ill-conditioning of the optimisation problem, the treatment planner must provide the system with a set of constraints. This can include setting the number and orientation of the beams, as well as their energy and delivery method (e.g. step-and-shoot). Dose-volume based constraints can also be applied, such as 'allow no more than X% of the target volume to receive less than Y Gy'. Similar constraints usually also exist for OARs. During optimisation, each constraint has a 'cost' or 'objective value'. This is a measure of how well the constraint is being met by the current plan, and is defined by Zhang *et al* [17] as:

$$f = \frac{1}{\mathrm{N}} \sum_{n} \left(D_n - D_n^0 \right)^2 \qquad \text{(eq. 5)}$$

where N is the number of voxels in that constraint's region of interest, D is the current dose, and D^0 is the desired dose. As a measure of how the whole optimisation is progressing, the weighted sum of all objective values gives the 'composite objective function':

$$F = \sum_{i} w_i f_i \qquad \text{(eq. 6)}$$

where the w is an individual weighting or importance factor (often selected by the planner) for the constraint i. During inverse optimisation, the fluence b is first initialised with either uniform or small random values. A three-step process is then undertaken: 1) dose to the patient is calculated from the current fluences; 2) a search direction x is established from the cost function F, based on the desired objectives and current dose distribution, and a step size a is calculated; 3) the fluence is then updated by adding ($x.a$) to the previous values, and the process begins again at step 1. After each dose calculation if a stopping criterion is met then the optimisation will finish and the plan is considered complete. Modern treatment planning systems have different methods for determining x and a: for example, the algorithm present within the Pinnacle planning system (Philips Medical Systems, Madison, USA) uses a gradient descent algorithm which only accepts changes which reduce the cost function. Other methods can include steepest descent methods, conjugate gradient algorithms or stochastic optimisation [18].

Once optimisation is finished, the result is a set of fluences which are ideal but not necessarily deliverable. As described earlier, some method is then required to approximate the ideal fluences if the step-and-shoot method is to be used. However, some modern planning systems now have methods for integrating machine constraints within the optimisation process, rather than afterwards [19]. This direct aperture optimisation (DAO) thus produces plans which are immediately deliverable:

i.e. they consist of a set of MLC segments and beam weightings. As will be shown within this thesis, this knowledge of the physical capabilities of the linac during inverse optimisation is essential for the production of accurate arc radiotherapy treatment plans.

1.2.3. Implementation of IMRT

IMRT presents specific challenges for radiotherapy departments that are not necessarily observed for conventional or conformal techniques [20]. These challenges exist at each stage of the radiotherapy process. In terms of planning, the use of inverse optimisation is computationally expensive, and requires robust determination of class solutions for various treatment sites [21]. Furthermore, from the clinician's perspective, if a process of dose escalation is to be undertaken which often requires a high degree of conformity to the target volumes with respect to nearby OARs – then accurate delineation is necessary. It may be applicable, therefore, to consider the use of more than one imaging modality, for example PET-CT for outlining the target volume in head and neck cancers [22]. The movement towards more targeted radiotherapy, often involving much sharper dose gradients from the PTV to nearby OARs, means that the patient set-up needs also to be closely controlled. The uptake of IMRT in many departments has been accompanied by increased use of on-treatment imaging [23], such as x-ray cone-beam computed tomography (CBCT). Figure 5 shows how such devices are positioned on the linear accelerator [24]. Image guided radiotherapy (IGRT) is the use of regular patient imaging over the course of treatment for the purposes of monitoring and, if necessary, adjusting the treatment position. IGRT may also be accompanied by patient immobilisation devices such as moulded shells for head and neck patients. There are presently a number of techniques and protocols for performing IGRT, with the overall aim of monitoring the internal anatomy in the region of the treatment volume, and ensuring that the patient is positioned at each fraction as close as possible to the planned geometry.

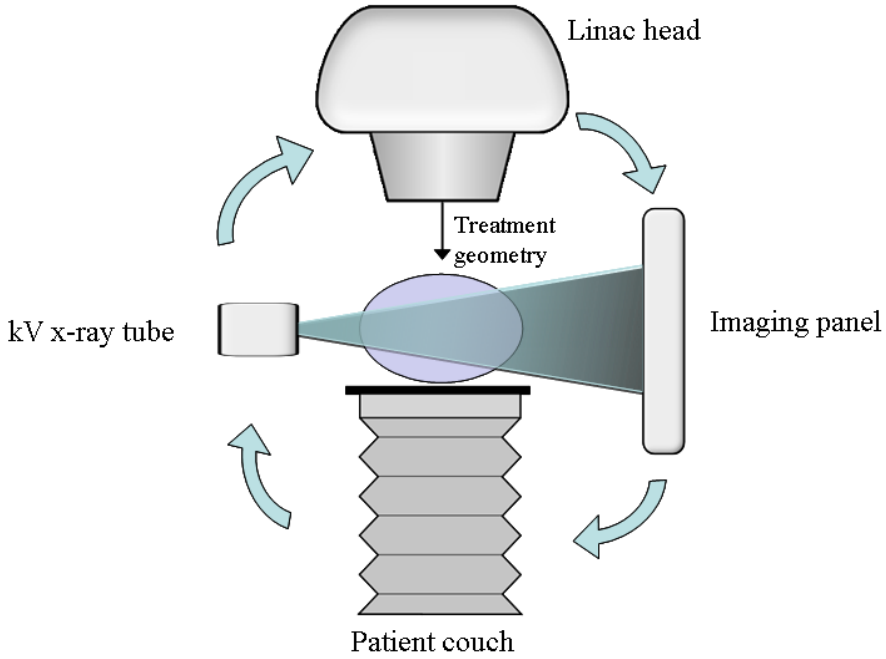

Figure 5. Geometry of the cone-beam CT (CBCT) system for Elekta linear accelerators. The imaging beam is normal to the treatment beam, and usually rotates in a complete 360° arc around the patient, or 200° for 'half-rotation' scans.

Another significant challenge for the practical implementation of IMRT is ensuring the accuracy of delivery. IMRT fields (both step-and-shoot and dMLC) require highly accurate positioning of the MLCs, and a number of quality control regimes have been proposed to monitor this [9]. Furthermore, IMRT control points can involve small field sizes and low radiation output (i.e. a small number of monitor units (MUs)), meaning that dose calculations have to be carefully characterised. A number of studies have discussed the accuracy of small-field dosimetry from commercial planning systems, which often employ analytical algorithms for the computation of dose [25]. Furthermore, the ability of the linac to reliably deliver short exposures in step-and-shoot IMRT has to be carefully characterised [26]. It is for this reason that IMRT is usually accompanied by a programme of pre-treatment, patient-specific quality assurance. Many dosimetric phantom devices now exist to verify that the delivered patient plan matches the calculated dose distribution within acceptable limits [27, 28]. It is also acknowledged that some method of secondary, independent dose calculation is important for IMRT, due to the small, potentially unusually-shaped fields and complexity of delivery [29, 30].

1.2.4. Clinical argument for IMRT

Despite these challenges, there is a clear clinical argument for IMRT [11]. A wide range of sites are now treated with IMRT as the standard of care, with the prostate being the most common site treated with IMRT worldwide [31]. The prostate presents a typical problem for radiotherapy, in that the treatment site is close to radiosensitive OARs such as the rectum, bladder and small bowel. Dose escalation to the prostate has been proposed by a number of studies [32, 33], and hypofractionated regimes (exploiting the possible low α/β ratio of prostate cancer) have also been suggested [34]. Ultimately, high rates of toxicity in the bladder and rectum have been the limiting factors in these studies, when using conventional or conformal radiotherapy. Zelefesky *et al* [35] noted that conformal radiotherapy allowed only an escalation of 65-70Gy_2 to the tumour leading to a poor level of local control (where Gy_2 is the radiobiologically equivalent dose delivered in 2Gy fractions). IMRT, however, allows for the delivery of concave fluences, reducing dose to the surrounding organs and thereby enabling escalation of the prescription dose (>81 Gy_2 proposed by [35]). Using a standard dose and fractionation, Zelefesky reported a reduction in late grade 2 rectal toxicity (proctitis) from 14% with conformal radiotherapy to 2% with IMRT, and other studies have reported similar outcomes [36]. A recent systematic review of IMRT for prostate cancer also noted the reduction of acute and late toxicity in the context of radical radiotherapy [6].

While prostate cancer remains the most commonly treated site with IMRT worldwide, two separate surveys have shown that head and neck cancer is the most commonly treated site in the UK [37, 38]. The argument for the use of IMRT in head and neck cancer follows similar reasoning to prostate cancer: with the proximity of numerous radiosensitive OARs there is difficulty in achieving local tumour control without also causing significant toxicity. The presence of highly serial organs such as the spinal cord, brainstem and optic nerves means that a sharp fall-off in dose is required if coverage to the target volume is to be maintained. Furthermore, there are also more parallel OARs which, if irradiated above certain dose-volume tolerances,

increase the likelihood and severity of toxicities which can impact on patient quality of life (such as the loss of salivary function through irradiation of the parotid glands). There is increasing evidence to suggest that IMRT reduces acute and late toxicity in head and neck patients. In particular, the PARSPORT study reported significant reduction in xerostomia (along with faster recovery of saliva production) when the parotid glands were spared using IMRT in the treatment of pharyngeal squamous-cell carcinoma [13]. A review by O'Sullivan *et al* [39] identifies other randomised clinical trials which demonstrate that IMRT provides improved parotid sparing, and hence improved salivary function, when compared to conformal radiotherapy [40].

Staffurth [11], in reviewing a number of clinical studies for IMRT, suggested that there is sufficient consistent evidence to widely implement IMRT in the United Kingdom for certain cancer sites. However, the UK uptake of IMRT since its introduction in the 1990s has been slow [41]. The National Radiotherapy Advisory Group (NRAG), established to address the shortfall in overall provision of radiotherapy in the UK, proposed that 33% of all radical fractions should be delivered with IMRT. In a 2007 survey it was reported that less than half of radiotherapy centres had any means of delivering IMRT [37], and a recent report has estimated that inverse-planned IMRT accounted for ~6.8% of all treatment episodes in 2011/12 [41]. A 2008 survey by Mayles [38] suggested that the main reasons for the slow uptake of IMRT are insufficient physics support, along with a lack of funding and appropriate equipment. Various studies have identified the additional planning complexity and quality assurance processes as also placing significant strains on resources for the implementation of IMRT [6, 20]. While IMRT has been deemed potentially cost effective with respect to improved patient quality of life [42], there remain challenges for its initial implementation in the clinic, and the most efficient use of resources to deliver IMRT.

1.3. Principles of VMAT

Volumetric modulated arc radiotherapy (VMAT) is a technique for the delivery of IMRT whereby the dose is delivered continuously in an arc around the patient [43]. As shown in Figure 6, VMAT can be delivered using a conventional linear accelerator by exploiting the dynamic aperture shaping from the multi-leaf collimators. Crucially, VMAT is capable of producing intensity modulated dose distributions similar to those achieved by fixed-beam IMRT, but in a much shorter delivery time [44]. VMAT has gained recent attention in the clinical setting due to the potential to increase the provision of intensity modulated treatments for a given linac.

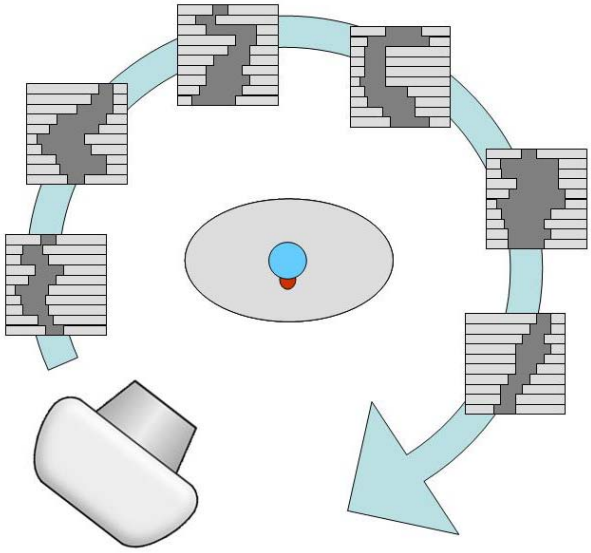

Figure 6. VMAT involves continuous radiation delivery while the linac rotates around the patient. MLC shapes are varied dynamically, while the dose rate and/or gantry speed can be modulated to achieve the desired dose delivery.

The development of VMAT closely tracked the development of IMRT from the early 1990s, but did not gain widespread interest until becoming commercially introduced in 2009 [43]. The delivery of radiotherapy using arcs rather than fixed beams is not a new concept, however, with a rudimentary form of conformal arc therapy proposed as early as 1965 [45]. In 1982, Brahme *et al* built on this work and demonstrated formally that to achieve a uniform dose to a nominal target wrapped within an organ at risk, then the radiation delivered in an arc around the target would need to have a non-uniform fluence distribution [46]. In the 1990s the concept of intensity-

modulated radiotherapy was the catalyst for the development of 'tomotherapy', whereby a megavoltage fan beam is rotated around the patient in geometry analogous to a CT scanner [47]. Through the use of a simple binary collimator, it is possible to build up an intensity modulated dose distribution in slices through the target volume, while indexing the patient through the machine on a couch. While highly effective, the requirement for a dedicated tomotherapy machine led some researchers to investigate the use of arc therapy on conventional linear accelerators fitted with MLCs. Yu [48] introduced intensity modulated arc therapy (IMAT) in 1995, whereby tomotherapy dose distributions were reproduced on a linac through the delivery of a series of overlapping arcs. At this stage, IMAT plans were produced with a forward-planned solution, which approximated tomotherapy intensity profiles using a sequence of MLC segments. However, the use of multiple forward-planned arcs (usually 3-5) only demonstrated a plan benefit over conventional or conformal therapy, rather than IMRT deliveries [49, 50].

In the past decade, the commercial TomoTherapy system (Accuray, Sunnyvale, USA) has demonstrated highly conformal dose distributions, allowing many centres to quickly implement complex intensity modulated treatments with a dedicated unit [51]. The search for an equivalent linac-based solution continued with several authors attempting to determine an inverse-planned technique for IMAT which would result in the desired dose distribution deliverable in a single arc [52, 53]. This was subsequently termed VMAT. It is possible to build up an analogy for VMAT inverse planning by considering the fixed-field IMRT method. For IMRT, equation 4 required the inverse optimisation of the fluence b to produce a desired dose distribution D. If b has uniform intensity but an arbitrary 2D shape (for example, defined by an MLC), then the fluence from one IMRT beam is:

$$\mathrm{b}_{\mathrm{IMRT}} = \sum_{i=1}^{N} \mathrm{b}_{\mathrm{i}} \qquad \text{(eq. 7)}$$

where, for an 'ideal' continuously variable IMRT field, $N \to \infty$. For M beams with different gantry angles (Ω), the complete radiation fluence would then be:

$$B_{IMRT} = \sum_{j=1}^{M} (b_{IMRT})_j \qquad \text{(eq. 8)}$$

Around a VMAT arc there is no instantaneous modulation of fluence, such that, at each gantry angle, $N = 1$ in equation 7. However, as VMAT involves the continuous delivery of radiation during rotation, then $M \to \infty$ in equation 8. For VMAT, therefore, the complete fluence is:

$$B_{VMAT} = \int b(\Omega)\, d\Omega \qquad \text{(eq. 9)}$$

Thus, IMRT allows only a coarse sampling of the gantry angles but with potentially highly modulated beams, whereas VMAT utilises all of the gantry angles, but without any instantaneous modulation of beam intensity. For inverse planning, it is not feasible to evaluate $B_{VMAT} = D/A$ as in equation 4. Firstly, it would be computationally expensive for the inverse optimiser, as there would be a large number of parameters if Ω is considered a continuous variable. Secondly, there are restrictions on the linac (such as maximum leaf speed) if the plan is to be delivered in practice. Furthermore, optimisation does not need to take place at every gantry angle. It has been shown that there is a number of beams above which no benefit is achieved to produce the desired intensity modulated dose distribution [54].

On this latter point, theoretical considerations of VMAT have focussed on determining what level of modulation is achievable in a single arc compared to fixed-field IMRT [55]. Bortfeld's work [54] extended the theory that only a finite number of intensity modulated beams are required to approximate an ideal dose distribution, to take account of VMAT delivery. It was shown that, if intensity modulated beams are delivered in short, abutting arcs rather than from fixed beam angles, then the delivered dose distributions are approximately equivalent. This was one of the first theoretical justifications demonstrating that VMAT could provide an equivalent level of modulation to IMRT. One conclusion to be drawn from this is that any inverse

optimiser for VMAT needs only to generate a set of fixed control points, separated by a gantry angle spacing (ΔΩ).

Thus, the development of single-arc VMAT, producing plans that are able to be delivered in a significantly shorter treatment time than IMRT, has required a practical planning methodology whereby MLC segments spaced equidistantly around an arc are inverse-optimised. The gantry spacing required is determined partly by the level of modulation required by the plan. However, it is also important to consider how the treatment planning system approximates the continuous dose delivery. As shown in Figure 7, if the treatment planning system only calculates dose through a coarse representation of the arc (e.g. every 10 degrees), then the patient dose will be under-sampled at distances far from the rotational axis (i.e. the isocentre). Furthermore, work by Webb and McQuaid [56] suggested that a gantry angle spacing of $\Delta\Omega < 5°$ was required if a fixed intensity modulated beam is to be approximated by a 'small arc' between control points. In practice, many treatment planning systems allow this parameter to be adjusted [57].

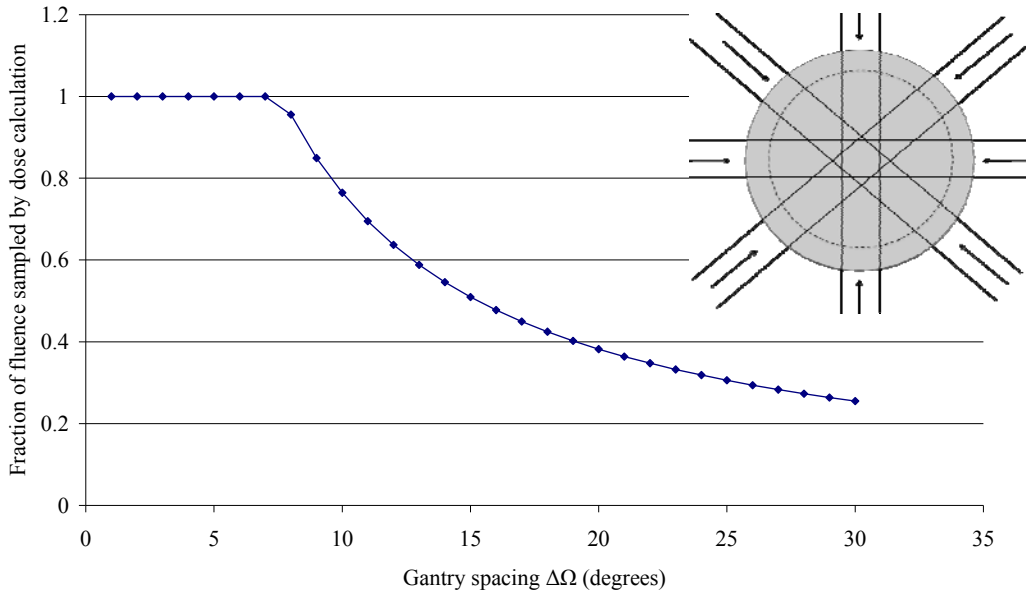

Figure 7. For a cylindrical model of a patient (inset) with a diameter 60cm, with equally spaced 4cm² beams applied to the isocentre, this graph indicates the fraction of the sampled fluence at 15cm from the isocentre (indicated by the dashed line). For increasing values of ΔΩ, the sampling of the fluence gets lower, and hence the dose calculation is a poorer approximation to continuous VMAT delivery.

The above theoretical considerations of VMAT planning require that the linear accelerator is able to deliver a sequence of arbitrary MLC shapes in an arc, each with an arbitrary number of monitor units. In reality, due to the physical constraints of the linac, this means that the dose rate and/or gantry speed needs to be modulated between each control point [43]. As will be examined further in this thesis, MLC motion ultimately determines the choice of gantry speed or dose rate. It has been suggested previously that one of the reasons for the relatively slow commercial interest in VMAT was the lack of suitable linac control systems to govern these dynamic changes [52]. However, modern control systems are now capable of varying gantry speed, dose rate, and individual MLC speed in order to achieve highly complex dose delivery. As this thesis will show, there are a number of physical linac limitations which need to be considered in the planning process to ensure accurate and deliverable VMAT treatments.

Since becoming commercially available in 2009, there have been two main implementations of arc radiotherapy: Elekta VMAT (Elekta, Crawley, UK) and Varian RapidArc (Varian Medical Systems, Palo Alto, USA). There exist also a number of software solutions for the production of VMAT plans, such as the Varian Eclipse planning system, Pinnacle, and the Elekta planning systems (XiO and Monaco). In the context of this thesis, only the Elekta VMAT delivery and the Philips Pinnacle system are used, although many of the conclusions are valid for other implementations. It should also be noted that 'VMAT' (as introduced by Otto [58]) is used throughout this thesis as a generic term for the delivery of arc radiotherapy through the modulation of MLC motion, dose rate and/or gantry speed. It is adopted here to avoid confusion with other forms of arc radiotherapy (such as IMAT), which have previously involved different modes of delivery.

1.4. VMAT research and context for thesis

VMAT remains a relatively novel treatment technique, and as such there has been a wide-ranging programme of research since its commercial introduction [43]. While

fixed-field IMRT remains the most common method for the delivery of modulated dose distributions, VMAT is gradually becoming a standard feature on many new linear accelerators. The ability to produce similar dose distributions to IMRT within a shorter delivery time is attractive to departments seeking an improvement in their provision of complex radiotherapy. However, in order to be considered a valid alternative to fixed-field IMRT, VMAT needs to demonstrate equivalence or improvement throughout the radiotherapy process. Broadly, the research topics for VMAT have been in three areas: treatment planning, delivery, and imaging. The purpose of this section is to provide the context for the research projects within the present thesis, and to identify the current clinical implementation of VMAT in these three areas.

1.4.1. Treatment Planning

As described in section 1.3, VMAT requires inverse planning to determine a sequence of MLC shapes, each with their own number of monitor units, in order to produce the desired dose distribution. For example, a single arc prostate VMAT plan with a 4° gantry angle spacing will have 90 available control points. Inverse optimisation, therefore, has to find the appropriate MLC shapes and beam weightings for all of these control points, given the objectives and constraints of the plan. Some inverse planning strategies for VMAT (Figure 8) have previously set up a series of fixed beams around the patient, and then searched for ideal fluence profiles for each [52, 59-61]. Then, these ideal profiles are converted into a sequence of MLC positions in an arc. At the conversion stage, the limitations of the delivery are taken into account - i.e. the sequence of MLC positions and monitor units must be such that the linac is able to select an appropriate, deliverable gantry speed and/or dose rate. This process of ideal fluence generation followed by conversion to a set of MLC instructions is analogous to the two-step IMRT inverse planning procedure described in section 1.2.

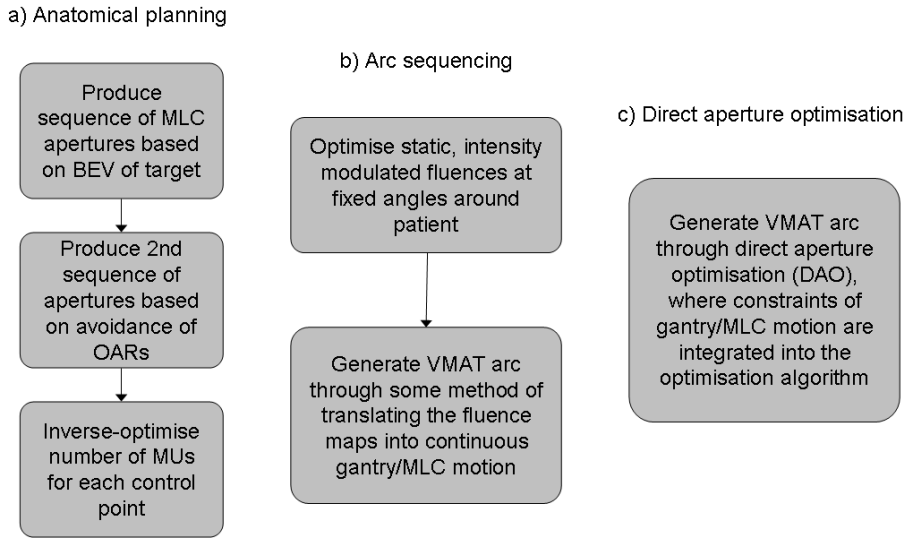

Figure 8. Overview of the different planning techniques for VMAT. Adapted from [60].

As also described in section 1.2, this two-step solution has a potential problem, in that the converted plan can only offer a broad approximation to the ideal fluences. This has led to more recent efforts determining an inverse planned solution for VMAT that incorporates direct aperture optimisation, where knowledge of the linac delivery constraints are incorporated within the optimisation [60]. One such DAO solution is that proposed by Otto [58], which was subsequently developed into the Eclipse planning system. This method begins by optimising a small number of discrete control points around an arc, where the MLC positions and MU weightings are optimised iteratively with respect to the objectives and constraints (including linac delivery constraints). After a number of iterations, a new control point is added halfway between the existing control points, and the optimisation continues. This process then repeats until the desired final control point spacing is reached (e.g. 4°). Otto demonstrates that this algorithm is capable of dose distributions similar to IMRT. Importantly, the integration of linac constraints within the optimisation means that the plan deliveries are efficient, with a beam-on time of < 2 minutes for plans previously delivered with IMRT in ~ 7 mins. Within this thesis, Publication 1 (section 2.1) expands on the concept of DAO-based planning, by investigating whether an existing static IMRT optimisation technique can be used to produce high quality VMAT radiotherapy plans.

Following the availability of two commercial planning solutions ('RapidArc' within Eclipse and 'SmartArc' within Pinnacle), there have been a large number of treatment planning studies investigating the clinical potential of VMAT compared to IMRT. In the clinical sites of the prostate, lung and head and neck, VMAT has been shown to produce very similar dose distributions to fixed-field IMRT. Single dose level prostate VMAT has been demonstrated by a number of authors [62, 63]. In all of these studies, the VMAT solution demonstrated equivalence or improvement in PTV coverage compared to IMRT. A more complex test of VMAT is the application of a simultaneous boost, or the delivery of different dose prescriptions to multiple PTVs. Yoo *et al* [65] found that RapidArc plans performed worse than IMRT when treating the prostate, seminal vesicles and lymph nodes in a two dose-level protocol. Conversely, two studies delivering a SIB to an intraprostatic lesion found that VMAT allowed for improved sparing of OARs compared to IMRT [66, 67].

Head and neck VMAT has had slower uptake in clinics. Some studies have found that it is difficult to produce adequate dose distributions on complex head and neck geometries with one or two arcs [68]. Other studies have had more success, with Bertelsen [44] demonstrating the feasibility of single-arc VMAT for oropharynx and hypopharynx patients treated with a three dose-level prescription. In this study it was found that target coverage was comparable to IMRT while the dose conformity was significantly improved. As such, doses to the spinal cord, parotids, and submandibular glands were significantly reduced compared to the IMRT solution.

In general, VMAT vs. IMRT planning studies have shown a trend for similar coverage of target volumes. In some centres, arc therapy has been successfully implemented into clinical use as a supplement to the provision of IMRT, and no significant changes in patient management have been identified [69-72]. However, it is apparent from many of these studies that, in attempting to reproduce existing IMRT-like dose distributions, potential improvements in plan quality from VMAT have not been fully explored. Objectively identifying the potential benefits of VMAT over IMRT is hindered partly by the difficulty in performing technique planning studies.

Comparative planning studies are essential when assessing a new treatment technique, and often involve parallel planning of a cohort of patients with the established method (e.g. fixed-field IMRT) and the method under investigation (e.g. VMAT). However, many planning studies are subject to bias in their design: for example, inter-planner variability, or lack of equivalent experience with both techniques. Attempts to reduce bias in planning studies, such as choosing identical optimisation parameters for both methods, may also be invalid, particularly if the optimisation algorithm employed is significantly different between each technique. This question of bias in technique comparison studies is addressed in Publication 2, in which a novel approach was developed to compare VMAT and IMRT, whereby planner bias is minimised through the use of an automated planning system.

Concern has previously been expressed about the impact of the low dose component of VMAT [73] – a rotational delivery means a larger volume of the patient is observed to receive a low dose (i.e. < 10 Gy). While these doses may not result in acute harm to surrounding tissue, there is the need to assess the risk of radiation-induced secondary malignancies, and to quantify this risk against other forms of radiotherapy. Previously, the move from conventional to IMRT treatments elicited a similar debate within the literature [74, 75]. For VMAT, the use of a continuous rotational dose calculation, incorporating a characterisation of linac head leakage and scatter, would be required for accurate estimations of low dose within the patient. This is discussed further in section 3.5.

1.4.2. Delivery and Quality Control

It is well established in the literature that VMAT can reduce treatment times compared to IMRT. Several studies have reported a 30-50% reduction in delivery time for prostate plans [62, 63, 66], accompanied by a reduction in the total number of monitor units required. Matuszak *et al* [76], assessing the use of VMAT for a range of treatment sites, reported a mean delivery time reduction of 78% compared to IMRT. Such time advantage has been exploited particularly for the delivery of stereotactic

lung treatments [77-79] which, due to their high dose per fraction, often have long beam-on times using fixed-field IMRT. For complex head and neck treatments, Vanetti [80] found that RapidArc could deliver equivalent-quality dose distributions in 70-90s compared to ~15 minutes with IMRT. These reduced delivery times have a number of potential benefits. Many of the above papers refer to the ability for improved patient throughput, and acknowledge the improved patient comfort and potential reduction in intra-fraction motion (although this has not yet been formally demonstrated).

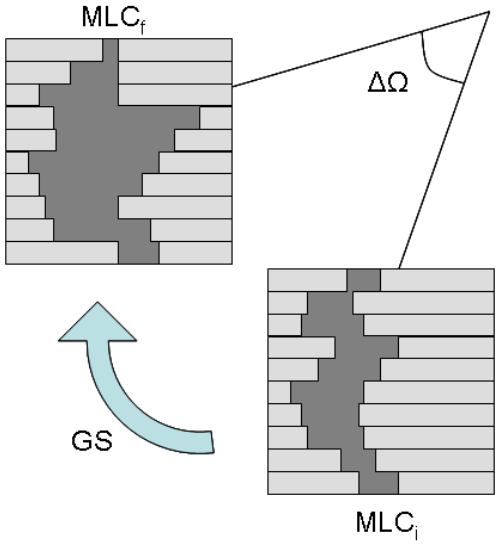

Figure 9. The required linac motion depends on the required MLC travel (MLCi to MLCf), over gantry distance ΔΩ.

The treatment time efficiency is determined partly by the planning system (as described in section 1.4.1), and partly by the linac itself. The Elekta VMAT system allows dose rate and gantry speed to be modulated in order to achieve the desired delivery [81]. As shown in Figure 9, from any given initial control point (MLC_i, MU_i) to the next (MLC_f, MU_f), the linac must first determine how many monitor units to deliver, and over what gantry distance. Thus the required gantry speed is:

$$GS = \frac{\Delta\Omega}{(MU_f - MU_i)/DR_{bin}} \qquad \text{(eq. 10)}$$

where DR_{bin} is the current dose rate of the linac. Equation 10 must be evaluated to ensure that it is <= GS_{max}, which is the maximum allowed gantry speed of 6°/s, set out

by the International Electrotechnical Commission (IEC) standards. The original Elekta VMAT system allowed for a fixed set of dose rate bins (e.g. 600 MU/min, 300 MU/min, 150 MU/min, 75 MU/min…). Once the appropriate DR_{bin} that satisfies equation 10 has been selected, then:

$$T_{CP} = \frac{\Delta\Omega}{GS} \qquad \text{(eq. 11)}$$

where T_{CP} is the control point time. However, the finite MLC speed provides another time constraint (T_{lim}) on the system:

$$T_{lim} = \frac{\max\left(MLC_f - MLC_i\right)}{v_{max}} \qquad \text{(eq. 12)}$$

where v_{max} is the maximum possible leaf speed. If $T_{lim} > T_{cp}$ then the dose rate bin again needs to be stepped down and equation 10 re-evaluated. This process is then repeated for every control point in a VMAT arc.

It is preferential for the dose rate to be as high as possible. Sequential MLC control points which require a slowing of the dose rate and gantry speed tend to be preferentially avoided in the plan optimisation process. In part this aids the overall speed of delivery, but it also acknowledges the observed adverse effects of low dose rates - particularly problems with beam stability, flatness and symmetry [82, 83]. The dosimetric output of linear accelerators (and most other quality control tests) tend to be performed at the maximum dose rate, and for fixed-field IMRT there was previously no requirement for the modulation of dose rate.

This raises an important aspect of VMAT delivery: one of the purported advantages of VMAT has been the ability to retrospectively install VMAT capability on existing linear accelerators. As such, existing MLC design and gantry motion capabilities have not necessarily been optimised to take account of the significant additional dynamic requirements for VMAT delivery. Rangaraj *et al* [81] noted that there has been a lack

of full characterisation of the constraints on VMAT delivery. Furthermore, Bortfeld and Webb [55] suggest that with VMAT there is currently a distinct trade-off between treatment efficiency and plan quality. It may be possible in the planning process to produce highly delivery-efficient plans (i.e. low modulation between consecutive control points), but this would reduce the overall plan quality. Within this thesis, Publication 3 (section 2.3) investigates the efficiency versus plan quality trade-off, and attempts to improve the characterisation of VMAT through the development of a delivery emulator.

Publication 3 also investigates the effects of allowing the dose rate to be continuously variable rather than restricted to fixed bins. Continuously variable dose rate (CVDR) VMAT was subsequently introduced onto the Elekta platform as part of the 'Integrity' control system update. Rather than 5 fixed bins, the CVDR system allows for 255 equally-spaced dose rate bins, such that there are smaller steps for the DR_{bin} variable. This has a number of consequences for delivery efficiency: the average dose rate will be higher, the gantry speed will be generally faster with fewer sharp changes in speed, and therefore delivery time will be shorter. In a validation study of the Integrity system, Bertelsen *et al* [84] confirmed that the introduction of CVDR resulted in faster deliveries than binned dose rate (BDR). Publication 4 (section 2.4) builds on this work by comparing BDR and CVDR delivery over a range of prostate and head and neck patients, and determines their effects on beam stability, MLC positioning accuracy, and overall plan dosimetry.

It is clear from this section that VMAT delivery is a complex process, requiring the linear accelerator to modulate various dynamic components simultaneously. As such, there is a strong requirement for routine preventative maintenance of the linacs, along with quality control (QC) regimes to ensure that the delivery system is working as expected. Whereas QC regimes for fixed-field IMRT are already well established in the literature [18], the question of what additional QC measures are required for VMAT remains a point of discussion [82, 83, 85]. Many VMAT QC papers recognise that there are three aspects of VMAT delivery which need to be routinely monitored:

leaf motion, gantry motion and dose rate variability. Ling *et al* [86] suggests QC tests which hold one of these variables constant while measuring the interdependency of the other two. An important aspect of quality control for VMAT is that, while the individual components of delivery can be checked independently, a set of tests need to be developed which check the synchronisation of these components. This is discussed further in section 3.4.

In clinical practice, radiotherapy treatments also require some provision for pre-treatment QC of patient plans [87]. For IMRT there are a number of established plan QC techniques for verification measurements on the linac. It is becoming increasingly common, however, for only a subset of IMRT plans to have dosimetric measurements, with the remainder having a secondary independent dose calculation, of which there are several commercial implementations [29, 30]. This is presently a source of debate within the literature [88]. The argument for reduced pre-treatment measurements is that dosimetric accuracy (and therefore patient safety) can be ensured with multiple redundant quality control procedures for the planning system, checking of the plan transfer integrity and monitoring the delivery. Advances in *in-vivo* dosimetry for IMRT also adds a further level of dosimetric confidence [89].

However, a strategy of reduced pre-treatment verification measurements could be problematic for VMAT. As discussed in this section, VMAT treatment plans are highly dependent on the ability of the linac to dynamically vary gantry speed, dose rate and MLC motion. Detailed knowledge of plan deliverability is not necessarily available in conventional planning systems or secondary dose calculators. Instead, as shown in Figure 10, there are a number of dosimetry devices for VMAT pre-treatment plan QC, many of which involve the delivery of the plan to detectors in a cylindrical geometry [90]. The proposed workflow benefit with VMAT may currently be offset by the requirement for additional plan verification time on the linac. The motivation for Publication 5 (section 2.5) was therefore to develop a novel software tool which is able to perform pre-treatment verification of VMAT plans without linac measurements. This publication details the integration of a software delivery

emulator with a Monte Carlo dose calculation algorithm in order to produce an independent secondary dose calculator for VMAT.

Figure 10. Pre-treatment plan QC devices for VMAT. Left, the Delta^4 phantom, consisting of two planes of diodes in a cylindrical geometry. Centre, the Octavius phantom, containing a 2D ion chamber array. Right, the ArcCheck phantom, in which diodes are placed around the circumference of the cylinder.

1.4.3. Imaging

As discussed in section 1.2, the use of image guided radiotherapy has been essential for the effective application of IMRT. Verellen *et al* [23] notes that the increasing use of IGRT is allowing the therapeutic ratio to be optimised by allowing for routine monitoring of the patient internal anatomy with reference to the PTV and nearby OARs. For high-risk prostate cases, a daily IGRT regime using electronic portal images and fiducial markers has also been associated with improved tumour control [91]. Furthermore, the use of cone-beam CT (Figure 5) has been demonstrated as effective by various authors for positional verification [92, 93], motion tracking [94] and adaptive re-planning [95].

The geometry of CBCT systems requires that the linear accelerator is rotated around the patient in order to acquire a sufficient number of projections for CT reconstruction. This rotational geometry has led to some investigations as to whether CBCT images can be acquired simultaneously during VMAT delivery [96]. Nakagawa [92] demonstrated that it was possible to reconstruct simultaneously-acquired CBCTs to verify the position of the prostate during VMAT treatment. This has a number of

potential benefits: firstly, knowledge of internal anatomy during treatment (rather than before or after) would provide more relevant information for positional verification and potential dosimetric assessment [92]. Some studies also suggest that knowledge of patient intra-fraction motion is important, and simultaneous imaging has been applied to track internal motion during delivery [97]. For highly complex radiotherapy (i.e. stereotactic treatments, dose escalation, and adaptive or margin-reduction strategies), such information would be valuable. Furthermore – in keeping with the other proposed benefits of VMAT - simultaneous CBCT can reduce the amount of in-room time for the patient, as both treatment and imaging are possible within one rotation of the linac gantry. This may in turn provide an extra advantage for patient throughput.

It should also be noted, however, that simultaneously-acquired CBCTs may only provide an 'offline' assessment of patient position, and some IGRT protocols may require pre-treatment positional verification. If systematic patient positioning errors are considered the most clinically important [98], then it is possible to envisage simultaneous CBCTs being used as part of an offline 'no action level' imaging protocol. Such a strategy would also require careful patient set-up procedures to minimise the risk of gross random positioning errors.

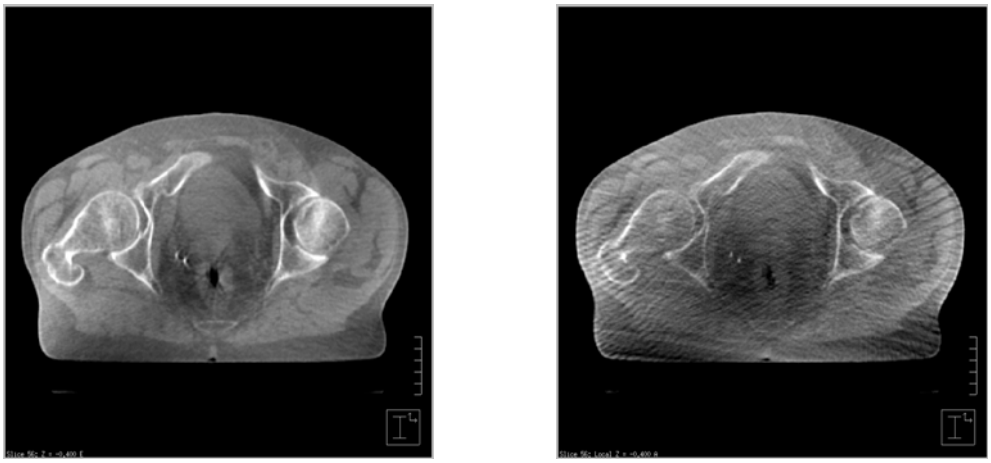

Figure 11. The effect of MV scatter on CBCT scans. On the left is a standard CBCT taken prior to VMAT delivery. On the right is the same patient scan taken during the delivery of the VMAT treatment.

Simultaneous CBCTs are only useful if they can provide images which are of sufficient clinical quality to perform IGRT. In practice, these acquisitions are degraded by treatment beam scatter from the patient, linac head and support structures onto the imaging panel. This is shown in Figure 11. The effect of this scatter has been discussed previously [99], whereby the visibility of low contrast soft tissue boundaries is reduced. As a consequence, simultaneous CBCTs require some method for scatter reduction (or avoidance) in order to recover the image quality. The main proposed methods are shown schematically in Figure 12.

Van Herk *et al* [100] proposed alternating the acquisition of the projections between 'kV-on' and 'kV-off', such that the imaging panel records an image of the MV scatter for each standard projection. This scatter image is then used to correct the corresponding projection image. The method proposed by Ling *et al* [101] divides the linac arc into interlaced sectors for imaging and treatment. As such, the kV and MV beams are not applied simultaneously, and no scatter is present within the reconstructed CBCTs. However, both of these correction techniques involve significant compromises. The van Herk method reduces the number of acquired projections by half, which (as is acknowledged by the authors) will impact upon image quality, particularly in the context of faster VMAT deliveries. While the Ling method is capable of producing scatter-free CBCT reconstructions, it increases the delivery time by periodically interrupting the treatment beam. It is also not clear what effect this latter methodology has on the quality of the plan or the accuracy of the delivery. Within this thesis, Publication 6 proposes an alternative scatter correction method for simultaneous VMAT-CBCT, which attempts to address the limitations of the other proposed methods.

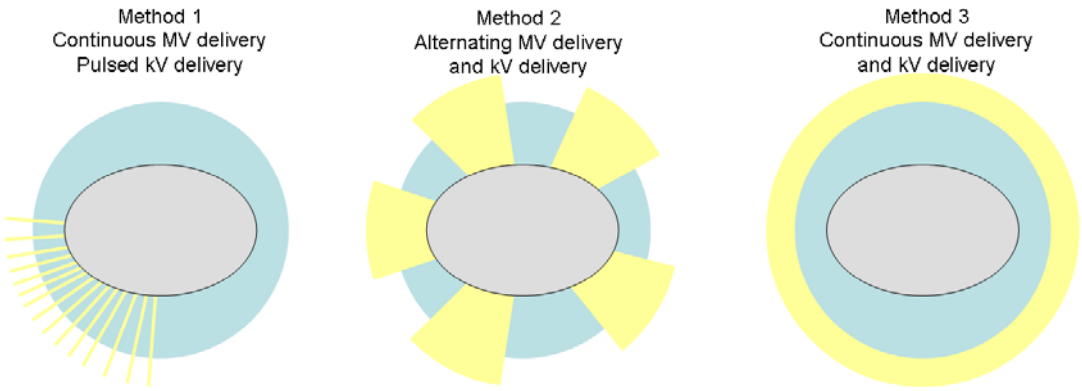

Figure 12. The various proposed techniques for scatter reduction in simultaneous CBCT acquisition. Yellow indicates kV delivery while blue indicates MV delivery over an arc. Method 3 is applied in publication 6, whereby a separate 'scatter map' is applied to correct the images.

1.5. Hypothesis and Aims

The overall aim of this thesis is to determine the most effective application of arc radiotherapy, and to investigate whether this relatively new technique can offer a benefit over IMRT in terms of the treatment quality and the impact on workflow. While the delivery time benefit of VMAT has already been well established, questions still remain about the overall effectiveness of VMAT as a potential replacement for fixed-field IMRT. If it is to be considered a viable, beneficial alternative, VMAT must offer equivalence or improvement throughout the radiotherapy process. Projects have been undertaken in the areas of treatment planning, delivery and imaging in order to improve the characterisation of VMAT and to determine the optimal application of this technique in the clinic. An overview of the aims are given below:

Treatment Planning

- Characterise VMAT plan optimisation by investigating whether static IMRT control points can be sequenced into a dynamic arc.
- Develop an objective, bias-free plan comparison methodology to investigate the difference between IMRT and VMAT for complex patient plans.

Delivery and Quality Control

- Investigate the limitations of various dynamic components of VMAT delivery through the development of a realistic linac emulator.
- Determine whether continuously variable dose rate VMAT demonstrates a dosimetric improvement over binned dose rate VMAT, and investigate the reasons for any such improvement.
- Determine whether it is possible to reduce the requirement for pre-treatment VMAT plan verification by developing an independent secondary dose calculation methodology.

Imaging

- Investigate the feasibility and practicability of simultaneous imaging during VMAT treatment, and develop a MV scatter correction method.

1.6. Structure of Thesis

Permission has been sought and obtained to submit this thesis in the alternative format. While the projects listed above are inter-related, they lend themselves to individual experimental investigations. The structure of this thesis, and hence the narrative of the research, is given below.

Publication 1 (section 2.1) investigates whether clinically-acceptable VMAT plans can be produced without a dedicated optimisation algorithm. Instead, a methodology was developed which sequences VMAT beams directly from static IMRT control points. Crucially, this methodology incorporates knowledge of the dynamic constraints of the linac, such that delivery efficiency can be considered during the planning process. A single-arc solution for prostate patients is demonstrated and plans are compared to the standard IMRT approach.

Due the potential difficulties in performing objective planning studies between VMAT and IMRT, Publication 2 details the development of an automated planning

technique. The technique - which involves the iterative adding and modification of optimisation objectives and constraints, governed by a set of clinically-defined rules - is demonstrated for complex three dose-level nasopharynx plans. Three strategies were investigated: comparing VMAT vs. IMRT for standard plan creation, parotid sparing, and dose escalation.

An important component of Publication 2 was that the delivery constraints were relaxed during VMAT optimisation, such that they have a low bearing on the plans. This assumed that the linac is capable of efficient, accurate delivery for complex treatments. The efficiency of VMAT delivery is considered in detail in Publication 3, which involves the development of a realistic linac emulator. For a set of prostate and head and neck plans, the software emulator is used to investigate the impact of leaf speed, jaw speed, and dose rate on VMAT delivery efficiency. Furthermore, the impact of continuously variable dose rate is investigated. Following the commercial availability of CVDR for the Elekta system, Publication 4 then experimentally investigates the effects of CVDR and BDR on beam stability, MLC positioning accuracy and overall plan dosimetry.

Both Publications 3 and 4 discussed the potential for ideally-efficient VMAT delivery, even for complex treatment plans. However, this delivery time benefit is currently offset by an increased burden of pre-treatment plan QC on the linac. Publication 5 addresses this point, and investigates the development of a Monte Carlo-based verification system for VMAT. The intention of this system is to incorporate knowledge of realistic linac motion into accurate calculations of dose, such that a full dynamic calculation (i.e. delivery between control points) can be performed. As such, it differs from other VMAT Monte Carlo systems which have previously focussed on simulating static control points [102], or retrospectively reproducing the motion from log files [103]. This model is assessed through comparison to measurements on the linac and is incorporated into an automated plan verification system, allowing direct Monte Carlo calculation scheduling from a treatment planning system export.

Publication 6 investigates an area in which VMAT may offer a benefit over IMRT for image guided radiotherapy. This publication investigates how workflow may be maximised by allowing for patient imaging during delivery, rather than before or after the treatment. A novel strategy for scatter correction is introduced, and image quality is assessed using both phantom and patient measurements.

Four of these papers have been published in academic journals (Publications 1, 3, 4, and 6), while two are currently in the peer-review process (2 and 5). Prior to each presented paper, a description of the author's contribution is given. A general discussion is given in section 3, in which the outcomes of each of the publications are considered. Additional work undertaken as part of this thesis, and proposed future investigations, are also discussed in section 3.

2. PUBLICATIONS

2.1. Publication 1

A VMAT planning solution for prostate patients using a commercial treatment planning system

Published in Physics in Medicine and Biology, 2010, vol. 55, pp. N395-N404

Authors:

CJ Boylan

C Golby

CG Rowbottom

Author Contributions

Hypothesis:

I proposed the hypothesis that statically-created IMRT segments could be used to generate VMAT plans of similar quality to the existing treatment method.

Methodology:

I developed the planning solution, including determining the optimum control point spacing and the strategy for the production of the static MLC segments. The external scripting software was written by a computer scientist in the department. I designed the experiments to test the VMAT planning solution. Myself and CG took the dosimetric verification, resilience and repeatability measurements.

Analysis:

I performed all of the analysis and wrote the manuscript, which was approved with minor modifications by the other authors.

10 pages

Phys. Med. Biol. **55** (2010) N395–N404 doi:10.1088/0031-9155/55/14/N01

NOTE

A VMAT planning solution for prostate patients using a commercial treatment planning system

C J Boylan, C Golby and C G Rowbottom

North Western Medical Physics, The Christie NHS Foundation Trust, Wilmslow Road, Manchester M20 4BX, UK

E-mail: Christopher.Boylan@physics.cr.man.ac.uk

Received 23 December 2009, in final form 15 June 2010
Published 5 July 2010
Online at stacks.iop.org/PMB/55/N395

Abstract

Volumetric modulated arc therapy (VMAT) is a rotational delivery technique which offers the potential of improved dose distributions and shorter treatment times when compared to fixed-beam intensity-modulated radiation therapy (IMRT). This note describes the use of an existing treatment planning system (Philips Pinnacle^3 v.8.0), supplemented by in-house software, to produce a single-arc VMAT prostate plan. While a number of planning systems for the Elekta VMAT platform are commercially available, the use of an in-house solution has allowed more detailed investigations of VMAT planning, as well as greater control over the optimization process. The solution presented here begins with a static step-and-shoot IMRT approach to provide initial segment shapes, which are then modified and sequenced into 60 equally spaced control points in a 360° arc. Dose–volume histogram comparisons demonstrate that this VMAT planning method offers multiple dose level target coverage comparable to that from a standard IMRT approach. The VMAT plans also show superior sparing of critical structures such as the rectum and bladder. Delivery times are reduced with the VMAT method, and the results of dosimetric verification, resilience and repeatability tests indicate that the solution is robust.

(Some figures in this article are in colour only in the electronic version)

1. Introduction

Volumetric modulated arc therapy (VMAT) offers the potential to deliver intensity-modulated dose distributions comparable to or better than those produced by conventional intensity-modulated radiation therapy (IMRT) treatments, in a shorter delivery time (Palma *et al* 2008, Shaffer *et al* 2010, Rao *et al* 2010). As described by Otto (2008), the technique involves varying a linear accelerator's dose rate, field shape and gantry speed in an arc to produce the desired dose distribution. The Elekta VMAT solution (Elekta Ltd, Crawley, UK) which

is considered in this note has been successfully commissioned by this centre and has been found by others to be a robust method for delivering conformal radiotherapy (Bedford and Warrington 2009).

In IMRT treatment planning, inverse-planned solutions are commonplace. However, VMAT provides a more complex problem for the optimization algorithm. There are a large number of parameters to be optimized, and a variety of machine limitations which must be taken into account. The maximum leaf speed, jaw speed and gantry speed affect the efficiency of VMAT delivery and the dosimetric quality of the plans. Furthermore, the Elekta VMAT system chooses from a discrete set of dose rates in order to deliver the desired dose. For example, a nominal maximum dose rate of 600 MU min^{-1} yields dose rate bins of 600 MU min^{-1}, 300 MU min^{-1}, 150 MU min^{-1}, 75 MU min^{-1}, 37 MU min^{-1} and 18 MU min^{-1}. Ideally these constraints should be considered as part of the inverse optimization, such that the resultant plan is capable of being delivered accurately and efficiently.

There are a number of planning solutions available for Elekta VMAT, including the SmartArc module for the Pinnacle^3 v.9.0 treatment planning system (Philips Medical Systems, WI, USA). SmartArc uses an optimization algorithm described by Bzdusek *et al* (2009), and although the clinical version of the software has only recently been released, it has been shown to produce VMAT plans of equivalent quality to IMRT for certain sites (Guckenberger *et al* 2009, Bertelsen *et al* 2010). Other VMAT planning methods have been proposed by Bedford (2009), Cao *et al* (2009) and Matuszak *et al* (2010)—all of which implement aspects of the earlier Pinnacle v.8.0 planning system.

While the initial results from SmartArc appear promising, 'in-house' planning methods currently allow for more detailed investigations of VMAT planning, providing more flexibility and control over the optimization process, and include the ability to adjust control point parameters (such as leaf positions and weighting) after the optimization process has finished (not currently possible with SmartArc).

This note describes the commissioning of a VMAT planning solution for prostate patients, using Pinnacle v.8.0 and software developed in-house. The solution, which delivers multiple dose level distributions comparable to IMRT, produces a single 360° arc which can be delivered in a short time and to a high degree of dosimetric accuracy. Dynamic machine constraints are considered in the in-house software, such that the resultant plan is deliverable and efficient. Comparisons are made with step-and-shoot IMRT by evaluating dose–volume parameters and conformity to the Conventional or Hypofractionated High dose Intensity-modulated radiotherapy for Prostate cancer (CHHIP) trial protocol (Khoo and Dearnaley 2008). The results of dosimetric verification using a three-dimensional detector array are described, and the repeatability and resilience of delivery are investigated.

2. Methods

2.1. Treatment planning process

2.1.1. Plan setup and prescription. The treatment planning system used was Pinnacle^3 v.8.0m, with the direct machine parameter optimization (DMPO) module for IMRT. Prostate patients were CT scanned in a supine position according to a standard protocol with 5 mm axial slice width. The organs at risk (OARs) were contoured (rectum, bladder, femoral heads, urethral bulb and bowel) and target volumes were expanded according to the CHHIP protocol. For the pre-clinical commissioning patients described in this note and the clinical VMAT patients, the dose prescribed was 57 Gy in 19 fractions (equivalent to group 3 of the CHHIP

Table 1. Selection of some of the relevant dosimetric quality parameters outlined in the CHHIP trial protocol.

CHHIP trial parameter	Constraint (%)
PTV1 min	76
PTV2 min	91
PTV3 min	95
PTV3 median	99–101
Bladder V68 max	50
Bladder V81 max	25
Bladder V100 max	5
Rectum V68 max	60
Rectum V81 max	50
Rectum V88 max	30
Rectum V95 max	15
Rectum V100 max	3

trial). The trial also specified three dose levels to three different planning target volumes (PTVs); these are detailed along with other specifications in table 1.

2.1.2. Initial optimization. 15 equi-spaced 8 MV beams (24° apart) were added to the plan starting at a gantry angle of 192° and ending at 168°. A fixed collimator angle of 10° was applied to avoid excessive inter-leaf leakage dose to the patient from the rotational delivery technique. DMPO was then used to create a 'step-and-shoot' plan, using a class solution of dose constraints derived from a standard IMRT solution. The optimization parameters were set such that the maximum number of control points was 26 (i.e. each beam contains 1 or 2 control points after optimization). The minimum segment area was set to 20 cm^2 and segments with less than 6 MUs were removed at this stage. Low-weighted segments can result in a poorer quality delivery, due to the inherent instability of the linear accelerator at low dose rates. The dose calculation was performed with a collapsed-cone convolution algorithm, using a dose grid resolution of 0.3 cm. Over 25 iterations, DMPO produced control points similar to those shown in figure 1.

2.1.3. External sequencing of control points. At this stage there were 15 equi-spaced beams each with one to two control points. A Java application was developed in-house which interrogated the Pinnacle file system and modified the plan, dividing each beam containing two control points into two separate beams containing one control point each. Optimizing 15 fluence maps with a coarse gantry angle spacing and then re-sequencing the control points into an arc reduced the computation time considerably compared to optimizing 26 fluence maps initially (this is a similar principle to the one employed by Bzdusek *et al* (2009)). The two new beams were shifted 6° in either direction, such that the spacing was 12° between the beams. The individual weighting of each control point, and hence the number of monitor units, was retained. For the beams that contained a single control point at the end of the DMPO optimization, the beam was split into two identical control points, shifted 6° in either direction, and the half the MUs from the original control point were given to each new beam. At the end of this process the arc contained 30 equi-spaced beams, from gantry angle 186° to 174°.

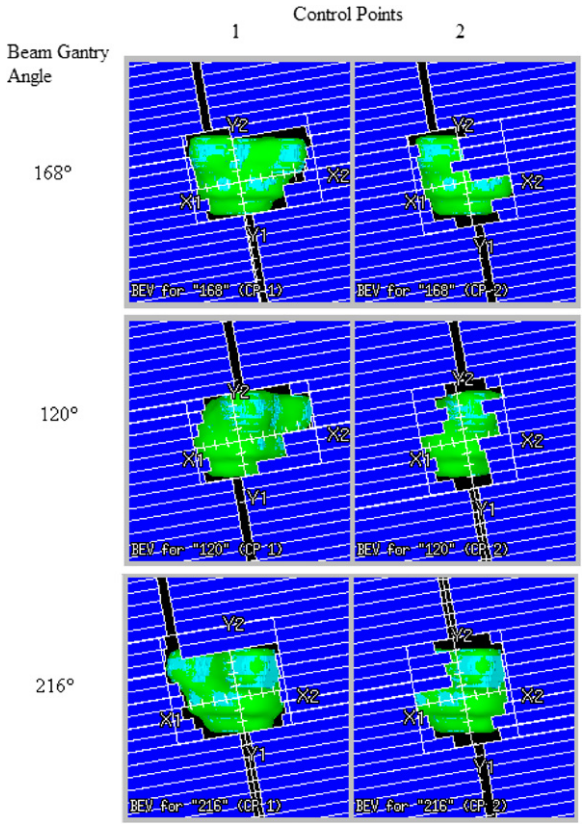

Figure 1. The two control points produced by DMPO for an example prostate patient for 3 of the 15 beams.

As there may be large differences in shape between each pair of control points, the amount of leaf motion between each of the newly created beams was minimized. In order to achieve this, the in-house software used a linear search (employing a 'greedy' algorithm) to determine the most efficient order of each pair of control points. The algorithm examined the leaf and jaw positions between adjacent control points, and ordered them such that leaf and jaw motion was minimized. In doing this, limitations of the VMAT delivery (i.e. maximum leaf and jaw travel per degree) were taken into account within the software to help to improve the efficiency of the resultant plan. The speed of delivery of a VMAT plan is determined by the dose rates selected by the linear accelerator, which is in turn determined by the difference between the positions of the leaves, jaws and gantry of adjacent control points. Minimizing leaf motion between the available control points ensures that the dose rate bins selected by the linac control system are as high as possible.

2.1.4. Interpolation of control points. Due to the continuous delivery of VMAT plans, initial testing indicated that the 30-beam step-and-shoot plan did not lead to a delivered dose distribution which matched the planning system prediction. Further investigation demonstrated that the coarse representation of 30 equi-spaced beams was not an adequate approximation to the continuous arc delivery employed by VMAT with a high degree of modulation between control points in the arc. Other authors have discussed the control point sampling required

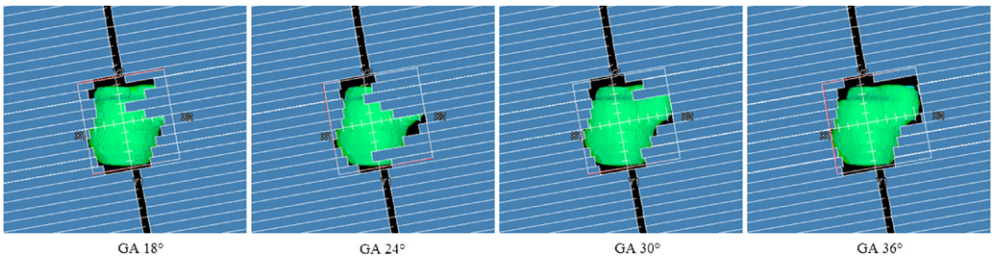

Figure 2. An example of four consecutive control points produced by the VMAT planning solution. Leaves outside of the field have been adjusted so that they remain stationary throughout the arc.

for accurate dosimetry (Otto 2008, Webb and McQuaid 2009, Feygelman *et al* 2010), and adequate results using 4 or 6° spacings for prostate cases have been demonstrated (Bzdusek *et al* (2009) and Cao *et al* (2009), respectively). Therefore, a series of interpolated beams were added midway between each existing beam, taking an average of the leaf and jaw positions between adjacent control points. This was done again using the in-house software, and a plan with 60 equi-spaced beams with 6° between each control point was produced. Monitor units were distributed such that half the MUs from the next control point in the arc were assigned to the interpolated beam.

2.1.5. Re-optimization and final dose calculation. After the control points were 'split' and interpolated, a further optimization step was required to refine the multi-leaf collimator (MLC) positions and beam weights and ensure that the dose distribution was clinically acceptable. This was achieved by running DMPO with the same parameters as the initial optimization, but using the 60 control points as the starting point for the optimization. The DMPO optimization process then made small changes to both the leaf positions and segment weights to minimize the overall cost function. The maximum number of iterations was set to ten and the final dose calculation was performed.

At this stage, steps were taken to ensure that the delivery was as efficient as possible. Due to the 10° collimator twist, the superior–inferior (Y) jaws were inspected and altered if the high dose region extended outside of the PTV. Following the final re-optimization and dose calculation it was found that leaves outside of the treatment field were required to move a significant amount between control points. This unnecessary motion increased the delivery time, as the gantry speed and dose rate had to be reduced to wait for the out-of-field leaf motion to finish. It was also found that these plans resulted in poorer dosimetric verification results. Therefore, leaf motion outside of the field was minimized on Pinnacle prior to export and delivery. Figure 2 shows an example of four adjacent control points after sequencing.

The approved plans were exported in DicomRT plan format to a record-and-verify system (MOSAIQ). MOSAIQ converts the exported files into RTP format, which are simple text files containing the plan details including the beam parameters and monitor units. At this stage, the RTP file consisted of 60 discrete beams each containing one control point. In order for MOSAIQ and the linear accelerator control system to recognize and deliver the plan as a VMAT treatment, the RTP file had to be reformatted to contain one beam with 60 control points with the gantry angle changing in each. This was achieved with a further piece of software, Arc Converter (William Beaumont Hospital, MI, USA), which was modified and tested in-house. The plans were then imported into MOSAIQ and could be delivered as VMAT prescriptions.

2.2. Pre-clinical testing and verification

Commissioning for the VMAT planning solution consisted of creating plans as described above on five randomly chosen prostate patients previously treated with IMRT. Dose–volume statistics were recorded for the IMRT and VMAT plans, along with CHHIP trial parameters.

Dosimetric verification was performed on the five patient plans using a three-dimensional detector array (Delta^4, Scandidos, Sweden). The Delta^4 has been demonstrated to be an appropriate device for the verification of VMAT treatments (Bedford *et al* 2009). Gamma analysis was performed at the 3%/3 mm level, within the 20% isodose.

The resilience of delivery was also investigated using one of the five patient plans as a reference plan. Using the Delta^4, the dosimetric effects of delivery under non-ideal scenarios were studied. These scenarios were: (a) interruption of the beam mid-treatment, (b) termination of the beam with completion on a partial beam, (c) simulated communication failure (i.e. manually disconnecting the MOSAIQ system from the linac control system mid-treatment) with completion on a partial beam, (d) termination of the beam on a symmetry error (i.e. manually changing the beam symmetry mid-treatment) with completion on a partial beam and (e) deliveries separated by a time frame of greater than 3 months.

Finally, the effects of symmetry and flatness on dosimetric repeatability were investigated. The reference plan was delivered to the Delta^4 with the symmetry of the treatment beam adjusted to be $\pm 5\%$ in both the gun-target (GT) and transverse (AB) directions. 5% asymmetry is an extreme test which lies beyond the clinical tolerance of the linear accelerator.

3. Results

3.1. Comparison to IMRT plans

A dose–volume histogram (DVH) comparison between the VMAT and IMRT plans for one of the commissioning patients is shown in figure 3. Target volume coverage (PTV1, PTV2 and PTV3) is equivalent for both techniques, demonstrating the ability of the VMAT solution to produce multiple dose level distributions. The VMAT plans offer superior avoidance of critical structures such as the rectum and bladder, which receive a lower volume of low to intermediate dose when compared to IMRT. The femoral heads receive a higher volume of low dose in the VMAT plan, although at around 15 Gy the histograms cross over and the VMAT plan is superior to the IMRT plan. In the example shown, dose to the bowel is higher in the VMAT plan, but at the CHHIP dose level of 38.76 Gy the absolute difference in irradiated volume between the VMAT and IMRT plans is 0.3 cc.

CHHIP parameters for all five patients are shown in figures 4(a)–(c). Again, target volume coverage is similar between the two techniques. OAR constraints are met by both techniques, with the VMAT plans performing better at the low to intermediate dose range for the rectum and bladder. The whole body volume receiving 20 Gy or more is lower for VMAT than for IMRT, indicating better conformality in the high dose region. As with many rotational delivery techniques, the volume of body receiving lower doses of >5 Gy and >10 Gy is higher for VMAT. However, the differences in low dose volumes between VMAT and IMRT are not significant; over the five patients the average V5 for the body (volume receiving 5 Gy or more) is 6558 (± 825) cc for VMAT compared to 5977 (± 632) cc for IMRT.

For the five patients examined as part of commissioning, the number of monitor units required for VMAT delivery is less than for step-and-shoot IMRT delivery (mean 521 MU versus 555 MU, respectively). Studies that compare SmartArc-produced single-arc VMAT

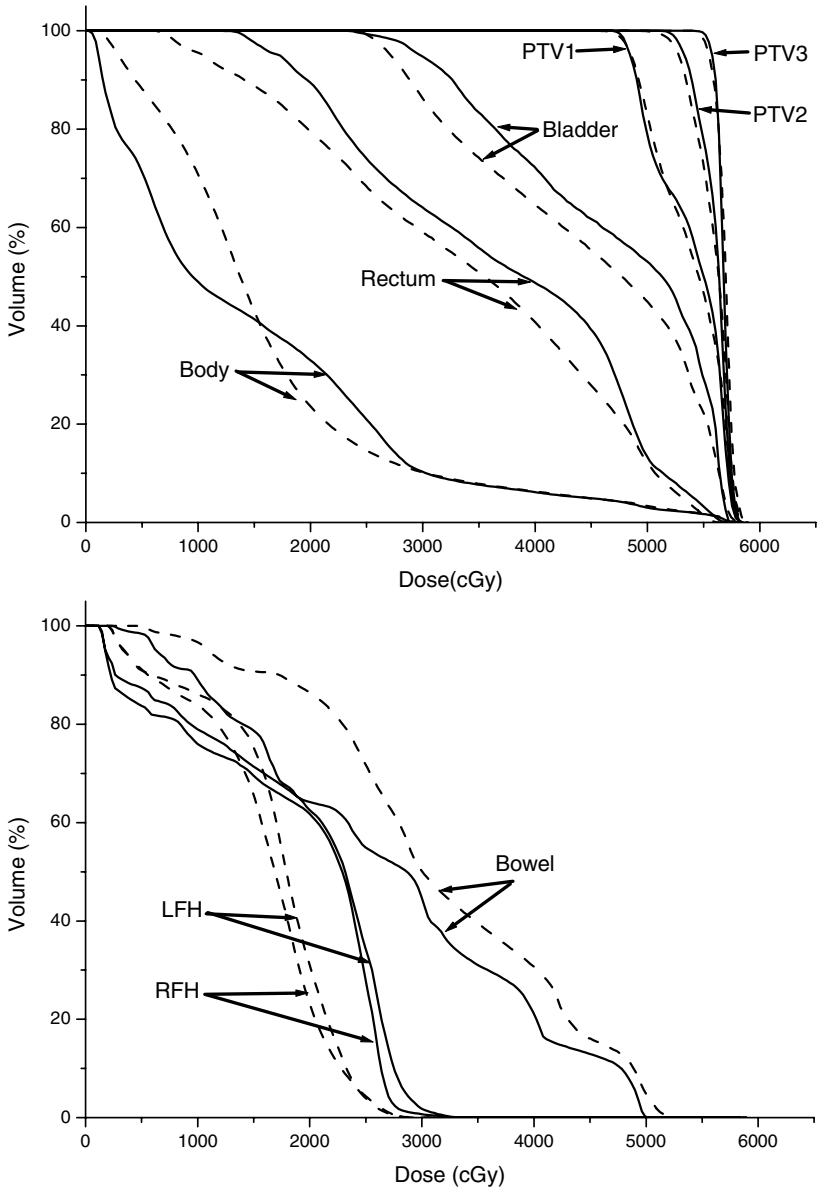

Figure 3. Dose–volume histogram (DVH) curves for one of the five prostate patients planned as part of the VMAT commissioning. The solid lines represent a standard IMRT approach, and the dashed lines represent the VMAT plan. LFH and RFH are the left and right femoral heads, respectively.

with step-and-shoot IMRT plans show a slightly larger reduction in monitor units (∼10% reported by Bertelsen *et al* (2010), Guckenberger *et al* (2009)). Much larger differences in MU (up to 50%) have been reported when comparing VMAT to sliding-window IMRT plans (Zhang *et al* 2009, Palma *et al* 2008), although this is mainly due to the nature of sliding-window delivery.

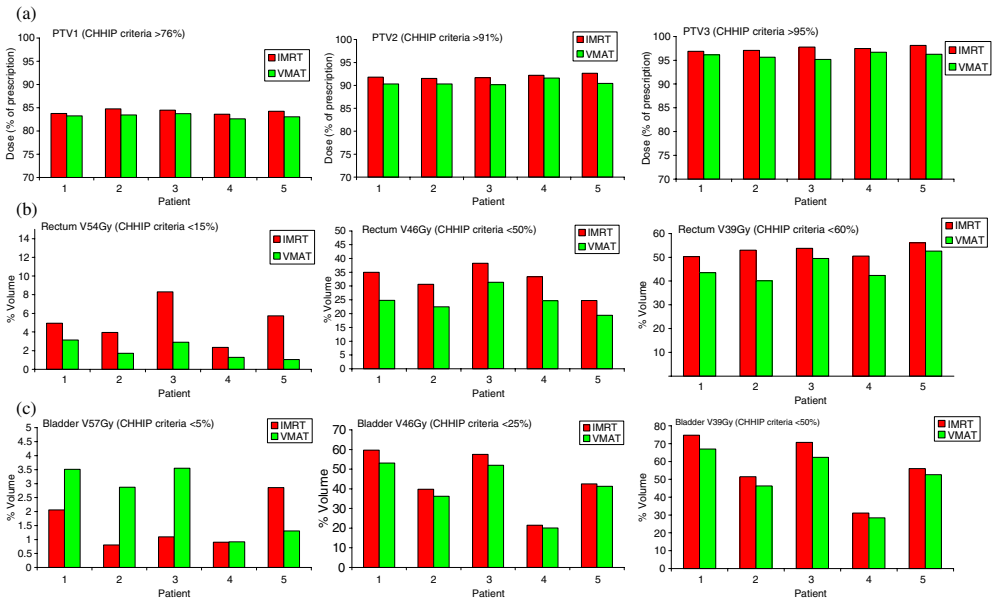

Figure 4. Comparison of CHHIP parameters for the IMRT and VMAT plans for the five commissioning patients. (a) Doses to the target volumes, which are similar between the two techniques. (b), (c) The volume of the rectum and bladder receiving three relevant CHHIP doses respectively (e.g. V54 Gy refers to the volume of the OAR receiving 54 Gy of the prescription dose).

3.2. Verification

All commissioned plans were transferred to the linear accelerator and delivered successfully. The mean delivery time was 2.5 min (range 2.3–2.9), and the clinical plans now being treated are of a similar duration. VMAT offers an improvement compared to the time taken to deliver five fixed IMRT fields, which for the commissioning patients examined here was on average 6.0 min (range 5.1–6.6).

All VMAT plans verified successfully on the Delta^4 with $>95\%$ of pixels within the 20% isodose having a gamma index of <1 at the $3\%/3$ mm level. This is a similar level of verification achieved when using the Delta^4 to verify IMRT prostate patients.

3.3. Delivery resilience

When using the original (uninterrupted) VMAT delivery as a reference on the Delta^4, no significant deviation was observed for any of the resilience scenarios studied with a 100% pass for a gamma analysis of $2\%/2$ mm within the 20% isodose being achieved in all cases. When a deliberate 5% asymmetry was introduced into the beam, the percentage gamma pass values remained at all times above 90% when compared to the reference plan delivered without any asymmetry.

4. Discussion

A VMAT planning solution has been developed using the Pinnacle v.8.0 treatment planning system supplemented by software developed in-house. Crucially, the VMAT solution

demonstrated here can produce a multiple dose level plan capable of being delivered in a single arc in a shorter treatment time than IMRT. DVH analysis shows that the planning process produces target volume coverage of equivalent quality to this centre's IMRT solution for prostate patients. The VMAT solution also achieves lower doses for the OARs. When considering the CHHIP trial parameters, which provide a good overall indication of dosimetric quality, the VMAT plans again performed well.

The process of beginning with static beams that contain several step-and-shoot segments and sequencing them into an arc has been demonstrated elsewhere (Cao *et al* 2009) and is the starting point of the Pinnacle SmartArc optimization (Bzdusek *et al* 2009). The method described here also orders each pair of control points so that leaf motion is minimized. Using an in-house solution has enabled this department to investigate in detail the planning and delivery aspects of VMAT, and has allowed a greater degree of flexibility and control over the optimization.

In terms of efficiency, the VMAT plans demonstrate a delivery time similar to that reported elsewhere for single-arc prostate treatments treated with an Elekta linac (Bedford 2009, Cao *et al* 2009). Shorter treatment times have been reported for the Varian RapidArc solution (∼1 min, Zhang *et al* (2009)), which is due in part to the availability of continuously variable dose rates for Varian linacs. Similarly, the modest reduction in monitor units required for VMAT plans compared to step-and-shoot IMRT plans is as expected. The literature suggests that SmartArc offers a potential ∼10% reduction in monitor units from step-and-shoot prostate IMRT, compared to ∼6% demonstrated here. Again, larger reductions have been reported comparing VMAT with sliding-window IMRT delivery.

The efficiency of VMAT delivery is strongly influenced by the planning strategy employed. While developing the prostate planning method outlined in this study, it was found that the speed and accuracy of VMAT delivery was improved when leaf motion outside of the treatment field was reduced. In practice, efforts can be made throughout the planning process to inspect the individual control points, identify any unnecessary leaf and jaw motion, and attempt to reduce it.

In summary, the VMAT planning solution demonstrated here delivers dose distributions of comparable quality to IMRT in a single arc and in a shorter treatment time. Delivery has been verified to a high degree of dosimetric accuracy and resilience tests also indicate that the solution is robust. This planning process has been introduced clinically for a subset of prostate patients at our institution.

Acknowledgments

The authors would like to thank Steve Smith for his assistance with the sequencing software, Dr Di Yan at the William Beaumont Hospital, Michigan, for help with the conversion into deliverable plans in MOSAIQ and the UK Elekta VMAT consortium.

References

Bedford J L 2009 Treatment planning for volumetric modulated arc therapy *Med. Phys.* **36** 5128–38

Bedford J L, Lee Y K, Wai P, South C P and Warrington A P 2009 Evaluation of the Delta^4 phantom for IMRT and VMAT verification *Phys. Med. Biol.* **54** N167–76

Bedford J L and Warrington A P 2009 Commissioning of volumetric modulated arc therapy (VMAT) *Int. J. Radiat. Oncol. Biol. Phys.* **73** 537–45

Bertelsen A, Hansen C R, Johansen J and Brink C 2010 Single arc volumetric modulated arc therapy of head and neck cancer *Radiother. Oncol.* **95** 142–8

Bzdusek K, Friberger H, Eriksson K, Hårdemark B, Robinson D and Kaus M 2009 Development and evaluation of an efficient approach to volumetric arc therapy planning *Med. Phys.* **36** 2328–39

Cao D, Afgan M K, Ye J, Chen F and Shepard D M 2009 A generalized inverse planning tool for volumetric-modulated arc therapy *Phys. Med. Biol.* **54** 6725–38

Feygelman V, Zhang G and Stevens C 2010 Initial dosimetric evaluation of SmartArc—a novel treatment planning module implemented in a multi-vendor delivery chain *J. Appl. Clin. Med. Phys.* **28** 3169

Guckenberger M, Richter A, Krieger T, Wilbert J, Baier K and Flentje M 2009 Is a single arc sufficient in volumetric-modulated arc therapy (VMAT) for complex-shaped target volumes? *Radiother. Oncol.* **93** 259–65

Khoo V S and Dearnaley D P 2008 Question of dose, fractionation and technique: ingredients for testing hypofractionation in prostate cancer—the CHHiP trial *Clin. Oncol.* **20** 12–4

Matuszak M M, Yan D, Grills I and Martinez A 2010 Clinical applications of volumetric modulated arc therapy *Int. J. Radiat. Oncol. Biol. Phys.* **77** 608–16

Otto K 2008 Volumetric modulated arc therapy: IMRT in a single arc *Med. Phys.* **35** 310–7

Palma D, Vollans E, James K, Nakano S, Moiseenko V, Shaffer R, McKenzie M, Morris J and Otto K 2008 Volumetric modulated arc therapy for delivery of prostate radiotherapy: comparison with intensity modulated radiotherapy and three-dimensional conformal therapy *Int. J. Radiat. Oncol. Biol. Phys.* **72** 996–1001

Rao M, Yang W, Chen F, Sheng K, Ye J, Mehta V, Shepard D and Cao D 2010 Comparison of Elekta VMAT with helical tomotherapy and fixed field IMRT: plan quality, delivery efficiency and accuracy *Med. Phys.* **37** 1350–9

Shaffer R, Nichol A M, Vollans E, Fong M, Nakano S, Moiseenko V, Schmuland M, Ma R, McKenzie M and Otto K 2010 A comparison of volumetric modulated arc therapy and conventional intensity-modulated radiotherapy for frontal and temporal high-grade gliomas *Int. J. Radiat. Oncol. Biol. Phys.* **76** 1177–84

Webb S and McQuaid D 2009 Some considerations concerning volume-modulated arc therapy: a stepping stone towards a general theory *Phys. Med. Biol.* **54** 4345–60

Zhang P, Happersett L, Hunt M, Jackson A, Zelefsky M and Mageras G 2009 Volumetric modulated arc therapy: planning and evaluation for prostate cancer cases *Int. J. Radiat. Oncol. Biol. Phys.* **76** 1456–62

(page intentionally blank)

2.2. Publication 2

A bias-free, automated planning tool for technique comparison in radiotherapy – application to nasopharyngeal carcinoma treatments

Accepted by Journal of Applied Clinical Medical Physics, July 2013

Authors:

CJ Boylan

CG Rowbottom

Author Contributions

Hypothesis:

I proposed that a planner-free methodology for the comparison of different radiotherapy techniques would allow a fairer evaluation of VMAT versus IMRT.

Methodology:

I proposed and developed the automated planning methodology, wrote the software and scripts within Pinnacle

Analysis:

I performed the comparison study, performed the data analysis and wrote the manuscript.

20 pages

Abstract

Background and Purpose

In this study a novel, user-independent automated planning technique was developed to objectively compare volumetric modulated arc therapy (VMAT) and intensity modulated radiotherapy (IMRT) for nasopharyngeal carcinoma planning, and to determine which technique offers a greater benefit for parotid-sparing and dose escalation strategies.

Material and Methods

Ten patients were investigated, with a standard prescription of three dose levels to the target volumes (70, 63 and 56 Gy), using a simultaneous integrated boost in 33 fractions. The automated tool was used to investigate three planning strategies with both IMRT and VMAT: clinically-acceptable plan creation, parotid dose sparing, and dose escalation.

Results

Clinically-acceptable plans were achieved for all patients using both techniques. For parotid-sparing, automated planning reduced the mean dose to a greater extent using VMAT rather than IMRT (17.0 Gy and 19.6 Gy, respectively, $p < 0.01$). For dose escalation to the mean of the main clinical target volume, neither VMAT nor IMRT offered a significant benefit over the other. The OAR-limiting prescriptions for VMAT ranged from 84 – 98 Gy, compared to 76 – 110 Gy for IMRT.

Conclusions

Employing a user-independent planning technique, it was possible to objectively compare VMAT and IMRT for NPC treatment strategies. VMAT offers a parotid-sparing improvement, but no significant benefit was observed for dose escalation to the primary target.

Introduction

Intensity modulated radiotherapy (IMRT) is an established treatment option for patients with nasophanyngeal carcinoma [1, 2]. The ability to deliver complex dose distributions has allowed the delivery of simultaneous integrated boosts (SIB) to gross tumour volumes (GTV) alongside lower dose levels to at-risk nodal regions [3]. With intensity-modulated plans it has been possible to reduce doses to nearby organs at risk (OAR). It has been shown that xerostomia rates in nasopharynx patients can be significantly reduced by lowering the mean parotid doses using IMRT [4]. Conversely, studies have indicated that IMRT (accompanied by advances in functional imaging) may be effective in improving the therapeutic ratio by escalating the dose to the tumour bed [5-7]. The concept of isotoxic planning – escalating the prescription dose until limiting organ at risk tolerances are met – has been demonstrated in a variety of clinical sites, including head and neck [8]. Such a technique is reliant on the ability to deliver highly complex, modulated treatment fields.

In many centres, the provision of IMRT has been accompanied (and in some cases supplanted) by the availability of volumetric modulated arc radiotherapy (VMAT). VMAT allows intensity-modulated dose distributions to be delivered by rotating the linear accelerator (linac) around the patient while dynamically varying the gantry speed, dose delivery rate, and multi-leaf collimator (MLC) positions [9]. This delivery method results in a much faster treatment time, and is often accompanied by a lower number of monitor units when compared to sliding window delivery of IMRT fields [10-12]. Several treatment planning studies have compared VMAT to IMRT for head and neck treatments [13-16], including nasopharyngeal carcinoma [17-19]. Generally, VMAT has been found to provide similar target coverage to 7-9 field IMRT, while maintaining an acceptable or lower dose to nearby organs at risk. Mean parotid doses have also been shown to be similar or slightly lower with VMAT [17, 19].

When moving to a new technique such as VMAT, planning studies are essential to determine any dosimetric differences to the established technique (in this case IMRT). However, there are a number of inherent problems and difficulties with computerized treatment planning studies. Foremost amongst these is the influence of the planner. VMAT, like IMRT, involves the selection of constraints for inverse optimization and an appropriate selection of constraints is essential to produce a plan which meets all of the treatment objectives. Many planning studies do not account for the possibility that the planner experience with each treatment technique may not be the same. Furthermore, there is the question of whether these studies are subject to expectation bias – that is, un-blinded treatment planning may lead to users inadvertently biasing their plans in favour of the new technique. Some planning studies attempt to reduce user bias by using identical optimization constraints for both techniques (in this case IMRT and VMAT). However, the optimization algorithms themselves may be quite different [20, 21], such that this may not allow a fair comparison.

Ideally, comparative planning studies should involve a user-independent selection of treatment planning parameters, with the plan aims clearly defined by the clinician from the outset. Automating the choice of optimization constraints would thus eliminate user-dependence of the results, and allow for a fair comparison between treatment methodologies. Such automated decision-making techniques have been demonstrated previously, such as the use of artificial neural networks to determine appropriate beam orientations [22]. More recently, an algorithm has been introduced which allows for multi-criteria optimization of beam orientations and profiles in IMRT [23, 24], and automated techniques have also been demonstrated for the selection of IMRT optimization structures [25].

The aim of this study is to compare dual-arc VMAT to 7-field IMRT for different NPC treatment strategies. Firstly, the ability of each technique to produce a plan which meets the clinical objectives is investigated. Secondly, the ability to reduce dose to the parotid glands is assessed, while maintaining all other planning

objectives. Finally, the ability of VMAT and IMRT to escalate dose to the tumour bed is investigated, keeping OAR doses within a tolerated range. In order to ensure a bias-free comparison between the techniques, a novel automated planning method has been developed which requires a set of dosimetric aims and planning rules, defined *a-priori* and identical for both planning methods. This system works within the environment of a commercial treatment planning system, such that the planning system's own direct aperture optimization is provided with a set of automatically-generated optimization constraints. The comparison is made over ten NPC patients, with the aim of objectively quantifying any benefit from rotational radiotherapy.

Methods and Materials

Patients and treatment protocol

Ten nasopharyngeal carcinoma patients who had been previously treated with IMRT were randomly selected for this study. The median age at diagnosis was 55 (range 27 – 64), with 2 patients originally presenting with stage I, 4 with stage II, and 4 with stage III disease. The standard treatment protocol employed was a three dose-level prescription delivered in 33 fractions using a simultaneous integrated boost (SIB). The primary clinical target volume (CTV1) received 70 Gy, the high-risk lymphatic nodes (CTV2) were treated with 63 Gy, and CTV3, representing the lower risk lymphatic involvement, received 56 Gy. Planning target volumes (PTVs) were created by adding a uniform margin of 3mm around each CTV. For optimization and evaluation, these PTVs were constrained to avoid areas within the build-up region (5mm from the body surface) – the modified volumes are labelled PTV_IMRT. All plan objectives, including maximum doses to organs at risk (OARs), are set out in Table 1.

Volume	Objective(s)	
PTV1_IMRT	95% volume > 95% prescription dose (66.5 Gy) 99% volume > 90% prescription dose (63 Gy)	Level 1
PTV2_IMRT	95% volume > 95% prescription dose (59.9 Gy) 99% volume > 90% prescription dose (56.7 Gy)	
PTV3_IMRT	95% volume > 95% prescription dose (53.2 Gy) 99% volume > 90% prescription dose (50.4 Gy)	
Whole Body	Maximum 77 Gy	
Spinal cord PRV	Maximum 50 Gy	Level 2
Brainstem PRV	Maximum 60 Gy	
Optic chiasm and optic nerves	Maximum 55 Gy	
Cochleae	Maximum mean 40 Gy (target < 35 Gy)	Level 3
Parotids	Maximum mean 26 Gy	
Larynx	Maximum mean 50 Gy (target < 45 Gy)	
Oral cavity	Maximum mean 60 Gy (target < 55 Gy)	
Eyes	Maximum 45 Gy (target < 40 Gy)	

Table 1. Nasophanrynx target and OAR evaluation objectives. The spinal cord and brainstem tolerances are given for the planning reference volume (PRV), which includes a margin of 0.5 cm around the OAR.

The treatment planning system used was Pinnacle 9.0 (Philips Medical Systems, Madison, USA). For the IMRT plans, 7 equi-spaced coplanar beams were set, with the treatment isocentre in the centre of CTV1. The linac used for planning was an Elekta Synergy with a 1 cm MLCi head for step-and-shoot IMRT delivery. Pinnacle's direct machine parameter optimization (DMPO) method was used [26], with the maximum number of control points (i.e. MLC segments) set to 100. The minimum segment area was set to 4 cm^2 and the minimum segment MUs was set to 2. This was done to allow for a high complexity of treatment plan.

Pinnacle's SmartArc optimization module was used to produce the VMAT plans [21]. A dual arc strategy was employed, with the gantry rotating from 182º to 178º and vice versa. The collimator angle for each arc was set to 10º in order to reduce the cumulative contribution of inter-leaf leakage. A control point spacing of 4º was used, such that 90 control points per arc were available for optimization. The aim of this study was to compare the ability of IMRT and VMAT to produce highly

complex treatment plans, neglecting any potential delivery time benefit with VMAT. As such, the constraints within SmartArc which aim to improve delivery efficiency (for example, maximum treatment time, and maximum leaf motion per gantry degree) were relaxed so as to have a low bearing on the optimization (Table 2).

IMRT	VMAT
7 co-planar beams (gantry angles 205º, 255º, 305º, 0º, 50º, 105º, 155º)	2 arcs (clockwise and anticlockwise, 182º to 178º)
Minimum segment area 4 cm^2	4º control point spacing
Minimum MU per segment 2	Maximum delivery time 300 s
Maximum number of segments 100	Leaf motion unconstrained between control points
Final dose calculation: Adaptive collapsed cone convolution	Final dose calculation: Adaptive collapsed cone convolution

Table 2. Planning parameters used for optimization.

Automated planning tool

A software tool has been developed which automatically adds and modifies optimization constraints based on the progress of the plan, through regular comparison to the plan objectives. The software, which follows a process shown schematically in Figure 1, was written using the Pinnacle scripting code alongside a Java application.

The software works by dividing the plan objectives into levels of importance. Initially, a set of optimization constraints are added which only aim to cover the target volumes (level 1). The plan is then optimized (using DMPO or SmartArc, as described above) and the dose is calculated. The current set of optimization constraints is then replaced by the evaluation objectives (Table 1). The evaluation objectives are a set of parameters that, if met, would likely result in a clinically acceptable plan. Optimization constraints are used to drive the optimization such that the clinical requirements are met, and are generally not the same as the evaluation objectives. By recalculating the cost function of each evaluation

objective, it is possible to determine which are passing or failing. If any evaluation objectives are not met at the current level, the software follows a set of pre-defined rules to generate a new set of optimization constraints. The new constraints are then loaded and the optimization restarts. This process repeats until all of the evaluation objectives are met for this level.

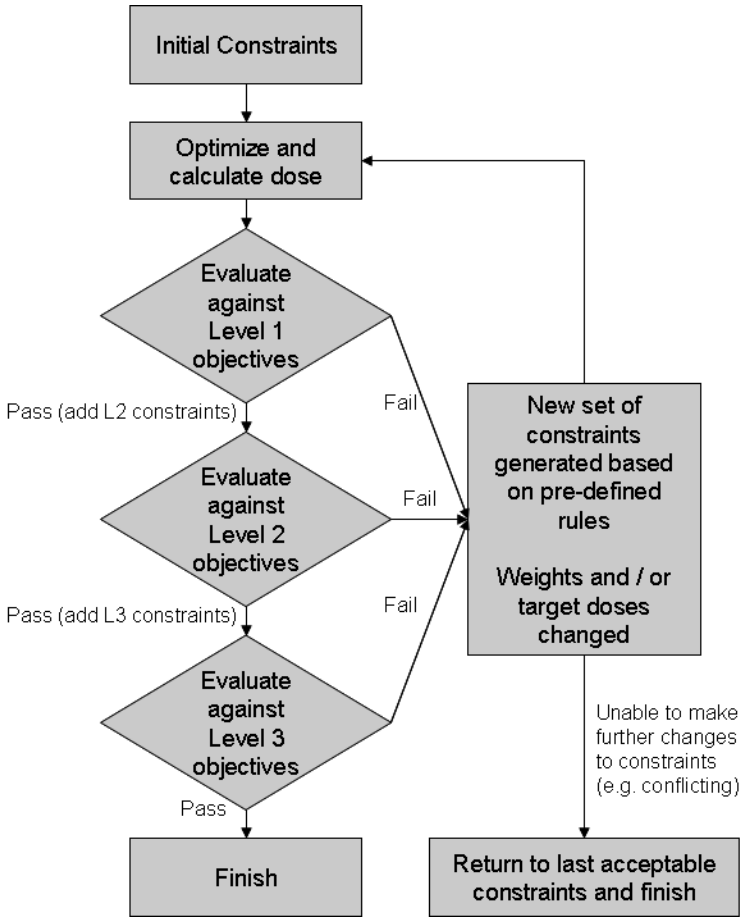

Figure 1. Flowchart describing the automated planning process employed.

Within Pinnacle, constraints can be modified by adjusting their weighting factor or, if this is not possible, their target dose. For example, if the minimum PTV1_IMRT objective is not being met (99% of the volume should receive at least 63 Gy), then the corresponding optimization constraint will be adjusted initially by increasing the weighting on a scale from 1-100. If the objective is still not met, the minimum dose constraint will then be increased in 1 Gy steps (i.e. 64 Gy, 65 Gy, 66 Gy…) until the evaluation objective is met.

Once the target coverage level passes, a second set of constraints are added to optimize serial-like organs at risk (level 2). Again, the plan is optimized and then compared to the evaluation objectives to determine any failures. This time, if any of the level 1 objectives fail, then those constraint modifications are made ahead of any failures in level 2. This ensures that the higher priority objectives are always worked on ahead of lower importance objectives. This cycle of optimization, evaluation, and constraint modification is repeated until all of the level 1 and 2 objectives are passed.

Following this, level 3 constraints are added, which consist of mainly parallel OARs where a lower dose is preferred, provided it is not at the expense of coverage to the targets (level 1) or exceeding the tolerance of serial OARs (level 2). Also included at this stage are dummy optimization structures, as shown in Figure 2. The purpose of these structures is to aid the conformity and homogeneity of dose to the target volumes. Again the software makes changes to the constraints based on order of priority. Ultimately, the software will continue making adjustments until one or more of the constraints can no longer be adjusted (for example, if it conflicts with another constraint). At this stage, the software 'rolls back' to the last set of constraints that met all of the plan evaluation objectives.

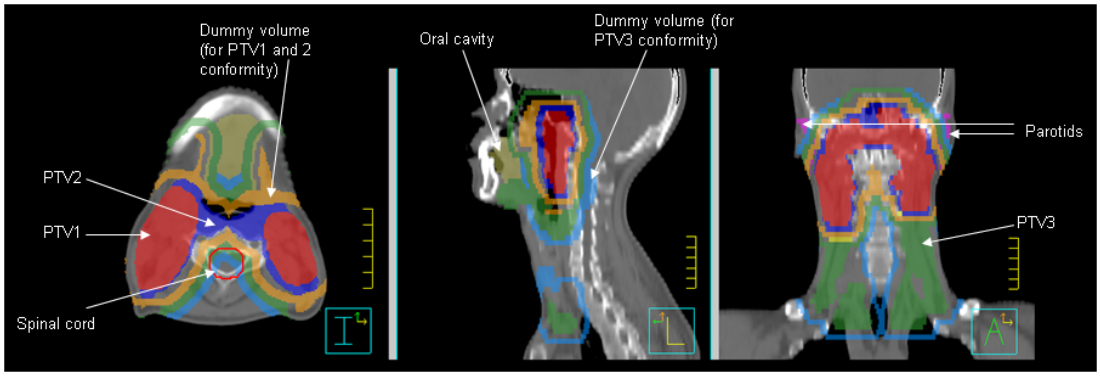

Figure 2. Typical regions of interest for one of the nasopharynx patients. Dummy structures were used alongside target volumes and organs at risk to aid optimization.

Experimental treatment strategies

The automated planning method was used to investigate three treatment strategies. Firstly, the ability of each technique to produce a standard, clinically-acceptable plan was investigated. The objectives as set out in Table 1 were used in this instance. The automated planning system followed the set of rules detailed above – i.e. target coverage, then serial OAR avoidance, followed by parallel OAR reduction as far as possible.

Secondly, a parotid-sparing strategy was investigated. For the purposes of this experiment, all other level 3 OARs were provided with tolerance doses which, once reached, were considered acceptable and no longer optimized. For example, the target mean cochlea dose was set to 35 Gy in the evaluation objectives. For the mean parotid OAR, no such target dose was set, so the system lowered the parotid dose until a higher level objective irreversibly failed.

The final treatment strategy to be investigated was the ability to escalate the prescription dose to the primary target volume (CTV1). In this case, the automated planning system maintained the level 2 and 3 OAR doses below the maximally tolerated levels set out in Table 1. Whenever all objectives were met, however, the system escalated the prescription (to the mean of CTV1) by 2 Gy. The process of optimization and dose escalation continued until one of the OAR doses exceed their tolerance, and it was not able to make further changes to the constraint parameters. The prescription dose at this stage is then taken as the limiting prescription dose for that patient.

All strategies were applied over the ten patients using both IMRT and VMAT. The modification rules and evaluation objectives were the same for both delivery methods. As the entire process was automated, there was no requirement for the planning to be supervised or interrupted. The total number of optimization steps was recorded along with the total planning time for each patient. Dose-volume

parameters were then retrieved for comparison between the IMRT and VMAT plans.

Statistics

All comparisons were made using a non-parametric Wilcoxon signed-rank test, where statistical significance was taken if $p < 0.05$. Where applicable mean values have been quoted with 1 standard deviation in parentheses.

Results

Standard Planning

Both VMAT and IMRT were capable of meeting the objectives set out in Table 1 to produce clinically-acceptable plans. The number of optimization cycles required (i.e. the number of times the constraints were modified and the optimization was restarted) to produce an acceptable VMAT plan was lower than that for IMRT (mean 36 steps compared to 50 for IMRT, $p < 0.05$). While the number of cycles was lower for VMAT, the total planning time was significantly longer at 7.0 hours compared to 1.8 hours for IMRT ($p < 0.01$), which was due to the increased time per SmartArc optimization.

The number of monitor units for the IMRT plans was 731.8 (± 62.5) MU compared to 642.2 (± 51.6) MU for the VMAT plans. For all 10 plans with both delivery techniques, the stopping point for the automated system was when the minimum PTV1_IMRT constraint exceeded the uniform dose constraint, resulting in a conflict and hence a rolling back to previously acceptable values. Figure 3 shows an averaged dose-volume histogram comparing VMAT and IMRT. Dosimetric results are given in Table 3. Heterogeneity index, defined as the ratio of the dose received by 5% and 95% of the volume, is also reported for each PTV. For all the target volumes, level 2 and level 3 OARs, no significant differences were identified between VMAT and IMRT ($p > 0.2$ for all objectives).

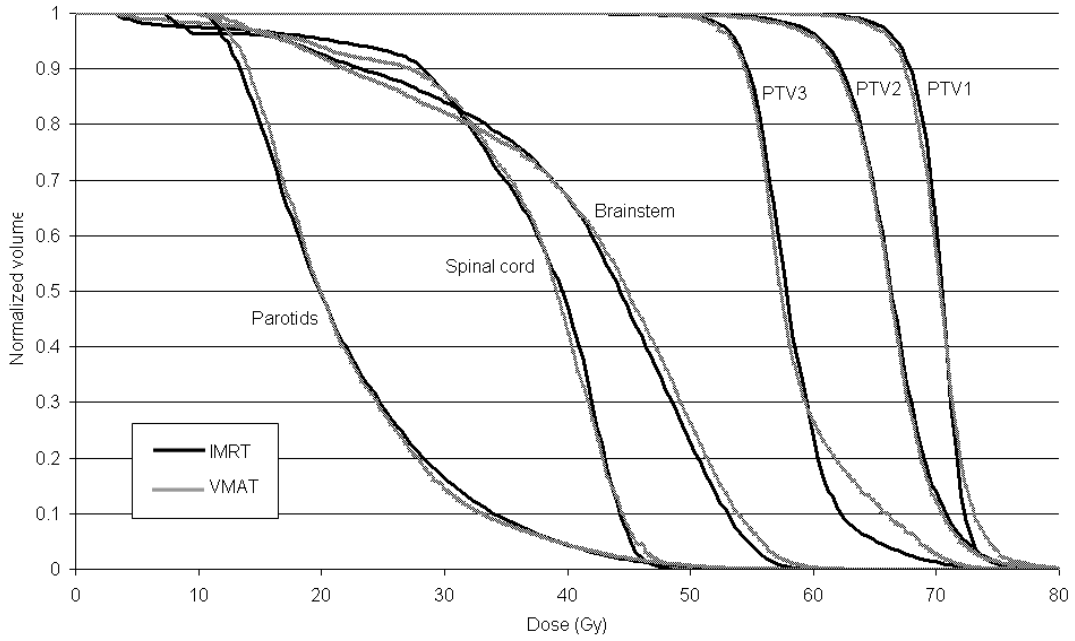

Figure 3. Averaged dose-volume histogram over all 10 nasopharynx patients, comparing the VMAT and IMRT automatically-generated solutions.

Volume		IMRT	VMAT
PTV1_IMRT	V95%	95.8 (± 1.3) %	97.1 (± 2.3) %
	V90%	99.3 (± 0.4) %	99.4 (± 0.2) %
	HI (D95/D5)	1.09 (± 0.03)	1.12 (± 0.02)
PTV2_IMRT	V95%	96.9 (± 0.5) %	97.6 (± 1.4) %
	V90%	99.0 (± 0.3) %	99.2 (± 0.7) %
	HI (D95/D5)	1.19 (± 0.05)	1.17 (± 0.03)
PTV3_IMRT	V95%	96.8 (± 1.2) %	97.4 (± 1.8) %
	V90%	99.2 (± 0.4) %	99.4 (± 0.6) %
	HI (D95/D5)	1.21 (± 0.09)	1.16 (± 0.08)
Spinal cord PRV		46.8 (± 0.7) Gy	47.4 (± 1.3) Gy
Brainstem PRV		56.6 (± 1.1) Gy	56.9 (± 3.6) Gy
Optic chiasm and optic nerves		45.5 (± 5.6) Gy	45.7 (± 3.8) Gy
Cochleae		39.3 (± 1.6) Gy	37.1 (± 2.9) Gy
Parotids		25.9 (± 3.2) Gy	26.8 (± 1.5) Gy
Larynx		48.3 (± 1.2) Gy	45.6 (± 4.3) Gy
Oral cavity		50.7 (± 1.6) Gy	48.9 (± 8.7) Gy
Eyes		29.7 (± 11.9) Gy	31.2 (± 9.7) Gy

Table 3. Dosimetric results for the standard VMAT and IMRT planning, averaged over the 10 patients. Standard deviation is shown within parentheses.

	Mean parotid dose (Gy)		
	IMRT	**VMAT**	**Δ (IMRT-VMAT)**
P1	19.4	19.1	0.3
P2	18.3	16.7	1.6
P3	13.9	13.8	0.1
P4	25.0	23.8	1.2
P5	20.6	15.5	5.0
P6	18.8	17.2	1.6
P7	23.4	21.5	1.9
P8	20.5	15.6	4.9
P9	19.1	13.1	5.9
P10	16.7	13.9	2.7
Average	**19.6**	**17.0**	**2.5**

Table 4. Lowest parotid doses achieved using IMRT and VMAT, while maintaining all other plan objectives.

Parotid Sparing

With the automated system adjusted to concentrate only on lowering the mean parotid dose, VMAT was found to be capable of a greater reduction than IMRT. All other objectives remained within the acceptable tolerances. The minimum parotid doses for each patient are displayed in Table 4. For the IMRT patients, the planning tool reduced the mean parotid dose to 19.6 Gy over the 10 patients (range 13.9 – 25.0 Gy). For the VMAT plans this figure was 17.0 Gy (13.1 – 23.8 Gy). The biggest reduction was observed in patient 8, whose mean parotid dose was reduced from 19.0 Gy with IMRT to 13.1 Gy with VMAT, a difference of 5.9 Gy. On average, the mean parotid dose was reduced by 2.5 Gy using VMAT compared to IMRT ($p < 0.01$). Figure 4 demonstrates how the dose-volume histogram changes over the automated planning process. For these plans, the mean number of MUs was 800.6 (± 87.0) for IMRT and 665.9 (± 72.1) for VMAT.

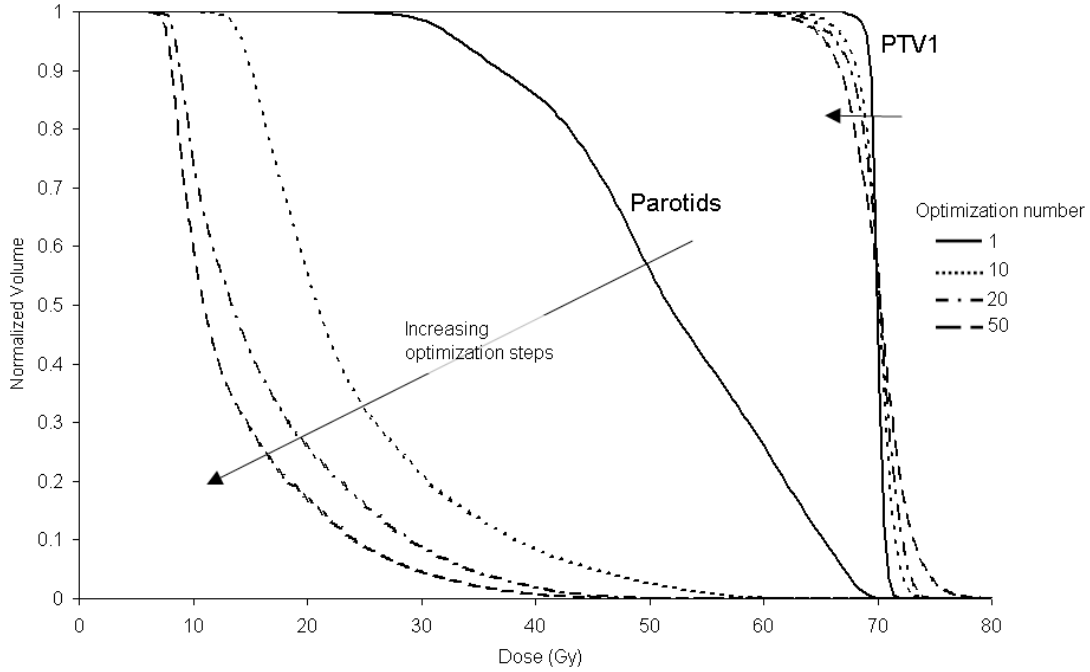

Figure 4. Example of the progress of the dose volume histograms over the course of the parotid dose optimization.

Dose Escalation

For the third strategy under investigation, dose escalation, all OARs were kept within their maximally tolerable doses set out in Table 1. The limiting prescription doses (prescribed to the mean of CTV1) are given for each patient in Table 5. On average, the system was able to escalate the dose to 91.6 (± 8.2) Gy for IMRT patients and 90.8 (± 5.8) Gy for VMAT patients. No statistically significant difference was observed between the ability of the two treatment techniques to escalate to a maximum limiting dose ($p > 0.5$ over the 10 patients). The stopping point for the automated system varied between patients – the most common limiting objective was the PTV2_IMRT prescription (5 patients), followed by the brain stem maximum dose (3 patients) and the spinal cord maximum dose (2 patients). These limiting objectives were the same using both the IMRT and VMAT planning techniques.

	Prescription dose (mean to CTV1 in Gy)		
	IMRT	**VMAT**	**Δ (IMRT-VMAT)**
P1	94.0	96.0	-2.0
P2	88.0	86.0	2.0
P3	102.0	84.0	18.0
P4	82.0	88.0	-6.0
P5	86.0	96.0	-10.0
P6	76.0	86.0	-10.0
P7	88.0	84.0	4.0
P8	92.0	92.0	0.0
P9	98.0	98.0	0.0
P10	110.0	98.0	12.0
Average	**91.6**	**90.8**	**0.8**

Table 5. Highest prescription dose achieved (using 2 Gy steps from the standard prescription of 70 Gy) to the mean of CTV1, maintaining all other objectives and OAR doses within tolerance. Shaded cells indicate the technique with the higher escalated dose.

Discussion

The value of arc radiotherapy in the clinic remains a popular topic of research, with many publications investigating the similarities and differences to static beam IMRT [10, 11, 13-16]. Many of these comparative studies demonstrate a significant improvement with VMAT in terms of the monitor unit efficiency and delivery time. If the delivery benefit is disregarded, however, it is more difficult to identify situations in which VMAT offers a dosimetric treatment benefit over IMRT. In this study, by attempting to remove planner bias, and by reducing the influence of VMAT's delivery constraints, it has been possible to more objectively compare these two treatment paradigms for nasopharyngeal patients.

For standard planning, the automated tool was able to produce plans which met the clinical objectives in all of the patients. As the system was provided with the same set of decision rules for both VMAT and IMRT, it is expected that the target coverage and serial OAR doses are similar for both techniques – the automated tool is designed to take these values to close to their tolerance. However, when the parotid doses were optimized, the VMAT plans were able to generate a significantly

lower mean dose before one of the higher-level objectives failed. The difference between the VMAT and IMRT mean parotid doses was 2.5 Gy on average. The QUANTEC project reviewed several dose-response studies for xerostomia and found that, for studies with long-term follow up (>12 months), the reduction in stimulated salivary flow rate was approximately 1.5% for every 1 Gy of mean dose received by the parotids [27]. Based on this, a reduction of 2.5 Gy could represent a 3.75% improvement in long-term salivary flow rate. It should be stressed, however, that this is highly patient-specific and will be influenced by other factors such as baseline function.

These results agree with previous comparisons between IMRT and VMAT, which have shown parotid doses to be either equivalent [11, 15], or slightly lower with VMAT [10, 13, 17, 18, 28]. Other planning studies also reported marginal improvements in target coverage with VMAT, although this was not observed in this study. One of the main differences between this planning study and others reported in the literature is the use of an automated system. The purpose of this was to ensure that the planning was independent of user experience with both techniques. Previously, some planning comparison studies have attempted to address user bias by using identical optimization constraints for both the techniques being investigated [29]. The use of identical optimization constraints, however, may not produce a fair comparison if the optimization algorithm itself is significantly different (as with the Pinnacle system).

While VMAT was found to provide a potential benefit for the reduction of parotid doses, no such benefit was determined for a dose escalation strategy. The automated system was able to produce plans which allowed substantive simultaneous boosts to the primary target volume (up to 110 Gy in one patient). However, the limiting prescriptions between the IMRT plans and VMAT plans showed significant variation – differences of up to 18 Gy between each technique. There were no trends suggesting whether IMRT or VMAT is a more suitable technique for dose escalation. One conclusion which can be drawn from this is that inter-patient variability is

larger than the difference between IMRT and VMAT planning. The large variation in results may suggest that certain aspects of patient geometry have a large impact on the ability to escalate dose. Work is now underway to determine whether the anatomical characteristics of the patient (such as target shape and proximity to nearby OARs) can be used to predict whether VMAT or IMRT is a better candidate for dose escalation. It should be noted that the clinical benefit of such dose escalation is beyond the scope of this paper. Consideration will need to be given to OARs other than those in Table 1. OARs such as the mandible, submandibular glands, temporal lobes, temporomandibular joint and brachial plexus may further limit the achievable escalated prescription dose.

While the automated planning tool described here can produce acceptable plans in Pinnacle unsupervised, there remain some limitations. Only the optimization constraints were automatically generated. As such, this system still required a planner-based choice of beam parameters (i.e. number of beams, number of arcs, collimator rotation and control point spacing) – although the parameters were identical for all patients. The length of time taken to create these plans means that the automated system may not currently be suitable for routine plan creation. Work is underway to develop strategies for speeding up the process, such as providing an initial 'rough' solution, or by varying the step sizes used between optimizations. Presently, the intention is to use this system to perform automated isotoxic planning – i.e. to generate individualized, dose-escalated plans. Further anticipated applications of the automated system include a) treatment technique comparisons, b) benchmarking of new planning software or c) development of class solutions for new clinical sites.

The automated plan methodology adopted here – i.e. the use of a set of rules to 'search' for appropriate optimization parameters within a commercial planning system – can be contrasted with other systems. In particular, the iCycle algorithm is an independent optimization system, guided by priority-assigned clinical objectives [23]. This system allows for a wide range of parameters to be optimized (including

beam and couch orientation), potentially making it a candidate for bias-free plan comparison studies. Another automated option has been proposed by Janssen *et al* [30]. This system creates a large number of IMRT and VMAT plans using a commercial planning system with a range of optimization constraints, forming a pareto front for a given set of objectives. By producing pareto fronts for both techniques, it is possible to determine which technique is optimal by comparing the fronts. As this system requires many hundreds of optimizations, the plans take a number of days to produce. Other studies have demonstrated the use of unsupervised learning systems for the creation of treatment plans [31, 32], determining IMRT beam angles [22], and identifying optimum patient position [33]. However, we have been unable to find previous studies demonstrating the use of a planner-free system to compare two techniques (e.g. VMAT and IMRT), within the environment of a commercial planning system.

Conclusion

An automated planning tool has been developed to perform a comparison study between 7-field IMRT and dual-arc VMAT. The system was able to generate clinically acceptable plans with both treatment techniques, and when given instructions to reduce mean parotid doses as far as possible it was found that the VMAT plans were capable of a significantly lower mean parotid dose compared to IMRT. This study indicates that VMAT offers a parotid-sparing benefit over IMRT in the treatment of nasopharyngeal carcinoma, which could lead to reduced xerostomia rates. Conversely, investigating a strategy of dose escalation to the primary target volume, VMAT and IMRT gave a large range of maximally tolerated doses, with no technique superior over all 10 patients.

Conflict of Interest Statement

This work was partly funded by an Elekta research grant.

References

1. J. C. Cheng, K. S. Chao, and D. Low. Comparison of intensity modulated radiation therapy (IMRT) treatment techniques for nasopharyngeal carcinoma. Int J Cancer 2001; 96(2):126-31.
2. Z. Taheri-Kadkhoda, N. Pettersson, T. Bjork-Eriksson, et al. Superiority of intensity-modulated radiotherapy over three-dimensional conformal radiotherapy combined with brachytherapy in nasopharyngeal carcinoma: a planning study. Br J Radiol 2008; 81(965):397-405.
3. E. Peponi, C. Glanzmann, G. Kunz, et al. Simultaneous integrated boost intensity-modulated radiotherapy (SIBIMRT) in nasopharyngeal cancer. Strahlenther Onkol 2010; 186(3):135-42.
4. M. K. Kam, S. F. Leung, B. Zee, et al. Prospective randomized study of intensity-modulated radiotherapy on salivary gland function in early-stage nasopharyngeal carcinoma patients. J Clin Oncol 2007; 25(31):4873-9.
5. J. Qian, L. Lee, W. Liu, et al. Dose reconstruction for volumetric modulated arc therapy (VMAT) using cone-beam CT and dynamic log files. Phys Med Biol 2010; 55(13):3597-610.
6. J. Belec, N. Ploquin, D. J. La Russa, et al. Position-probability-sampled Monte Carlo calculation of VMAT, 3DCRT, step-shoot IMRT, and helical tomotherapy dose distributions using BEAMnrc/DOSXYZnrc. Med Phys 2011; 38(2):948-60.
7. J. M. Moran, M. Dempsey, A. Eisbruch, et al. Safety considerations for IMRT: executive summary. Med Phys 2011; 38(9):5067-72.
8. A. Lauve, M. Morris, R. Schmidt-Ullrich, et al. Simultaneous integrated boost intensity-modulated radiotherapy for locally advanced head-and-neck squamous cell carcinomas: II--clinical results. Int J Radiat Oncol Biol Phys 2004; 60(2):374-87.
9. C. X. Yu and G. Tang. Intensity-modulated arc therapy: principles, technologies and clinical implementation. Phys Med Biol 2011; 56(5):R31-54.
10. A. Bertelsen, C. R. Hansen, J. Johansen, et al. Single Arc Volumetric Modulated Arc Therapy of head and neck cancer. Radiother Oncol 2010; 95(2):142-8.
11. M. Guckenberger, A. Richter, T. Krieger, et al. Is a single arc sufficient in volumetric-modulated arc therapy (VMAT) for complex-shaped target volumes? Radiother Oncol 2009; 93(2):259-65.
12. P. Zhang, L. Happersett, M. Hunt, et al. Volumetric modulated arc therapy: planning and evaluation for prostate cancer cases. Int J Radiat Oncol Biol Phys 2010; 76(5):1456-62.
13. E. Vanetti, A. Clivio, G. Nicolini, et al. Volumetric modulated arc radiotherapy for carcinomas of the oro-pharynx, hypo-pharynx and larynx: a treatment planning comparison with fixed field IMRT. Radiother Oncol 2009; 92(1):111-7.
14. J. Alvarez-Moret, F. Pohl, O. Koelbl, et al. Evaluation of volumetric modulated arc therapy (VMAT) with Oncentra MasterPlan(R) for the treatment of head and neck cancer. Radiat Oncol 2010; 5(110):110.

15. F. Stieler, D. Wolff, H. Schmid, et al. A comparison of several modulated radiotherapy techniques for head and neck cancer and dosimetric validation of VMAT. Radiother Oncol 2011; 101(3):388-93.
16. R. Wiehle, S. Knippen, A. L. Grosu, et al. VMAT and step-and-shoot IMRT in head and neck cancer: a comparative plan analysis Strahlenther Onkol 2011; 187(12):820-5.
17. M. Johnston, S. Clifford, R. Bromley, et al. Volumetric-modulated arc therapy in head and neck radiotherapy: a planning comparison using simultaneous integrated boost for nasopharynx and oropharynx carcinoma. Clin Oncol (R Coll Radiol) 2011; 23(8):503-11.
18. T. F. Lee, P. J. Chao, H. M. Ting, et al. Comparative analysis of SmartArc-based dual arc volumetric-modulated arc radiotherapy (VMAT) versus intensity-modulated radiotherapy (IMRT) for nasopharyngeal carcinoma. J Appl Clin Med Phys 2011; 12(4):3587.
19. S. H. Lu, J. C. Cheng, S. H. Kuo, et al. Volumetric modulated arc therapy for nasopharyngeal carcinoma: A dosimetric comparison with TomoTherapy and step-and-shoot IMRT. Radiother Oncol 2012; 9:9.
20. K. Otto. Volumetric modulated arc therapy: IMRT in a single gantry arc. Med Phys 2008; 35(1):310-7.
21. K. Bzdusek, H. Friberger, K. Eriksson, et al. Development and evaluation of an efficient approach to volumetric arc therapy planning. Med Phys 2009; 36(6):2328-39.
22. C. G. Rowbottom, S. Webb, and M. Oldham. Beam-orientation customization using an artificial neural network. Phys Med Biol 1999; 44(9):2251-62.
23. S. Breedveld, P. R. Storchi, P. W. Voet, et al. iCycle: Integrated, multicriterial beam angle, and profile optimization for generation of coplanar and noncoplanar IMRT plans. Med Phys 2012; 39(2):951-63.
24. L. Rossi, S. Breedveld, B. J. Heijmen, et al. On the beam direction search space in computerized non-coplanar beam angle optimization for IMRT-prostate SBRT. Phys Med Biol 2012; 57(17):5441-58.
25. I. Xhaferllari, E. Wong, K. Bzdusek, et al. Automated IMRT planning with regional optimization using planning scripts. J Appl Clin Med Phys 2013; 14(1):4052.
26. S. Jones and M. Williams. Clinical evaluation of direct aperture optimization when applied to head-and-neck IMRT. Med Dosim 2008; 33(1):86-92.
27. J. O. Deasy, V. Moiseenko, L. Marks, et al. Radiotherapy dose-volume effects on salivary gland function. Int J Radiat Oncol Biol Phys 2010; 76(3 Suppl):S58-63.
28. R. Wiehle, S. Knippen, A. L. Grosu, et al. VMAT and step-and-shoot IMRT in head and neck cancer: a comparative plan analysis. Strahlenther Onkol 2011; 187(12):820-5.
29. N. P. Nguyen, L. Smith-Raymond, V. Vinh-Hung, et al. Feasibility of Tomotherapy to spare the cochlea from excessive radiation in head and neck cancer. Oral Oncol 2011; 47(5):414-9.
30. T. Janssen, Z. van Kesteren, E. Damen, et al. Clinically relevant pareto fronts (Abstract). Radiother Oncol 2011; 99:S99.

31. F. Stieler, H. Yan, F. Lohr, et al. Development of a neuro-fuzzy technique for automated parameter optimization of inverse treatment planning. Radiat Oncol 2009; 4(39):39.
32. H. Yan, F. F. Yin, and C. Willett. Evaluation of an artificial intelligence guided inverse planning system: clinical case study. Radiother Oncol 2007; 83(1):76-85.
33. X. Zhao, D. Kong, G. Jozsef, et al. Automated beam placement for breast radiotherapy using a support vector machine based algorithm. Med Phys 2012; 39(5):2536-43.

(page intentionally blank)

2.3. Publication 3

The use of a realistic VMAT delivery emulator to optimize dynamic machine parameters for improved treatment efficiency

Published in Physics in Medicine and Biology, 2011, vol. 56, pp. 4119-4133

Authors:

CJ Boylan

CG Rowbottom

RI Mackay

Author Contributions

Hypothesis:

I developed the hypothesis that a software emulator could be used to investigate dynamic limitations of various linac components during VMAT delivery.

Methodology:

I wrote the VMAT emulator software, designed all of the experiments and took the measurements. The VMAT treatment plans were previously-treated clinical plans, produced by a number of different staff members (including myself).

Analysis:

I performed all of the analysis and wrote the manuscript, which was subject to minor changes from CGR, RIM and Elekta, to help with the clarity of the paper.

15 pages

Phys. Med. Biol. **56** (2011) 4119–4133 doi:10.1088/0031-9155/56/13/024

The use of a realistic VMAT delivery emulator to optimize dynamic machine parameters for improved treatment efficiency

C J Boylan[1,2], **C G Rowbottom**[1,2] **and R I Mackay**[1,2]

[1] North Western Medical Physics, The Christie NHS Foundation Trust, Wilmslow Road, Manchester M20 4BX, UK
[2] Manchester Academic Health Science Centre (MAHSC), Faculty of Medical and Human Sciences, University of Manchester, Manchester M13 9PL, UK

E-mail: Christopher.Boylan@physics.cr.man.ac.uk

Received 17 March 2011, in final form 6 May 2011
Published 21 June 2011
Online at stacks.iop.org/PMB/56/4119

Abstract
The delivery of volumetric modulated arc therapy (VMAT) requires the simultaneous movement of the linear accelerator gantry, multi-leaf collimators and jaws while the dose rate is varied. In this study, a VMAT delivery emulator was developed to accurately predict the characteristics of a given treatment plan, incorporating realistic parameters for gantry inertia and the variation in leaf speed with respect to gravity. The emulator was used to assess the impact of dynamic machine parameters on the delivery efficiency, using a set of prostate and head and neck VMAT plans. Initially, assuming a VMAT system with fixed dose rate bins, the allowable leaf and jaw speeds were increased and a significant improvement in treatment time and average dose rate was observed. The software was then adapted to simulate a VMAT system with continuously varying dose rate, and the increase in delivery efficiency was quantified, along with the impact of an increased leaf and jaw speed. Finally, a set of optimal dynamic machine parameters was derived assuming an idealized scenario in which the treatment is delivered in a single arc at constant maximum gantry speed.

(Some figures in this article are in colour only in the electronic version)

1. Introduction

In recent years there has been increasing interest in the use of dynamic arcs rather than static beams to deliver radical radiotherapy (Yu and Tang 2011). While commercial planning and delivery solutions for arc therapy are still relatively in their infancy, a number of studies have already demonstrated significantly reduced treatment times without compromising the dose distribution when compared to fixed-field intensity modulated radiotherapy (IMRT)

(Matuszak *et al* 2010, Palma *et al* 2008). Planning solutions for sites such as the prostate (Zhang *et al* 2010, Wolff *et al* 2009), head and neck (Bertelsen *et al* 2010, Vanetti *et al* 2009) and lung (McGrath *et al* 2010, Verbakel *et al* 2009) have been demonstrated, indicating that arc therapy may be able to at least complement the provision of IMRT in the radiotherapy department.

Volumetric modulated arc therapy (VMAT) refers to the delivery of dose using a conventional linear accelerator moving in an arc around the patient. The field shape, defined by multi-leaf collimators (MLCs) and jaws, is dynamically varied during the arc along with the dose rate and gantry speed to produce an intensity-modulated dose distribution (Otto 2008, Cao *et al* 2009). VMAT delivery often requires only one complete arc around the patient, although larger and more complex treatment sites may require more (Guckenberger *et al* 2009). A number of authors have reported a delivery time benefit of 50–100% compared with fixed field IMRT (Zhang *et al* 2010, Verbakel *et al* 2009, Shaffer *et al* 2009).

When formulating VMAT as a method of delivering IMRT in a single arc, Bortfeld and Webb (2009) describe both techniques as having compromises: standard IMRT can produce highly modulated fields, but from a coarse sampling of fixed gantry angles, whereas VMAT uses all gantry angles but has no instantaneous modulation. A further practical limitation of VMAT is that adjacent control points ('segments') around the arc must be achievable with the linear accelerator. That is, the linac control system must be able to move the MLCs, jaws and gantry, whilst modulating the dose rate, in order to deliver the correct dose. In theory, for finite leaf and jaw speeds, the linac should be able to deliver any control point provided it is able to reduce the gantry speed and dose rate low enough. Practically, however, very low dose rates are undesirable in VMAT delivery due to their impact on treatment time efficiency—widely reported as the most significant advantage of this technique. While good dosimetric results have been demonstrated on plans utilizing a large range of dose rates, adverse effects on the beam stability, flatness and symmetry have also been observed at very low rates (Bedford and Warrington 2009).

In order to ensure delivery efficiency, many planning systems for VMAT include delivery constraints within the optimization. The method described by Otto (2008), which is now part of the Varian RapidArc system, incorporates factors such as the maximum leaf speed and gantry speed into the optimization algorithm. These 'efficiency constraints' ensure that the dose rate on the machine is maximized for each control point. Similar constraints are used within the Philips Pinnacle^3 SmartArc system (Bzdusek *et al* 2009). SmartArc requires user-inputted values for maximum allowable leaf, jaw and gantry speed, as well as the minimum and maximum number of MUs per gantry angle degree. Users can also specify the maximum leaf travel per gantry degree, and can specify a maximum delivery time.

Successful dosimetric verification has been demonstrated with both RapidArc and SmartArc on Varian and Elekta linear accelerators (Rao *et al* 2010, Feygelman *et al* 2010). However, the impact of a linac's dynamic parameters (leaf, jaw, gantry speed and dose rate) on delivery efficiency has not yet been fully characterized. This paper considers this problem through the use of a realistic VMAT delivery emulator and a cohort of plans. Machine constraints were adjusted within the software and by modelling the delivery, their effect on treatment efficiency was investigated. Initially, the existing Elekta VMAT system, which uses fixed dose rate bins, was considered and the impact of adjustments to the leaf and jaw speed was assessed. The effect of continuously variable dose rate was then investigated to quantify the time advantage when using a larger number of dose rate bins. Finally, the emulator was used to model a scenario in which treatment is delivered in a single arc at constant gantry speed. This represents a fast and highly efficient method of delivery, limited only by the maximum allowable gantry speed of the linac.

2. Materials and methods

2.1. VMAT system

The VMAT system described in this paper consists of the Pinnacle^3 v.9.0 SmartArc planning module, and delivery with an Elekta Synergy linear accelerator (RTD v.6.0). Plans produced using SmartArc are exported to a record and verify system (MOSAIQ) via an 'RTP' file, which contains the instructions for the linac (gantry angle, MLC and jaw positions, and monitor units for each control point).

In order to achieve delivery of the control points, the linac is able to adjust the gantry speed and dose rate. Elekta linacs were previously only able to choose from a fixed set of dose rate bins, from the machine's maximum decreasing by a factor of 2 (e.g. 600 MU min^{-1}, 300 MU min^{-1}, 150 MU min^{-1}, 75 MU min^{-1} etc). The linac will preferentially deliver dose at the highest rate possible, but will step down to a lower bin to satisfy the maximum gantry speed constraint, and to allow time for the leaves and jaws to reach their next position. The latest release of the Elekta VMAT system allows for continuously variable dose rate. Rather than the 4–5 fixed bins described above, the linac will be able to choose from 255 dose rates up to the maximum.

2.2. Development of emulator

Software was written in Java which emulates the VMAT delivery. There are three main stages for the emulator: firstly, the software reads in a VMAT RTP file and builds a set of instructions for the linac. Secondly, the software interprets the instructions and calculates the appropriate gantry speed and dose rate bin for each control point (figure 1).

Initially, the gantry speed required to deliver the prescribed number of MU at the maximum dose rate is calculated. If this gantry speed exceeds the physical limit of the machine, then the dose rate is dropped to a lower bin and the speed is recalculated:

$$\Omega_G = \frac{\Delta^\circ}{(\Delta \mathrm{MU}/\mathrm{DR}_{\mathrm{bin}})} \leqslant \Omega_G^{\max} \tag{1}$$

where Ω_G is the gantry speed ($^\circ$/s), Δ° is the gantry angle interval, ΔMU is the control point MU, $\mathrm{DR}_{\mathrm{bin}}$ is the current dose rate bin (MU/s) and $\Omega_G^{\max}$ is the maximum allowable gantry speed. Using this value for gantry speed, the time for the control point can be calculated ($t_{\mathrm{cp}} = \Delta^\circ/\Omega_G$). The emulator then calculates how much time the leaves and jaws require to travel from their previous position to the current control point:

$$t_{\mathrm{lim}} = \max\left(\frac{\Delta L_{\max}}{v_{\mathrm{leaf}}}, \frac{\Delta J_{\max}}{v_{\mathrm{jaw}}}\right) \tag{2}$$

where t_{lim} is the limiting time, $\Delta L_{\max}$ and $\Delta J_{\max}$ are the maximum leaf and jaw distances to travel (cm) and v_{leaf} and v_{jaw} are the nominal leaf and jaw speeds (in cm s^{-1}). The emulator evaluates t_{cp} and t_{lim}, and ensures that the condition $t_{\mathrm{cp}} > t_{\mathrm{lim}}$ is met by stepping down to a lower dose rate bin if necessary and re-evaluating equation (1). This process is repeated over all the control points, and the emulator outputs the gantry speed and dose rate.

In the final module of the software, the target gantry speeds and dose rate bins are sent to a realistic machine emulator, which models the actual delivery characteristics. The model includes

(a) the acceleration or deceleration of the gantry between control points;
(b) the variation in the *actual* leaf speed with respect to gravity around the arc;
(c) the acceleration and deceleration of the leaves.

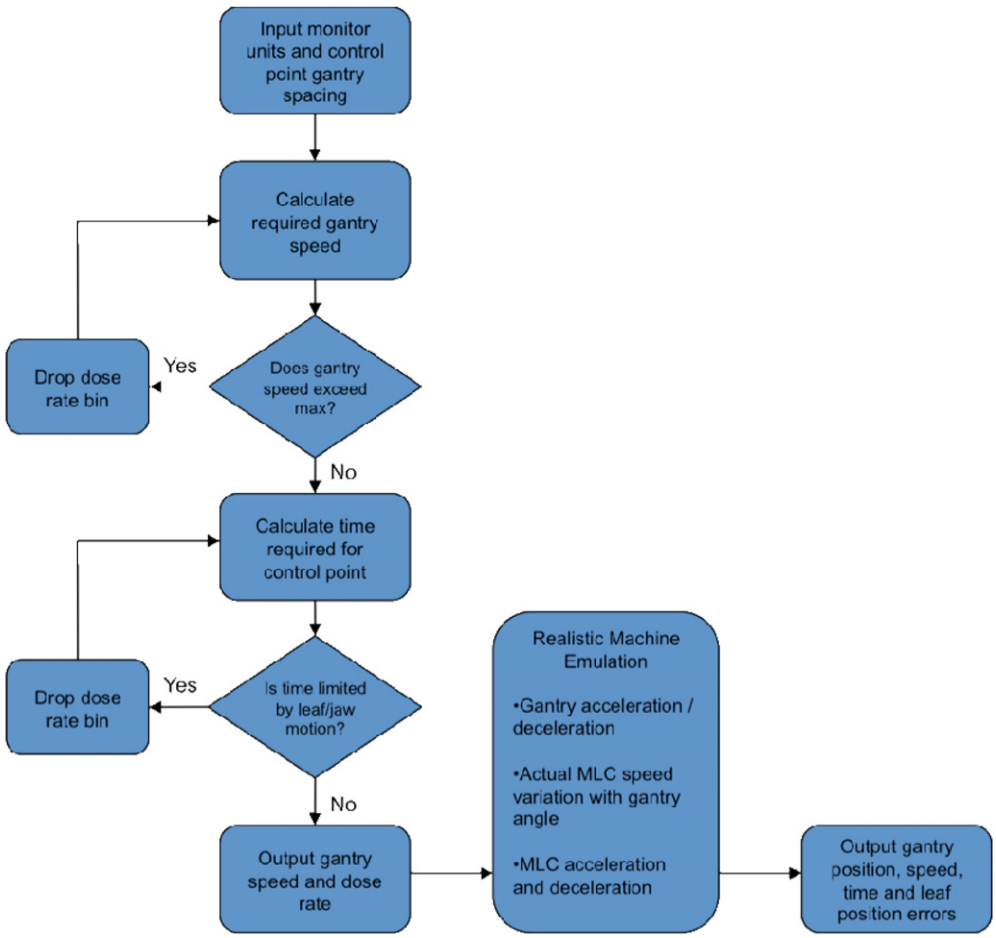

Figure 1. Flowchart describing the emulator software process.

The models for each of these parameters were derived from actual machine measurements using the Elekta 'service graphing' function. This is a software tool accessible within the service mode of the linac, which allows various machine parameters (e.g. gantry position) to be logged during delivery, with a time resolution of 250 ms. The log files can later be interrogated to determine the machine state at a given point in the delivery, including the dose rate, leaf, jaw and gantry speed.

Details of the model parameters are found in table 1. The nominal maximum leaf and jaw speeds (v_{leaf} and v_{jaw}) are intentionally set lower than the actual speeds (which vary from 2.2 to 3.4 cm s^{-1} depending on the MLC orientation with respect to gravity). This is done to ensure that t_{cp} is very often greater than t_{lim}, i.e. the MLCs reach their required position well before the gantry has reached the next control point. The emulator software monitors the number and magnitude of leaf-positioning problems, and records an 'error' if a leaf is >1 mm from its intended position at the end of the control point. The emulator ultimately outputs the gantry speed and dose rate bin for each control point, along with the delivery time.

The emulator was assessed for accuracy by comparing its output to the actual machine deliveries for a range of patient plans. For these commissioning tests, the

Table 1. List of values used to model the linear accelerator within the emulator. The values were derived from experiments on an Elekta Synergy linac. It was estimated that each of the simplifying assumptions will contribute $\ll$0.1 s error in the calculation of each control point.

Machine parameter	Magnitude in the emulator model	Notes and model assumptions
Gantry acceleration	1.8–3.2° s^{-2}	Varies with gantry angle
Gantry deceleration	3.4–4.3° s^{-2}	Varies with gantry angle
Leaf speed	2.2–3.2 cm s^{-1}	Varies with gantry angle. At gantry angle 0°, assume opposing leaf banks are identical, and speed of leaf motion inwards = speed outwards
Leaf acceleration and deceleration time	0.25 s	Assume acceleration = deceleration, and no impact due to MLC orientation with respect to gravity

software constants were set to the same as the actual linac control system: $v_{\text{leaf}} = 2.0$ cm s^{-1}, $v_{\text{jaw}} = 2.0$ cm $s^{-1}\Omega_G^{\max} = 6°$ s^{-1} (this gantry speed limit is specified by the IEC standard 60601). The realistic machine parameters were set as in table 1. A 'benchmarking' cohort of ten Pinnacle-planned VMAT treatments (five prostate and five head and neck) was delivered on an Elekta Synergy linac and live parameters were recorded using the service graphing function. The measured parameters were then plotted against the emulator's output and the overall treatment time was compared.

2.3. Virtual experiments

Experiments using the emulator were performed with a separate 'experimental' cohort of ten VMAT plans (again consisting of five prostate and five head and neck). The single-arc prostate plans (mean 474 MU) were created according to the local three-dose level protocol for VMAT. The head and neck plans (all oropharynx treatments with mean 533 MU) were produced on patients previously treated with IMRT. They consisted of two counter-rotating arcs, and aimed to achieve a dose distribution which approximates the IMRT solution. Each plan was exported to MOSAIQ and the RTP file was retrieved for input into the emulator.

2.3.1. Effect of dynamic parameters on treatment efficiency. The first experiment examined the impact of leaf and jaw speed on the duration and efficiency of delivery. Maximum gantry speed was held constant for these tests, and dose rate bins were fixed at 600, 300, 150 and 75 MU min^{-1}. For each plan, the emulator was run for various values of v_{leaf} and v_{jaw}, with the corresponding 'real' parameter adjusted by the same margin. Delivery time was calculated, as well as the percentage of monitor units delivered in each dose rate bin.

2.3.2. Effect of continuously variable dose rate. A modification to the software allowed the emulator to select a much greater range of dose rates, as in the recent Elekta VMAT update. 255 dose rate bins were allowable, up to the maximum dose rate (in this case set at

600 MU min^{-1}). The treatment time reduction was quantified for the plan cohort, and again the impact of increasing v_{leaf} and v_{jaw} was investigated.

2.3.3. Determining 'ideal' machine parameters. The minimum possible delivery time for a single 360° arc is 60 s (based on the IEC-defined maximum gantry speed of 6° s^{-1}). If $\Omega_G^{\max}$ is set to 6° s^{-1} in equation (1), then for each control point

$$\text{DR} = \frac{\Delta\text{MU}}{(\Delta^\circ/6)}. \tag{3}$$

This requires a continuous range of deliverable dose rates in order to maintain constant gantry speed (as ΔMU is a continuous variable). It can therefore be seen that, in order to satisfy the requirement $t_{\text{cp}} > t_{\text{lim}}$

$$v_{\text{leaf}} > \frac{\Delta L_{\max}}{(\Delta^\circ/6)} \quad \text{and} \quad v_{\text{jaw}} > \frac{\Delta J_{\max}}{(\Delta^\circ/6)} \tag{4}$$

which is true for both leaf motion and jaw motion. For the cohort of five prostate and five head and neck plans, these parameters (maximum dose rate, leaf speed and jaw speed) were calculated in order to achieve the required maximal delivery time. The effect of increasing the number of bins from 255 to 1023 was also assessed.

3. Results

3.1. Commissioning results

When compared to actual deliveries on the linac, the emulator produced realistic results. A typical comparison is shown in figure 2(a), demonstrating that the emulator selects the appropriate dose rate bins as the treatment progresses. Over five prostate VMAT plans, the emulator treatment time differed from the actual time by an average of –1.5 s (±1.4 s 1SD) for each beam. For the head and neck patients, the difference was –3.9 s (±1.2 s) per arc. Figure 2(b) shows a comparison between the emulator and the actual machine when gantry position is plotted against time. The complete data of timing comparisons are shown in table 2. Mean delivery time, as determined by the emulator, was 116.1 s for the prostates and 239.9 s for the dual-arc head and neck patients.

3.2. Virtual experiments

3.2.1. Effect of dynamic parameters on treatment efficiency. For the single-arc prostate treatments, the effect of increasing the allowable leaf speed is shown in figure 3. A leaf speed increase from 2.0 to 3.0 cm s^{-1} reduced the delivery time by an average of 21.0 s. Beyond 3.0 cm s^{-1} there was no significant time reduction. Figures 3(b) and (c) demonstrate how with an increased leaf speed the linac was able to select higher dose rate bins for delivery. The mean dose rate was increased from 294 MU min^{-1} at 2.0 cm s^{-1} to 351 MU min^{-1} at 3.0 cm s^{-1}. The number of monitor units delivered in the top dose rate bin increased by an average of 13.8%, and the histogram also shows a reduction in the number of MUs delivered in the lower dose rate bins.

For the head and neck plans, an increase in maximum leaf speed of 2.0–3.0 cm s^{-1} reduced the average delivery time by 37 s for the first arc and 42 s for the second arc. Figure 4(a) shows that this time improvement was due to the linear accelerator being able to select 150 MU min^{-1} rather than 75 MU min^{-1}. The histogram of MUs delivered in each dose bin shows a significant positive shift with increased leaf speed (figure 4(b)).

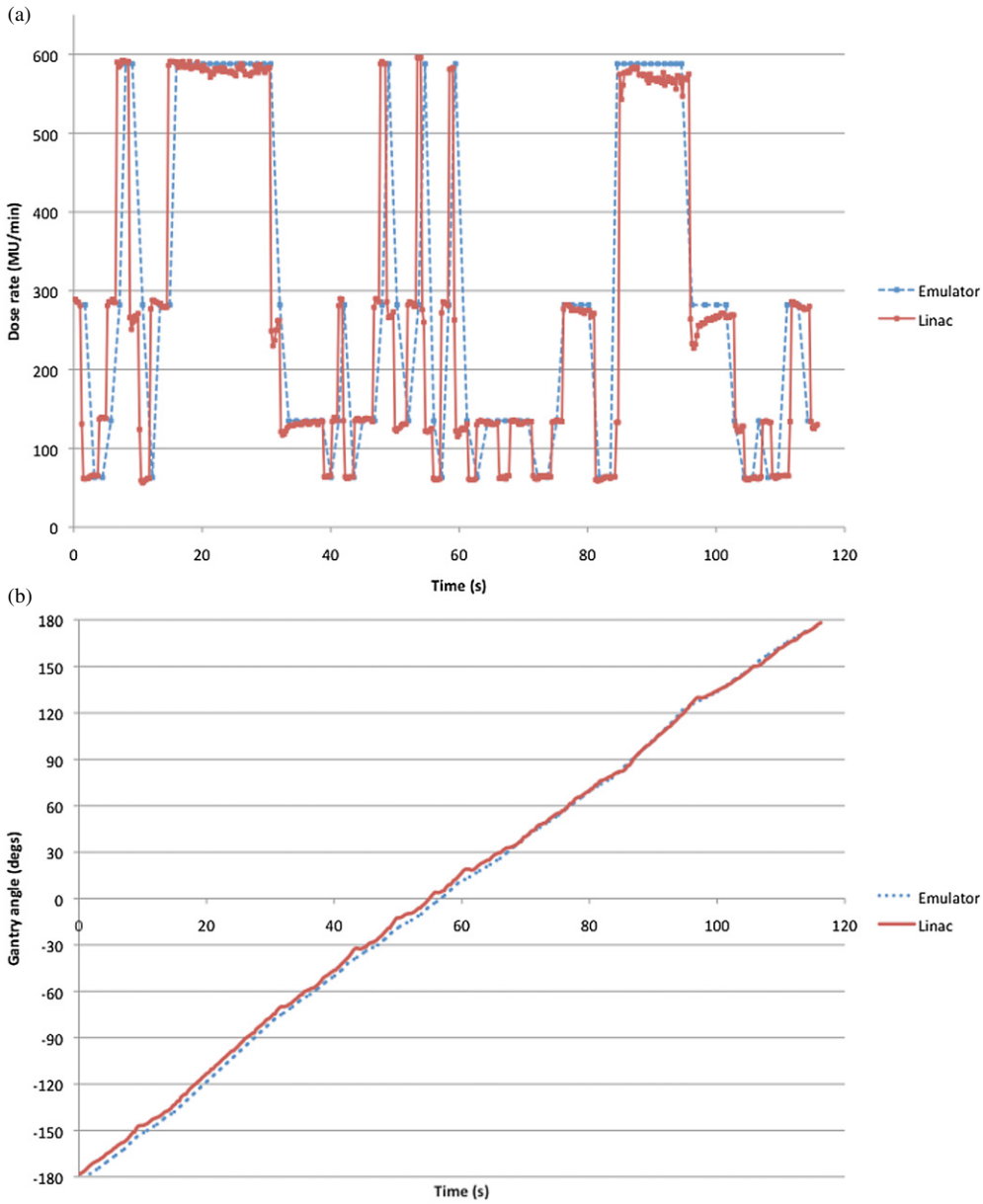

Figure 2. (a) Comparison of the emulator-predicted dose rate against time versus the measured dose rate on the machine, for a typical protate plan. (b) For the same plan, a comparison of the gantry position with time demonstrating the agreements between the emulator and the linac measurements.

The mean dose rate increased from 144 to 199 MU min^{-1}, while the number of MUs being delivered in the lowest bin (75 MU min^{-1}) was reduced by 25%.

When assessing the impact of leaf speed changes on the realistic delivery parameters, no leaf-positioning errors were recorded when increasing the nominal leaf speed from 2.0 to 3.0 cm s^{-1}, provided the actual leaf speed increases by the same amount. Furthermore,

Table 2. Comparison of the total delivery times between the linac and the emulator for the cohort of benchmarking plans.

Prostate	Emulator time (s)	Linac time (s)
1	113.4	117.3
2	114.3	115.8
3	116.7	117.5
4	113.4	114.5
5	122.5	122.8
Mean	116.1	117.6
Head and Neck		
1	125.9 + 123.4	129.5 + 125.5
2	114.3 + 104.9	120.3 + 108.3
3	125.6 + 121.2	130.0 + 126.5
4	122.5 + 115.6	126.8 + 119.0
5	124.4 + 121.5	128.8 + 123.8
Mean	122.5 + 117.3	127.1 + 120.6

the estimated leaf acceleration/deceleration time of 0.25 s needs to be maintained if leaf-positioning errors are to be avoided.

In contrast to leaf speed, the maximum jaw speed was not a limiting factor in any of the plans considered in this study. The magnitude of jaw position changes between control points was small compared to leaf position changes, and so when evaluating equation (2) the limiting leaf travel time was always greater than the limiting jaw travel time. Increasing jaw speed had no effect on any of the plans, and so no data are presented.

3.2.2. Effect of continuously variable dose rate. With 255 dose rate bins, the treatment time was significantly reduced when using the parameters of $v_{\text{leaf}} = 2.0$ cm s^{-1}, $v_{\text{jaw}} = 2.0$ cm s^{-1} $\Omega_G^{\max} = 6^\circ$ s^{-1}. Figure 5 shows how the linac was able to select a much higher range of dose rates. For the five prostate patients, the average reduction in delivery time was 31.7 s and the average dose rate increased from 294 to 376 MU min^{-1}. For the head and neck patients, the delivery time advantage was 43 s per arc compared to the standard binned dose rate system, representing a 35% reduction in overall treatment time.

Increasing the maximum leaf speed with continuously variable dose rate had a similar effect of reducing the delivery time and increasing the average dose rate. Figure 5(b) shows that the reduction in delivery time peaks at a leaf speed of 3.0 cm s^{-1}, where the time benefit was $\sim$13 s compared to 2.0 cm s^{-1}. The average dose rate also increased from 376 to 436 MU min^{-1}. For head and neck patients, increasing to 3.0 cm s^{-1} reduced each arc time by 19 s and increased the average dose rate from 202 to 262 MU min^{-1}.

With such a significant decrease in the time per control point, leaf-positioning errors were observed if the acceleration/deceleration time was kept at 0.25 s. On average, each delivery had 8.8 control points where at least one leaf was >1 mm from its intended position by the time the gantry reached its next position. Reducing the MLC acceleration/deceleration time to 0.2 s reduced the number of errors to zero in all the plans.

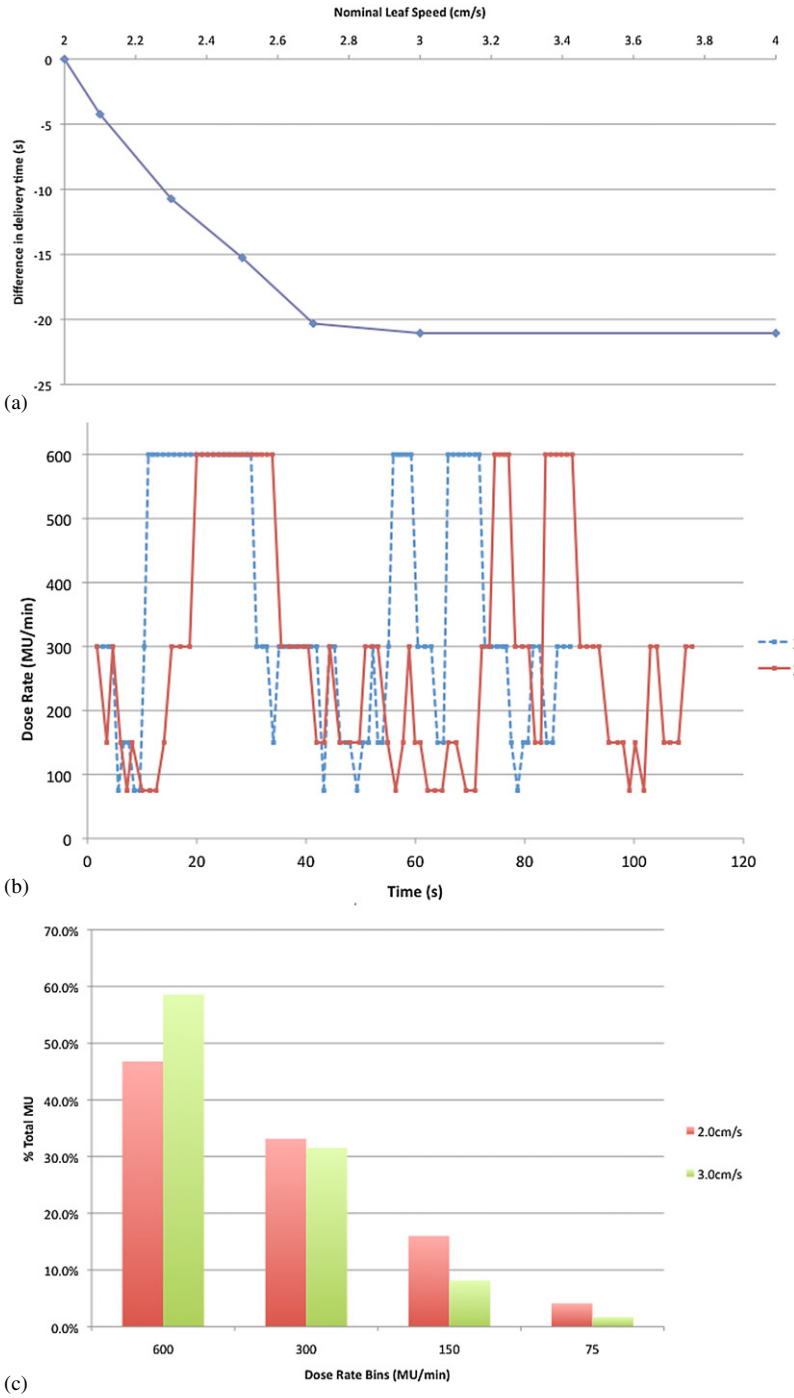

Figure 3. Increasing the nominal leaf speed from 2.0 to 3.0 cm s^{-1} for the prostate patients: (a) averaged over all patients, the maximum time advantage is 21 s, (b) comparing the selection of dose rate bins over a typical treatment (prostate patient 3), (c) demonstrating that, with a higher nominal leaf speed, the linac preferentially selects higher dose rate bins.

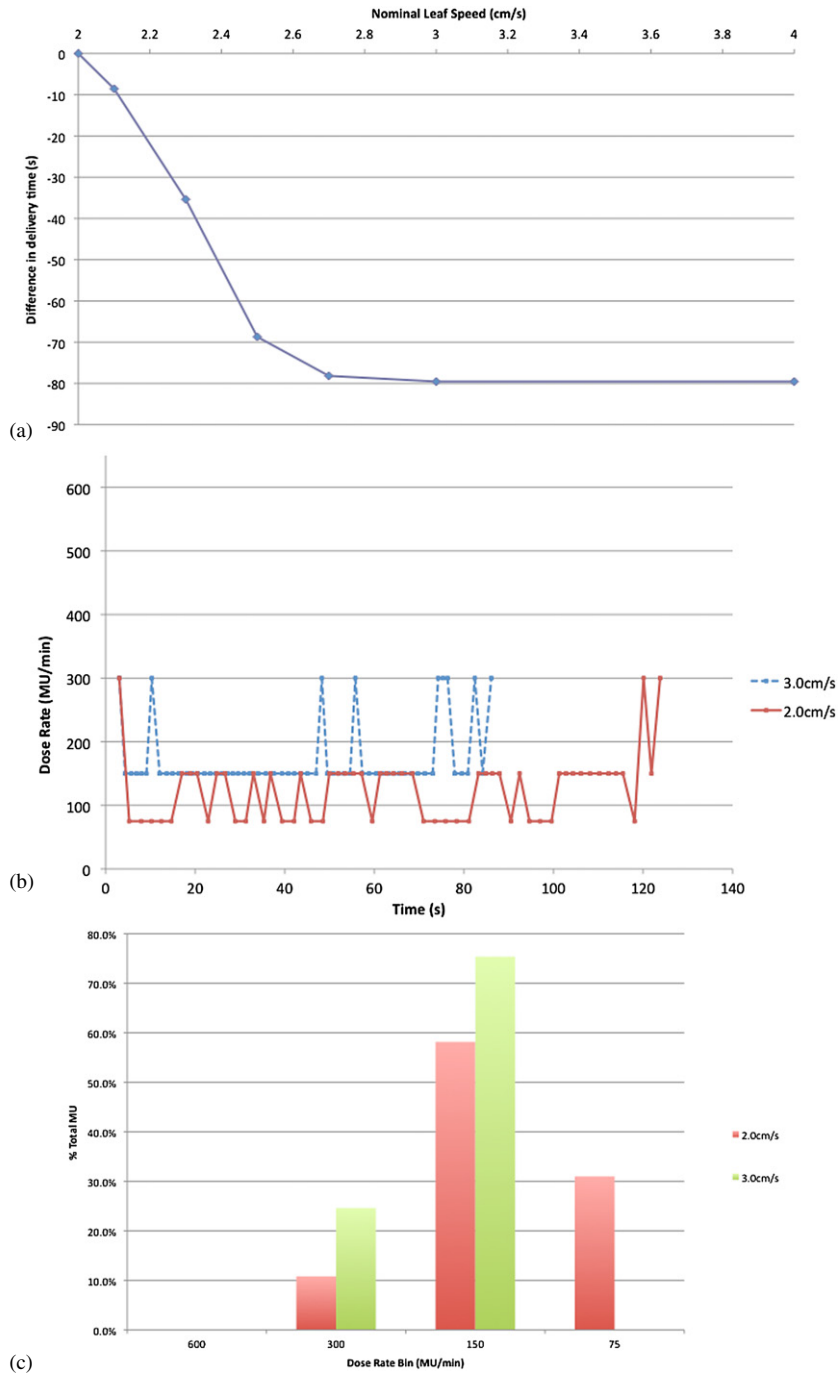

Figure 4. Increasing the nominal leaf speed from 2.0 to 3.0 cm s^{-1} for the head and neck patients: (a) averaged over all patients, the maximum time advantage is 79 s in total over both arcs, (b) comparing the selection of dose rate bins over a typical treatment (first arc of head and neck patient 3), (c) demonstrating that the linac preferentially selects higher dose rate bins, such that, in this example, no dose is delivered in the bottom dose rate bin.

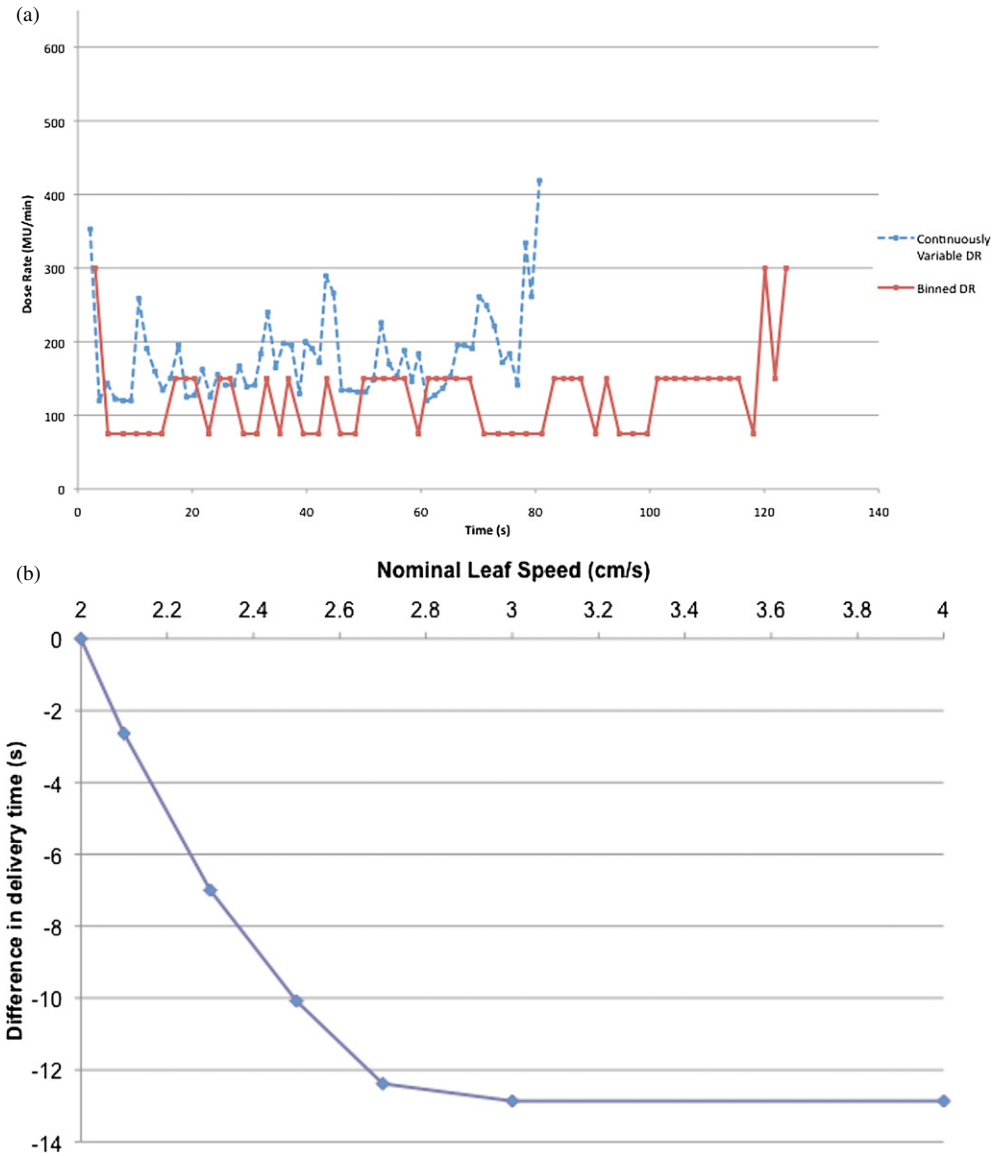

Figure 5. Continuously variable versus binned dose rates. (a) Typical head and neck beam delivered with binned and continuously variable dose rates, where all other parameters (including leaf speed) are kept constant. (b) Time advantage when increasing nominal leaf speed with continuously variable dose rate.

3.2.3. Determining 'ideal' machine parameters. Applying equations (3) and (4) to the prostate and head and neck plans gave the results shown in table 3. For the five prostate plans, a maximum dose rate of approximately 1400 MU min^{-1}, a nominal leaf speed of 2.8 cm s^{-1} and a jaw speed of 1.5 cm s^{-1} were required to deliver the plan at a constant gantry speed of 6° s^{-1}. For head and neck treatments, the maximum dose rate needed to be approximately 1180 MU min^{-1}, with a nominal leaf speed of 2.8 cm s^{-1} and a jaw speed of 2.0 cm s^{-1}. These

Table 3. Idealized machine parameters for the ten VMAT plans.

Prostate	Ideal max dose rate (MU min^{-1})	Ideal max leaf speed (cm s^{-1})	Ideal max jaw speed (cm s^{-1})	Delivery time with emulator (s)
1	1392	2.8	1.5	61.4
2	1392	2.8	1.5	61.5
3	1392	2.8	1.5	61.5
4	1404	2.8	1.5	61.5
5	1386	2.8	1.5	61.4
Mean	1393	2.8	1.5	61.5
Head and Neck				
1	1119	2.8	1.8	62.1 + 62.4
2	1171	2.8	1.8	62.1 + 62.1
3	844	2.8	1.8	62.2 + 62.1
4	1104	2.8	1.8	62.2 + 62.2
5	933	2.8	1.8	62.1 + 62.4
Mean	1034	2.8	1.8	62.1 + 62.2

values were entered into the emulator to calculate the resulting delivery times, which are also shown in table 3.

Again, leaf-positioning errors were observed due to the significantly shorter control point time. On average, across the 10 patients, 12.7 control points contained positioning errors >1 mm. When the acceleration/deceleration time for the leaves was reduced from 0.25 to 0.2 s, the number of errors returned to zero.

4. Discussion

VMAT introduces a set of specific and unique problems for linac-based radiotherapy. Whereas static fields require modelling of beam profiles and modifiers within the planning system, dynamic arcs also require knowledge of the dynamic capabilities of the machine—particularly if the delivery time is to be optimized during planning. With the availability of variable dose rates, it also becomes more important to ensure that the linac delivery is efficient. Furthermore, the linear accelerator design (including the leaf, jaw and gantry speed) may not currently be optimized for VMAT delivery. The purpose of this study was to better understand the impact of these dynamic machine parameters on VMAT treatment delivery.

The emulator produced reasonable predictions of the actual delivery of the linear accelerator. While a number of realistic parameters were added to improve the accuracy of the model, some simplifying assumptions were made. The emulator assumes an idealized picture of the dose rate—that it is constant for each control point and bin switching is instantaneous—whereas it is apparent from the linac plot in figure 2 that it is not. Furthermore, the service graphing function will likely include measurement dead time, which has not been measured or accounted for in this study. These factors may explain the discrepancies between the real and predicted delivery times. Finally, it should be noted that the leaf acceleration/deceleration time was estimated at $\sim$0.25 s, based on an average of measurements with a range 0.22–0.30 s. This is similar to the minimum resolution of the measurement, such that the real

acceleration/deceleration may at times be greater, and therefore the average value of 0.25 s represents a conservative estimate.

Rangaraj *et al* (2010) have previously investigated the properties of VMAT delivery through the use of an ideally efficient formulation of the RapidArc delivery process. Large discrepancies (>10 s) were found between the predicted and actual treatment times for five plans—a point which the paper acknowledges may be due to the lack of a full characterization of all of the constraints on VMAT delivery. In this study, the optimal (or 'ideally efficient') plan is subject to discretization of the dose rates (whether 4 or 255 bins), nominal and actual leaf speed constraints and the acceleration/deceleration of the gantry. Inclusion of these factors has led to accurate modelling of VMAT delivery, and also allowed investigations into the effects of changing real machine constraints.

Increasing the allowable leaf speed means that t_{lim} is reduced, allowing the linac to select higher dose rate bins and a faster gantry speed. Using the emulator allowed the efficiency to be quantified for a number of VMAT patient plans. Figure 3 shows that an improvement in efficiency is seen even with a modest increase in leaf speed. For prostates, increasing the leaf speed to 2.5 cm s^{-1} increases the number of monitor units in the top dose rate bin by approximately 10%. Similarly, for the head and neck patients, increasing the leaf speed to 2.5 cm s^{-1} reduced the proportion of MUs delivered in the bottom dose rate bin (75 MU min^{-1}) to almost zero for the five plans considered. For the prostate and head and neck patients, the maximal time advantage was achieved with a leaf speed of 3.0 cm s^{-1}.

It is important to emphasize again that the nominal maximum leaf speed of 2.0 cm s^{-1} is a conservative value stored within the software of the linac, and actual leaf speeds are greater. Thus, a v_{leaf} of 3.0 cm s^{-1} will actually require a real speed of between 3.2 and 3.8 cm s^{-1} (depending on the MLC orientation with respect to gravity). It may be feasible for manufacturers to achieve these speeds, given that the current maximum speed measured on the Elekta machine in this study was 3.4 cm s^{-1}. For Varian linacs, the nominal leaf speed has been reported to be 2.9 cm s^{-1} (Feygelman *et al* 2010), whereas the Siemens 160 MLC can achieve a maximum of 4.3 cm s^{-1} (Tacke *et al* 2008).

Continuously variable dose rate is a recent addition to the Elekta VMAT system. As expected, increasing the number of available dose rate bins to 255 significantly reduced the treatment time using the emulator. It will be of future interest to compare the results presented here to actual measurements on a continuously variable dose rate system. Again, it was found that increasing the leaf speed enabled a higher average dose rate and shortened treatment time for prostates and head and neck plans.

In principle, the fastest delivery time for a single arc is 60 s, assuming the delivery is limited only by the IEC maximum gantry speed of 6.0° s^{-1}. It was calculated that a linac would need to be able to deliver ∼1400 MU min^{-1} for prostate plans and ∼1180 MU min^{-1} for the head and neck plans in order to deliver at the maximum gantry speed. These dose rates are significantly higher than those used for the majority of linac-based radiotherapy. However, higher dose rates have been achieved by removing the flattening filter in the head of the linac. In particular, Cashmore (2008) reports an increase of 2.3 times the maximum dose rate for an open field. Further work would be required to assess whether VMAT could be delivered using a flattening filter-free beam, in order to facilitate maximum gantry speed delivery.

It is of interest to note that the quoted delivery times as estimated by the emulator are slightly greater than 60 s (table 3). One reason for the discrepancy is the gantry acceleration time at the beginning of the beam. However, when looking at the emulator's predicted output over the course of treatment (figure 6), it appears that the gantry speed fluctuates between 5.8 and 6° s^{-1}. The use of an 8 bit variable for the dose rate (giving a range of 255 possible values) may not approximate well to a truly continuous variable, especially if the maximal dose rate

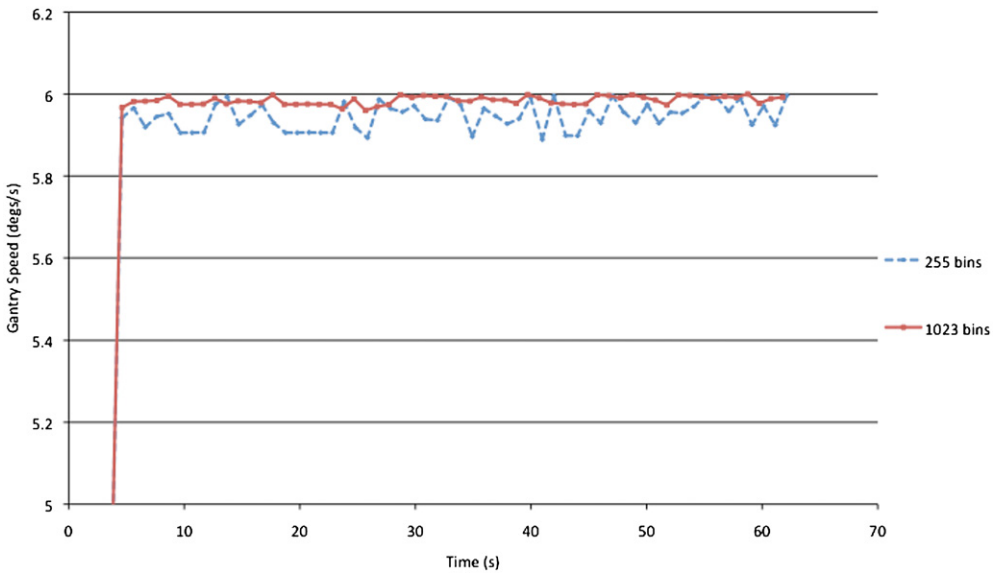

Figure 6. Comparison between the required gantry speeds for 8 bit (255 values) and 10 bit (1023 values) dose rate bins, for an idealized machine that can deliver ∼1180 MU min^{-1}.

is high. Increasing the bin range to 1023 values (10 bit) reduces the delivery time per arc by approximately 1 s and allows for a higher and smoother gantry speed (figure 6).

Using a software emulator has enabled an analysis of the relative importance of different dynamic delivery parameters. It will be of future interest to use the emulator to aid the planning process as well. The SmartArc plans used in this study were all subject to 'efficiency constraints' with the aim of ensuring deliverability and dosimetric quality on the linac. It is not clear to what extent these constraints affect the plan quality, although limiting leaf travel between control points will inevitably restrict the shapes of segments that can be selected. Using the emulator as a testing tool, it will be of interest to investigate the deliverability of increasingly unconstrained and complex plans. Treatment efficiency may then be predicted, as will any potential errors, which could then be fed back to planning in order to improve the balance between plan quality and deliverability.

5. Conclusion

Through the use of a realistic delivery emulator and a set of treatment plans, the impact of a range of dynamic parameters has been assessed for the Elekta VMAT system. Increasing the maximum MLC speed led to an increase in the number of monitor units delivered at higher dose rates, and significantly reduced the overall treatment times. The efficiency improvement due to continuously variable dose rate was also quantified for a cohort of prostate and head and neck plans. Finally, the required dose rate, leaf and jaw speeds were calculated for an idealized delivery scenario where the gantry maintains a constant maximum gantry speed of $6^\circ\ s^{-1}$.

Acknowledgments

The authors are grateful to Elekta for their constructive comments on the preparation of this paper. The lead author's work is also partly funded by an Elekta research grant.

References

Bedford J L and Warrington A P 2009 Commissioning of volumetric modulated arc therapy (VMAT) *Int. J. Radiat. Oncol. Biol. Phys.* **73** 537–45

Bertelsen A, Hansen C R, Johansen J and Brink C 2010 Single arc volumetric modulated arc therapy of head and neck cancer *Radiother. Oncol.* **95** 142–8

Bortfeld T and Webb S 2009 Single-Arc IMRT? *Phys. Med. Biol.* **54** N9–20

Bzdusek K, Friberger H, Eriksson K, Hardemark B, Robinson D and Kaus M 2009 Development and evaluation of an efficient approach to volumetric arc therapy planning *Med. Phys.* **36** 2328–39

Cao D, Afghan M K, Ye J, Chen F and Shepard D M 2009 A generalized inverse planning tool for volumetric-modulated arc therapy *Phys. Med. Biol.* **54** 6725–38

Cashmore J 2008 The characterization of unflattened photon beams from a 6 MV linear accelerator *Phys. Med. Biol.* **53** 1933–46

Feygelman V, Zhang G and Stevens C 2010 Initial dosimetric evaluation of SmartArc—a novel VMAT treatment planning module implemented in a multi-vendor delivery chain *J. Appl. Clin. Med. Phys.* **11** 3169

Guckenberger M, Richter A, Krieger T, Wilbert J, Baier K and Flentje M 2009 Is a single arc sufficient in volumetric-modulated arc therapy (VMAT) for complex-shaped target volumes? *Radiother. Oncol.* **93** 259–65

Matuszak M M, Yan D, Grills I and Martinez A 2010 Clinical applications of volumetric modulated arc therapy *Int. J. Radiat. Oncol. Biol. Phys.* **77** 608–16

McGrath S D, Matuszak M M, Yan D, Kestin L L, Martinez A A and Grills I S 2010 Volumetric modulated arc therapy for delivery of hypofractionated stereotactic lung radiotherapy: a dosimetric and treatment efficiency analysis *Radiother. Oncol.* **95** 153–7

Otto K 2008 Volumetric modulated arc therapy: IMRT in a single gantry arc *Med. Phys.* **35** 310–7

Palma D, Vollans E, James K, Nakano S, Moiseenko V, Shaffer R, McKenzie M, Morris J and Otto K 2008 Volumetric modulated arc therapy for delivery of prostate radiotherapy: comparison with intensity-modulated radiotherapy and three-dimensional conformal radiotherapy *Int. J. Radiat. Oncol. Biol. Phys.* **72** 996–1001

Rangaraj D, Oddiraju S, Sun B, Santanam L, Yang D, Goddu S and Papiez L 2010 Fundamental properties of the delivery of volumetric modulated arc therapy (VMAT) to static patient anatomy *Med. Phys.* **37** 4056–67

Rao M, Yang W, Chen F, Sheng K, Ye J, Mehta V, Shepard D and Cao D 2010 Comparison of Elekta VMAT with helical tomotherapy and fixed field IMRT: plan quality, delivery efficiency and accuracy *Med. Phys.* **37** 1350–9

Shaffer R, Morris W J, Moiseenko V, Welsh M, Crumley C, Nakano S, Schmuland M, Pickles T and Otto K 2009 Volumetric modulated Arc therapy and conventional intensity-modulated radiotherapy for simultaneous maximal intraprostatic boost: a planning comparison study *Clin. Oncol.* **21** 401–7

Tacke M B, Nill S, Haring P and Oelfke U 2008 6 MV dosimetric characterization of the 160 MLC, the new Siemens multileaf collimator *Med. Phys.* **35** 1634–42

Vanetti E *et al* 2009 Volumetric modulated arc radiotherapy for carcinomas of the oro-pharynx, hypo-pharynx and larynx: a treatment planning comparison with fixed field IMRT *Radiother. Oncol.* **92** 111–7

Verbakel W F, Senan S, Cuijpers J P, Slotman B J and Lagerwaard F J 2009 Rapid delivery of stereotactic radiotherapy for peripheral lung tumors using volumetric intensity-modulated arcs *Radiother. Oncol.* **93** 122–4

Wolff D *et al* 2009 Volumetric modulated arc therapy (VMAT) versus serial tomotherapy, step-and-shoot IMRT and 3D-conformal RT for treatment of prostate cancer *Radiother. Oncol.* **93** 226–33

Yu C X and Tang G 2011 Intensity-modulated arc therapy: principles, technologies and clinical implementation *Phys. Med. Biol.* **56** R31–54

Zhang P, Happersett L, Hunt M, Jackson A, Zelefsky M and Mageras G 2010 Volumetric modulated arc therapy: planning and evaluation for prostate cancer cases *Int. J. Radiat. Oncol. Biol. Phys.* **76** 1456–62

2.4. Publication 4

The impact of continuously-variable dose rate VMAT on beam stability, MLC positioning and overall plan dosimetry

Published in Journal of Applied Clinical Medical Physics, 2012, vol. 13, pp. 254-266

Authors:

CJ Boylan

A McWilliam

ER Johnstone

CG Rowbottom

Author Contributions

Hypothesis:

Following on from the previous paper, I proposed this study to investigate whether the newly-available CVDR-VMAT has improved delivery characteristics over BDR, and whether this has an impact on plan dosimetry.

Methodology:

I designed the experimental strategy and took the Delta^4 measurements on the linac before and after the Integrity upgrade. I developed the beam stability monitoring technique and took the measurements. AM and I produced the VMAT plans. EJ developed the MLC tracking as part of an MSc project with my supervision.

Analysis:

I performed the analysis of the results, generated the conclusions and wrote the manuscript.

13 pages

The impact of continuously-variable dose rate VMAT on beam stability, MLC positioning, and overall plan dosimetry

Christopher Boylan,[a] Alan McWilliam, Emily Johnstone, Carl Rowbottom
The Christie NHS Foundation Trust, Manchester and Manchester Academic Health Science Centre (MAHSC), Faculty of Medical and Human Sciences, University of Manchester, Manchester, Manchester, UK
christopher.boylan@christie.nhs.uk

Received 23 April, 2012; accepted 6 August, 2012

A recent control system update for Elekta linear accelerators includes the ability to deliver volumetric-modulated arc therapy (VMAT) with continuously variable dose rate (CVDR), rather than a number of fixed binned dose rates (BDR). The capacity to select from a larger range of dose rates allows the linac to maintain higher gantry speeds, resulting in faster, smoother deliveries. The purpose of this study is to investigate two components of CVDR delivery — the increase in average dose rate and gantry speed, and a determination of their effects on beam stability, MLC positioning, and overall plan dosimetry. Initially, ten VMAT plans (5 prostate, 5 head and neck) were delivered to a Delta^4 dosimetric phantom using both the BDR and CVDR systems. The plans were found to be dosimetrically robust using both delivery methods, although CVDR was observed to give higher gamma pass rates at the 2%/2 mm gamma level for prostates ($p < 0.01$). For the dual arc head-and-neck plans, CVDR delivery resulted in improved pass rates at all gamma levels (2%/2 mm to 4%/4 mm) for individual arc verifications ($p < 0.01$), but gave similar results to BDR when both arcs were combined. To investigate the impact of increased gantry speed on MLC positioning, a dynamic leaf-tracking tool was developed using the electronic portal imaging device (EPID). Comparing the detected MLC positions to those expected from the plan, CVDR was observed to result in a larger mean error compared to BDR (0.13 cm and 0.06 cm, respectively, $p < 0.01$). The EPID images were also used to monitor beam stability during delivery. It was found that the CVDR deliveries had a lower standard deviation of the gun-target (GT) and transverse (AB) profiles ($p < 0.01$). This study has determined that CVDR may offer a dosimetric advantage for VMAT plans. While the higher gantry speed of CVDR appears to increase deviations in MLC positioning, the relative effect on dosimetry is lower than the positive impact of a flatter and more stable beam profile.

PACS numbers: 87.56.bd; 87.55.km; 87.55.Qr

Key words: volumetric-modulated arc therapy, dose rate, intensity-modulated radiotherapy, treatment planning, dosimetric verification

I. INTRODUCTION

Dynamic arc radiotherapy has undergone several significant advancements since it was first proposed in 1995.[1] Many of the developments have related to formalizing and improving the efficiency of inverse planning,[2,3] such that highly modulated and conformal dose distributions

[a] Corresponding author: Christopher Boylan, Christie Medical Physics and Engineering (CMPE), The Christie NHS Foundation Trust, Wilmslow Road, Manchester M20 4BX, UK; phone: +44 (0)161 446 8443; fax: +44 (0)161 446 3545; email: christopher.boylan@christie.nhs.uk

can now be achieved for a range of sites.[4-6] Just as significant are the advances in linear accelerator design — particularly in the ability of linac control systems to now reliably vary gantry speed, dose rate, and aperture shape simultaneously over the treatment arc.[7] With the ability to deliver complex dose distributions efficiently and with a significant reduction in treatment time, arc radiotherapy is allowing many departments to improve their provision of intensity-modulated radiotherapy.[8]

One of the commercial solutions for arc radiotherapy is Elekta VMAT. Previously, the Elekta VMAT solution only allowed the linac to select from fixed dose rate bins during delivery.[9] The selection of dose rate bin and gantry speed for each control point is determined by the required change in multileaf collimator (MLC) shape and the number of monitor units to deliver. The binned dose rate (BDR) system, which is a feature of the Elekta Desktop 7.01 software, allows the dose rate to be reduced by factors of 2, such that for a maximum linac dose rate of 600 $MU.min^{-1}$, the available bins are 600 $MU.min^{-1}$, 300 $MU.min^{-1}$, 150 $MU.min^{-1}$, 75 $MU.min^{-1}$, and 37 $MU.min^{-1}$. A number of studies have shown good dosimetric results with BDR VMAT, using a variety of measurement techniques.[10-12]

A more recent version of VMAT, packaged with the Integrity linac control software, allows for a much larger range of dose rates to be selected. Rather than five fixed dose rate bins, Integrity allows 255 bins to be selected from a nominal range of 37 $MU.min^{-1}$ to 600 $MU.min^{-1}$. The initial, and most prominent, impact of continuously variable dose rates (CVDR) is the much reduced treatment times. This is due to the linac being able to switch between smaller dose rate intervals, and thus maintain a higher gantry speed during treatment. A recent report by Bertelsen et al.[13] has shown that CVDR VMAT provides good dosimetry and faster, smoother deliveries when applied to a number of clinical plans.

There is evidence to suggest that a higher average dose rate, which CVDR provides, can provide better beam stability during VMAT delivery. In particular, Bedford and Warrington[14] reported that beam symmetry was poorer in the low dose rate bins for the BDR system. Generally, VMAT delivery preferentially selects higher dose rates, as this is closer to the conditions at linac calibration (i.e., 600 $MU.min^{-1}$). Significant deviations from these calibration conditions, as Bedford and Warrington show, may lead to increased beam asymmetry and, hence, poorer dosimetry. It has been suggested that the increase in average dose rate offered by CVDR may therefore provide a dosimetric advantage.[13]

Conversely, an increase in average dose rate leads to an increase in gantry speed, and concern has been expressed that this may adversely affect the dynamic positioning of MLCs over treatment.[13,15,16] A recent study by Pasler et al.[15] saw an improvement in dosimetry for VMAT prostate plans as delivery time was reduced (i.e., average dose rate and gantry speed was increased), but complex head-and-neck plans did not benefit from faster delivery. For these patients, dosimetry was poorer when delivered with a higher dose rate. This was attributed to some MLCs not reaching their intended position at each control point. An increase in MLC positioning errors with the move to higher gantry speeds was also reported by Bertelsen et al.[13] for the Elekta Integrity system, and has also been observed with faster deliveries on the Varian RapidArc system.[16] With the trend towards faster VMAT treatments, the dosimetric impact of these MLC errors warrants further investigation.

The purpose of this study is to investigate the impact of CVDR on beam stability and MLC positioning accuracy, when compared to the BDR system. Initially, dosimetric verification was carried out on ten VMAT plans. In order to more fully understand the effects of increased dose rate and increased gantry speed, further tests were carried out utilizing the linac's electronic portal imaging device (EPID). Dynamic leaf positioning accuracy was investigated by tracking the MLCs over the course of delivery. Using the same EPID acquisitions, the effect of increased dose rate on beam stability was also characterized over the ten patient plans. The relative impact of each of these parameters on dosimetric performance could then be assessed.

II. MATERIALS AND METHODS

Ten patient plans were randomly selected, which consisted of five previously treated prostate VMAT patients, and five head-and-neck patients who had previously been treated with IMRT but were replanned with VMAT as part of a planning study. The plans were generated using Pinnacle version 9.0, utilizing the SmartArc optimization module (Philips Medical Systems, Madison, USA). The prostate patients were planned using a single arc technique, gantry rotating from 182° to 178°, with 4° between each control point, and a collimator angle of 45°. The beam energy was 10 MV and the final dose calculation was made using the adaptive collapsed cone convolution algorithm. A prescription of 57 Gy in 19 fractions to the prostate was set, with further dose levels covering the seminal vesicles, per group 3 of the CHHIP trial protocol.[17] The mean number of monitor units (and standard deviation) for the prostate patients was 465.1 ± 25.5 MU.

The five head-and-neck plans all involved complex shapes requiring a higher degree of modulation. All were three dose levels and consisted of three hypopharynx, one oropharynx, and one supraglottis. These were planned with a two arc solution, with gantry rotation from 182° to 178° and a collimator angle of 10° in both arcs. The control point spacing was again 4°, and the beam energy was 6 MV. 66 Gy was prescribed to PTV1, 60 Gy to PTV2, and 54 Gy to PTV3 using a simultaneous integrated boost (SIB) technique, in 30 fractions. On average, the total monitor units were 529.2 ± 66.2 MU for the head-and-neck plans.

The ten plans were delivered on an Elekta Synergy linear accelerator (Elekta, Crawley, UK) which was fitted with a MLCi head (1 cm leaf thickness). The linac had recently been upgraded to the Integrity control software such that in 'Service Mode', it was possible to deliver plans with either BDR or CVDR. Delivery times and dose rates were recorded for each plan.

A. Verification

Dosimetric verification was performed using each delivery method on the Delta^4 verification phantom (Scandidos, Uppsala, Sweden). The Delta^4 phantom consists of two planes of silicon diodes in a cylindrical PMMA phantom. With the application of appropriate correction factors, a pseudo three-dimensional analysis can be performed against the planned dose, and a gamma value calculated. This device has previously been shown to be an effective method for VMAT dosimetric verification.[18] The Delta^4 was set up at the isocenter of the linac and an inclinometer was fixed to the head to monitor gantry angle. Within the Delta^4 software, a correction factor was applied based on the linac's recorded output for that day. No automatic alignment of the measured dataset was performed. Gamma analysis was performed at the 2%/2 mm, 3%/3 mm, and 4%/4 mm levels for each of the plans, with measurement points < 20% of the maximum dose excluded from analysis.

B. EPID MLC tracking

A software tool has previously been developed and validated at this center to determine MLC positions using the EPID.[19,20] For this study, the software has been expanded to allow for tracking of MLC positioning during VMAT delivery. EPIDs have been shown to provide a sensitive and independent means of determining MLC positioning *in vivo* during radiotherapy.[21,22] With the Elekta iView system, a movie was acquired over the course of each VMAT delivery with a frame recorded approximately every 0.47 s. For each frame of the movie (Fig. 1) a histogram of pixel intensities was taken such that the exposed area could be identified. The field edge, and therefore the MLC positions, was then determined by thresholding the image at 50% of the modal pixel intensity.

As the iView system does not record the linac gantry angle for each image, the gantry angle was determined by using the Service Graphing function within the linac control system. Service Graphing records the state of various linac parameters every 0.25 s during treatment, so it was possible to 'tag' each EPID image with the appropriate gantry angle. The VMAT plans were

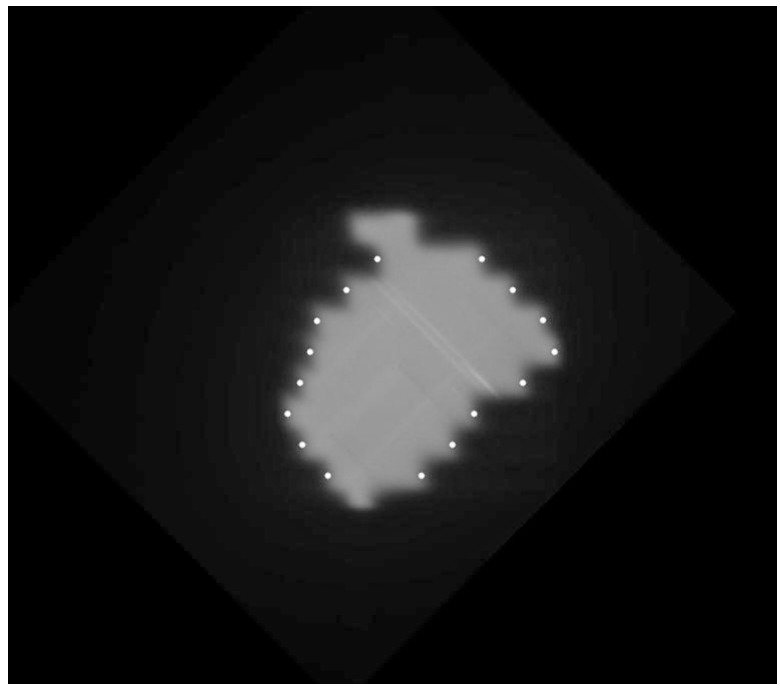

FIG. 1. A single portal image acquired during VMAT delivery, with the MLC positions identified (white dots).

retrieved from a commercial record and verify system (MOSAIQ), and interrogated to determine the expected position of the MLCs during treatment. As the plan file only contains MLC data at each control point (i.e., every 4º), it was necessary to interpolate the MLC positions for images acquired between these gantry angles.

The accuracy of the EPID at determining MLC positions was found to be within 0.5 mm compared to film measurements, and reproducibility of measurements was < 0.01 mm.[19] Prior to use with the VMAT plans, the system was tested under dynamic conditions using both a conformal (10 × 10 cm) and dynamic arc (a 2 cm sliding window defined by MLCs, similar to that described in Bedford and Warrington[14]). For the conformal arc, mean MLC deviation was determined to be -0.04 mm with a standard deviation (st. dev.) of 0.3 mm. For the sliding window the mean MLC deviation was -0.1 mm with a st. dev. of 1.2 mm.

C. Beam flatness and stability

Using the same data from the portal imager, beam stability was assessed over each treatment arc for the binned dose rate deliveries and the continuously variable dose rate. Software was written which analyzes each frame from the EPID movie and monitors the profile of the beam in the gun-target (GT) and transverse (AB) directions. Again, a histogram of the signal intensity in the image was used to identify the exposed area of the field, so that the effects of the penumbra and noise outside the field could be excluded. Then, the image was integrated across all rows (for the GT profile) and all columns (for the AB profile), taking a mean signal intensity per exposed pixel (Fig. 2). The standard deviation of each of these 1D profiles was recorded, and the process was then repeated over all of the frames of the EPID movie. The fluctuation of the beam profile could then be compared between the BDR and CVDR deliveries.

Due to the small sample size, the results of the gamma analysis, MLC deviations, and beam stability were statistically compared between BDR and CVDR over all deliveries using a non-parametric Wilcoxon signed-rank test. Significance was taken as $p < 0.05$. Where applicable, the standard deviation of results has been quoted in parentheses.

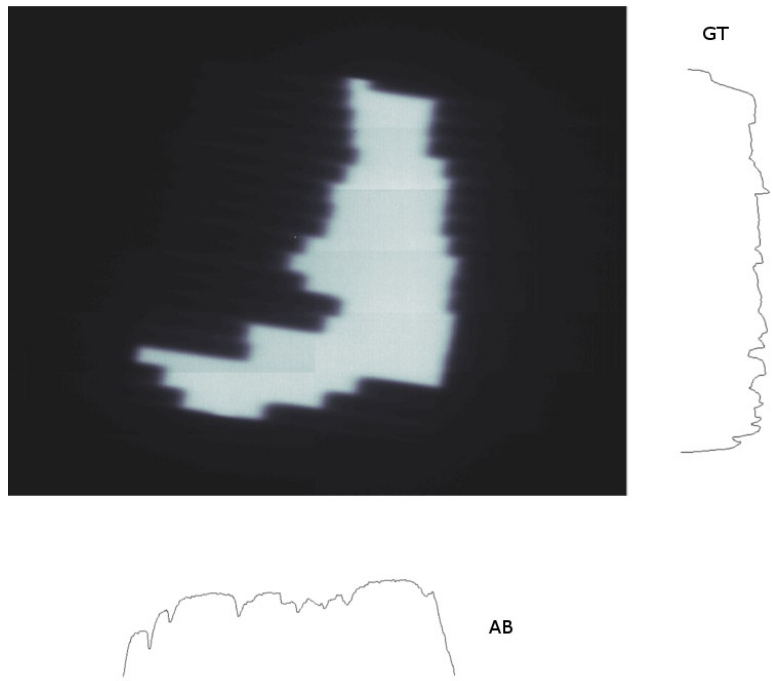

FIG. 2. Flatness monitoring of a portal image. The pixel intensity is integrated over the whole exposed field area in the GT and AB directions to determine the beam profile. The standard deviation of each profile is then calculated to measure the flatness.

III. RESULTS

Delivery times using continuously variable dose rate were reduced compared to the binned dose rate system (Table 1). The mean reduction in delivery time for both the prostate plans and for the head-and-neck plans was 30.2%. Figure 3 shows how the dose rate varies over one of the head-and-neck deliveries. As expected, the CVDR deliveries have smaller steps between dose rate bins and a higher average dose rate. The mean dose rate for the CVDR deliveries was 266 ± 67 MU.min^{-1} compared to 192 ± 55 MU.min^{-1} for the BDR deliveries ($p < 0.01$ over all

TABLE 1. Delivery times for the VMAT plans delivered with BDR and CVDR.

	Time (s)	
Plan	*Binned Dose Rate*	*Continuously Variable Dose Rate*
Prostate 1	118.9	80.8
Prostate 2	119.9	86.8
Prostate 3	119.6	83.2
Prostate 4	115.9	87.6
Prostate 5	122.6	78.4
Mean	119.4	83.4
Head and Neck 1	201.0	141.5
Head and Neck 2	210.3	146.0
Head and Neck 3	205.8	141.8
Head and Neck 4	204.5	144.3
Head and Neck 5	205.0	143.0
Mean	205.3	143.3

patients). Both delivery techniques were capable of switching between dose rate bins in less than 0.25 s (i.e., below the resolution of the Service Graphing function).

Results from the Delta^4 verifications are shown in Table 2. For the prostate patients, no statistically significant difference was observed at the 3%/3 mm gamma analysis between the BDR and CVDR deliveries. At 2%/2 mm, there was an improvement in gamma pass in favor of CVDR (2.0% pixels failing versus 5.2%, $p < 0.01$). For head-and-neck plans, a statistically significant improvement in gamma pass was observed with CVDR at all gamma levels for individual arc verifications on the Delta^4. However, the combined dose distributions (summing the contributions from both arcs) did not reflect this difference. The Delta^4 verifications were found to be reproducible, with intercomparison of repeat deliveries giving gamma pass rates of 100% at 2%/2 mm.

The mean MLC positioning deviations are shown in Table 3. Over all deliveries, CVDR deliveries resulted in larger mean MLC deviations than BDR deliveries ($p < 0.01$). For the head-and-neck plans, this difference was more pronounced than for the prostates, with a mean deviation of 0.06 cm measured for the BDR system versus 0.13 cm for the CVDR system. Averaged over all patients, the st. dev. of MLC positioning errors was similar for both BDR and CVDR ($p > 0.2$).

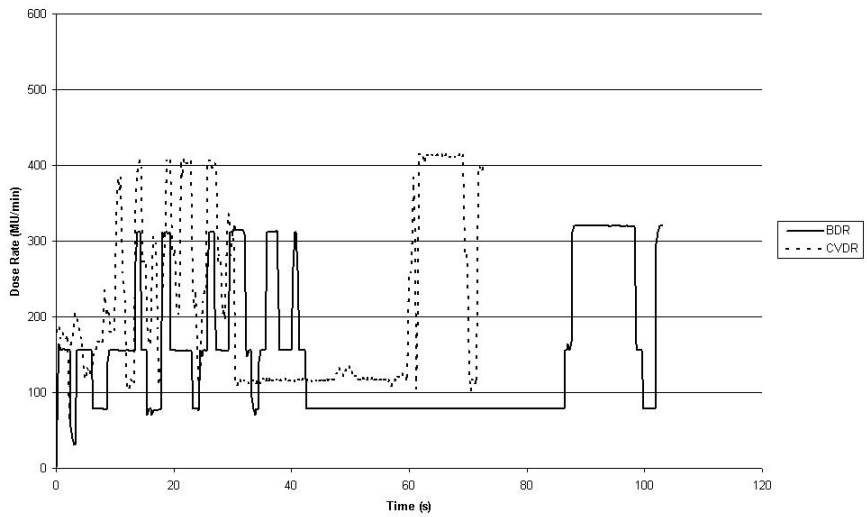

FIG. 3. Dose rate varying with time for the BDR and CVDR deliveries of one of the head-and-neck arcs.

TABLE 2. Delta^4 verification results for all plans delivered with BDR and CVDR. Values shown are the mean percent measurement points failing gamma analysis (± 1 st. dev.).

Prostate	*BDR*	*CVDR*	*p*
2%/2 mm	5.2±2.5%	2.0±1.5%	<0.01
3%/3 mm	0.6±0.8%	0.0±0.0%	>0.2

Head and Neck	*Arc 1*			*Arc 2*			*Combined*		
	BDR	*CVDR*	*p*	*BDR*	*CVDR*	*p*	*BDR*	*CVDR*	*p*
2%/2 mm	24.0±10.3%	23.4±6.0%	<0.01	17.2±10.5%	15.5±6.4%	<0.01	6.7±2.1%	6.5±2.6%	>0.2
3%/3 mm	7.0±5.1%	6.5±1.8%	<0.01	3.9±5.3%	3.1±1.7%	<0.01	1.1±0.4%	1.0±0.6%	>0.2
4%/4 mm	1.7±1.6%	1.4±0.5%	<0.01	1.0±1.3%	0.8±0.5%	<0.01	0.2±0.1%	0.1±0.1%	>0.2

Table 3. Mean and st. dev. of leaf positioning errors as determined by the EPID MLC tracking.

	BDR		*CVDR*	
Prostate Plan	*Mean Positional Error (cm)*	*St. Dev. (cm)*	*Mean Positional Error (cm)*	*St. Dev. (cm)*
1	0.08	0.18	0.09	0.17
2	0.07	0.24	0.08	0.21
3	0.09	0.17	0.09	0.22
4	0.07	0.76	0.09	0.31
5	0.08	0.21	0.09	0.17
Mean	0.08	0.31	0.09	0.22
Head and Neck Plan				
1	0.12	0.71	0.17	0.97
2	0.02	0.22	0.10	0.33
3	0.04	0.27	0.13	0.33
4	0.05	0.26	0.11	0.21
5	0.06	0.29	0.13	0.34
Mean	0.06	0.35	0.13	0.44

Using the portal images acquired during delivery, the standard deviation of the GT and AB profiles was calculated over each treatment arc. Figure 4 shows how the standard deviation varies over one of the head-and-neck arcs, for both CVDR and BDR. Over all the deliveries, the mean and maximum st. dev. of the profiles was higher for BDR deliveries compared to the CVDR deliveries ($p < 0.05$ for both prostate and head-and-neck deliveries). In all cases, st. dev. was larger in the GT profiles than in the AB direction (Fig. 5).

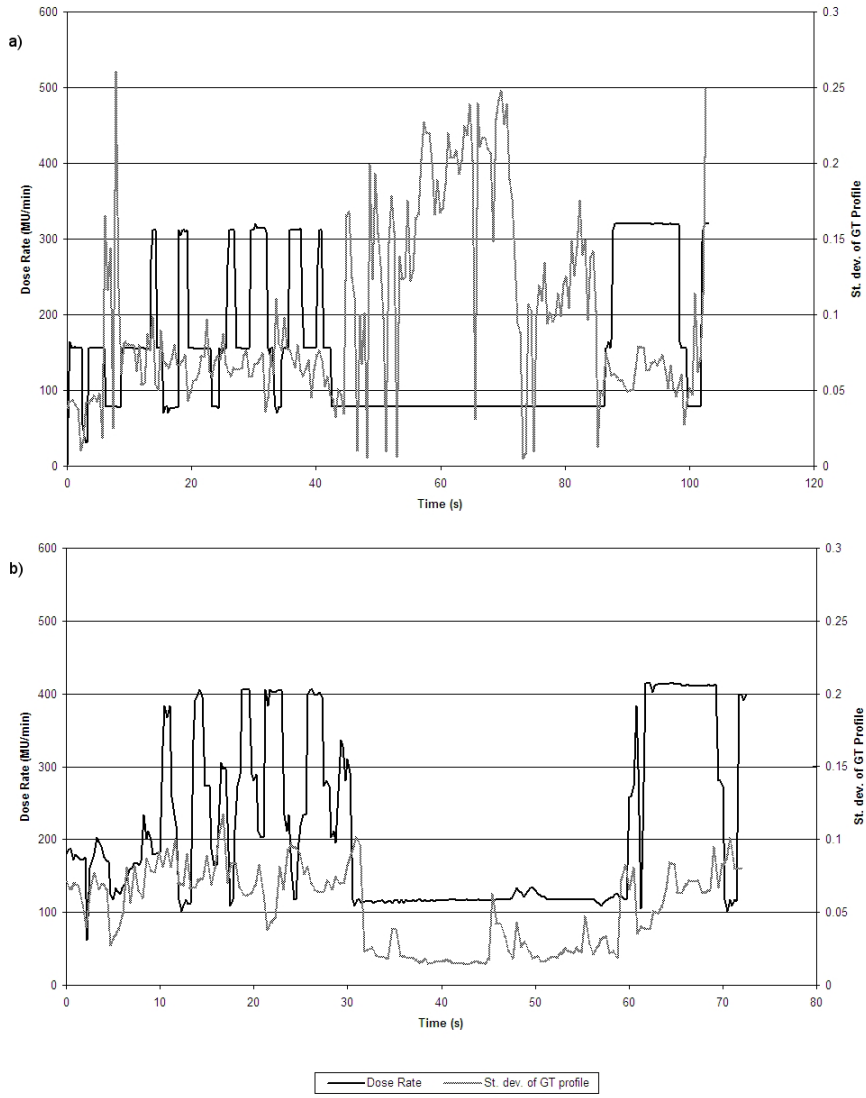

FIG. 4. Standard deviation of the GT profiles over a head-and-neck arc, plotted alongside dose rate for the BDR delivery (a), and for the CVDR delivery (b).

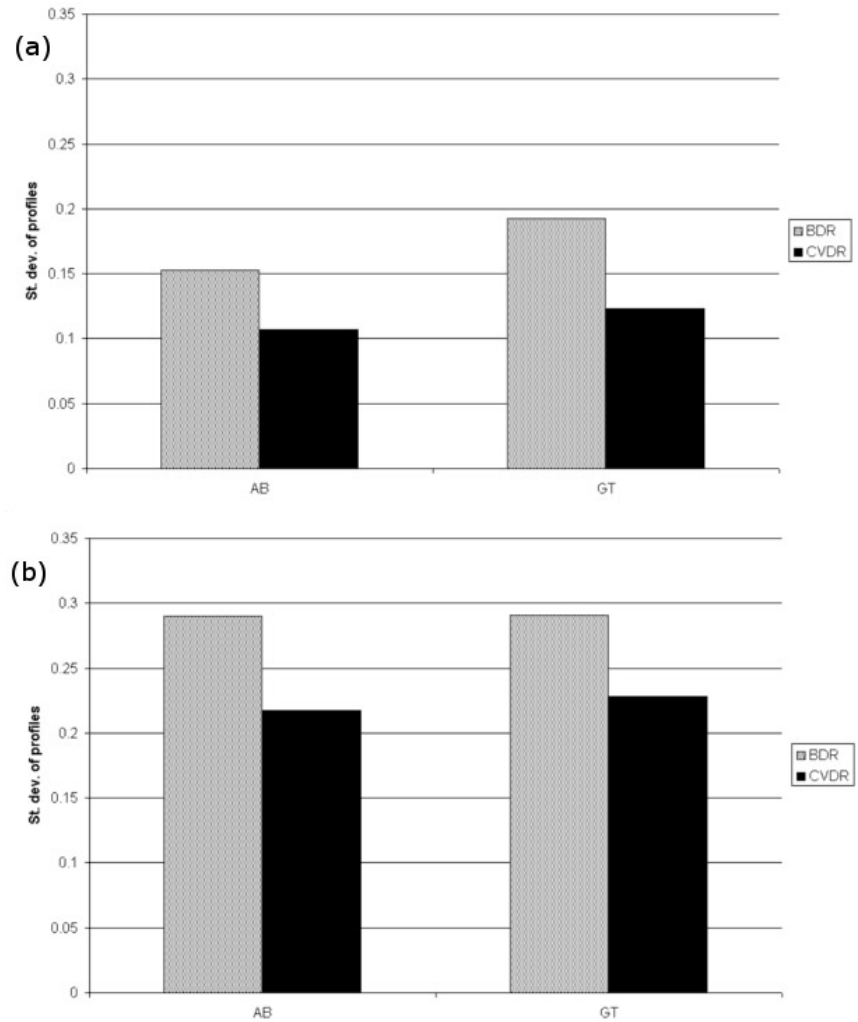

FIG. 5. Mean of the standard deviation of the AB and GT profiles for (a) all prostate patients, and (b) all head-and-neck patients.

IV. DISCUSSION

As expected, a reduction in delivery time was observed using continuously variable dose rate (~ 30.2%), which is in agreement with previous predicted and measured results.[13,23] This reduction is due to the ability to select a larger range of dose rates. On average, the increase in mean dose rate was 38.6% using CVDR compared to BDR.

In general, dosimetric verification was found to be satisfactory for both the BDR and CVDR systems. Following this center's requirements for gamma evaluation, all prostate and head-and-neck deliveries were considered clinically acceptable using the Delta^4 phantom. For the single arc prostate plans, no difference was observed between BDR and CVDR at the 3%/3 mm gamma level, although at the tighter tolerance of 2%/2 mm, the CVDR deliveries resulted in a higher pass rate. Similarly, for the complex two arc head-and-neck plans, the CVDR deliveries had a higher pass rate at all gamma levels for individual arcs. It is of interest to observe that the combined dose distributions (from both arcs) did not reflect this difference. Further

analysis reveals that, generally, the Delta^4 dose measurements of the first head-and-neck arc are systematically high, but are systematically low for the second arc (Fig. 6). As such, the combined dose distribution results in an acceptable gamma pass rate. The reason for this may be attributable to the way in which the dual arc plans are created. The SmartArc plans tended to produce one arc which conforms to the shape of the target volumes, and a second which is more heavily modulated to ensure a more uniform dose in the target, while maintaining the avoidance of organs at risk.

The study by Bertelsen et al.[13] reported higher gamma pass rates for head-and-neck plans, which may be due to differences in treatment protocol, and choice of VMAT parameters (a single arc, 2º control point spacing, compared to a dual arc, 4º solution in this study). However, the results presented here are in agreement with those reported previously, in that they indicate a slight improvement in dosimetry with CVDR compared to BDR.

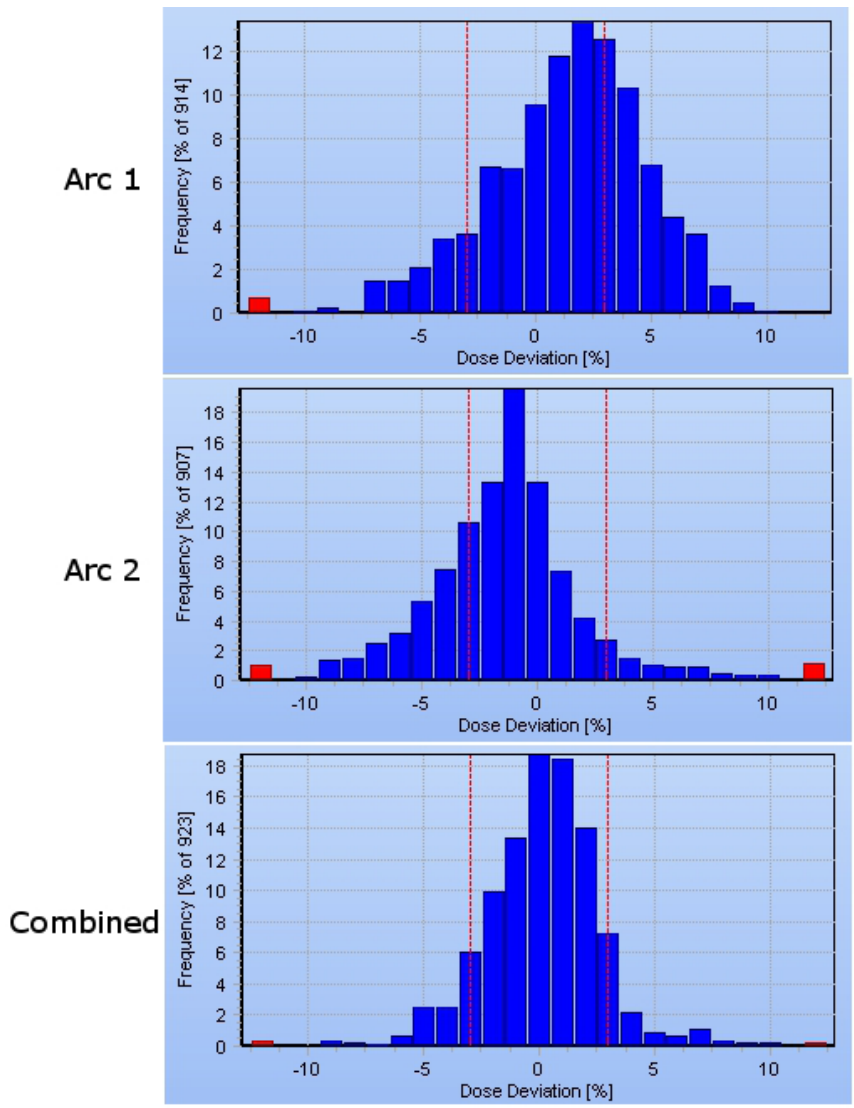

FIG. 6. Delta^4- measured dose deviations from one head-and-neck plan. The two individual arcs measure systematically low and high, such that the combined dose deviation is acceptable.

The fundamental difference between CVDR and BDR deliveries is the ability to select from a larger range of dose rates during treatment, which also allows higher gantry speeds to be selected. Using the EPID as an independent means of tracking MLC position, it was possible to determine the impact of these changes. While the mean MLC errors were small (head-and-neck plans gave 0.13 cm and 0.06 cm for CVDR and BDR, respectively), a statistically significant difference was observed between the delivery methods. This trend is similar to that noted by Bertelsen et al. However, the two methods are not directly comparable – the Bertelsen study uses the leaf error signal from the linac's service graphing function, whereas this study relates MLC position determined independently (from the EPID) with the planned position.

While it has been observed that the faster CVDR deliveries result in a higher mean MLC deviation over each treatment, it is more difficult to determine the whereabouts of any systematic positioning errors during the arc. A plot of gantry angle versus MLC deviations (Fig. 7) indicates that the leaf bank which is traveling against gravity has larger deviations. However, this trend is observed to be similar for both BDR and CVDR deliveries. An investigation of MLC deviation against instantaneous gantry speed would be of interest, but this is a difficult parameter to determine independently during VMAT delivery. Future work may involve the use of an external inclinometer (such as that used with the Delta^4 device) to reliably measure instantaneous gantry speed, and investigate any relationship to instantaneous MLC errors.

The dynamic monitoring of MLC position within the Elekta control system will temporarily interrupt the beam if a leaf error of > 0.4 cm is detected. With the move towards faster VMAT deliveries (through the use of CVDR, and potentially much higher dose rates[24]), the tolerance of this dynamic error monitoring may have to be tightened.

It is preferential for VMAT to be delivered with a dose rate which is closer to calibration and QA conditions.[14] Utilizing the portal imager, it has been possible to confirm that CVDR delivery, with its higher mean dose rate, leads to a flatter and more stable beam over the duration of delivery. Figure 4 shows how the st. dev. of the beam profiles varies over the treatment. With the BDR system it is possible to observe 'spikes' in the beam flatness which occur when there are large changes in dose rate. The CVDR system does not appear to contain these spikes due to the smaller intervals between dose rates. While both delivery methods are dosimetrically robust, the CVDR system presents an advantage in terms of beam stability during delivery.

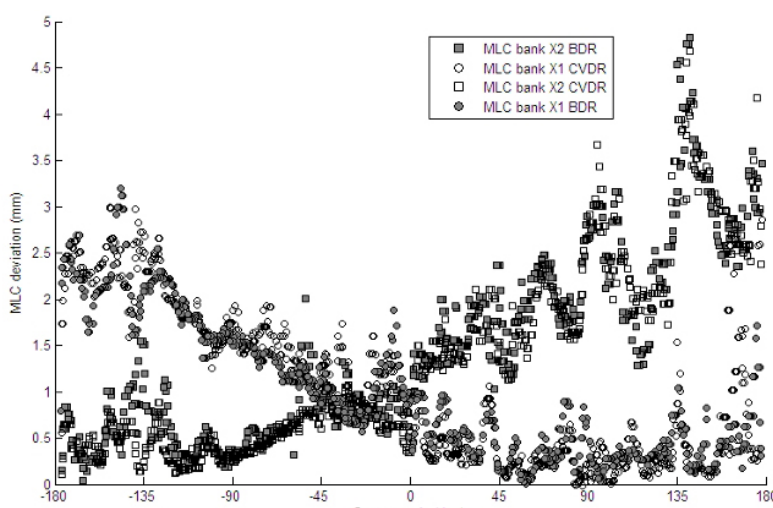

FIG. 7. Scatter plot of mean MLC deviations from each leaf bank (X1 and X2) over all prostate patients, plotted against gantry angle. Initially, leaf bank X1 is traveling against gravity. Shaded boxes and circles indicate CVDR delivery.

These results suggest that any negative dosimetric impact from MLC positioning which arises with the use of CVDR is smaller than the positive impact of the improved beam stability. It will be of future interest to determine what level of complexity can be achieved before the impact of MLC positioning errors becomes significant. It should also be noted that the ability of the linac to reach new aperture shapes is strongly dependant on the speed of the MLCs. In this study, the Elekta linac was fitted with standard 1 cm MLCi leaves. As VMAT becomes more widely used, modern MLC designs are placing greater importance on leaf speed, which will enable more complex changes in aperture shape without having to significantly reduce the dose rate or gantry speed.

It should be noted that the results presented here may be dependent on the planning system, and treatment protocols employed. At present this center uses VMAT for prostate treatments and selected head-and-neck sites. It will be of future interest to add to the small sample size considered in this study with more complex clinical sites, such as paraspinal tumours[25] and medulloblastoma (whole central nervous system) treatments.[26] Furthermore, it will be of use to investigate whether the EPID tracking and flatness measurements can be reproduced using other devices, such as a head-mounted diode or ion chamber array.

V. CONCLUSIONS

VMAT delivered with both continuously variable dose rate and binned dose rates provides high quality dosimetric verification for prostate and head-and-neck plans. The CVDR system, packaged with the Elekta Integrity software upgrade, is also capable of significantly shorter delivery times. Investigating two important components of the delivery, it was found that MLC positioning accuracy is slightly poorer with the faster CVDR deliveries, but that beam flatness and stability is improved compared to BDR. For complex VMAT deliveries, therefore, the superior beam stability (a result of the higher average dose rate with smaller intervals) appears to be the dominant factor in improved dosimetry for CVDR.

ACKNOWLEDGMENTS

The authors would like to thank Elekta for its assistance with the installation of the Integrity control software, and David Ryder for his help with the preparation of this paper. The lead author's work is partly funded by an Elekta research grant.

REFERENCES

1. Yu CX. Intensity-modulated arc therapy with dynamic multileaf collimation: an alternative to tomotherapy. Phys Med Biol. 1995;40(9):1435–49.
2. Bortfeld T and Webb S. Single-arc IMRT? Phys Med Biol. 2009;54(1):N9–N20.
3. Otto K. Volumetric modulated arc therapy: IMRT in a single gantry arc. Med Phys. 2008;35(1):310–17.
4. Zhang P, Happersett L, Hunt M, Jackson A, Zelefsky M, Mageras G. Volumetric modulated arc therapy: planning and evaluation for prostate cancer cases. Int J Radiat Oncol Biol Phys. 2010;76(5):1456–62.
5. Matuszak MM, Yan D, Grills I, Martinez A. Clinical applications of volumetric modulated arc therapy. Int J Radiat Oncol Biol Phys. 2010;77(2):608–16.
6. Bertelsen A, Hansen CR, Johansen J, Brink C. Single arc volumetric modulated arc therapy of head and neck cancer. Radiother Oncol. 2010;95(2):142–48.
7. Yu CX and Tang G. Intensity-modulated arc therapy: principles, technologies and clinical implementation. Phys Med Biol. 2011;56(5):R31–R54.
8. Popple RA, Fiveash JB, Brezovich IA, Bonner JA. RapidArc radiation therapy: first year experience at the University of Alabama at Birmingham. Int J Radiat Oncol Biol Phys. 2010;77(3):932–41.
9. Rao M, Yang W, Chen F, et al. Comparison of Elekta VMAT with helical tomotherapy and fixed field IMRT: plan quality, delivery efficiency and accuracy. Med Phys. 2010;37(3):1350–59.

10. Wolff D, Stieler F, Hermann B, et al. Clinical implementation of volumetric intensity-modulated arc therapy (VMAT) with ERGO++. Strahlenther Onkol. 2010;186(5):280–88.
11. Kaurin DG, Sweeney LE, Marshall EI, Mahendra S. VMAT testing for an Elekta accelerator. J Appl Clin Med Phys. 2012;13(2):3725.
12. Haga A, Nakagawa K, Shiraishi K, et al. Quality assurance of volumetric modulated arc therapy using Elekta Synergy. Acta Oncol. 2009;48(8):1193–97.
13. Bertelsen A, Lorenzen EL, Brink C. Validation of a new control system for Elekta accelerators facilitating continuously variable dose rate. Med Phys. 2011;38(8):4802–10.
14. Bedford JL and Warrington AP. Commissioning of volumetric modulated arc therapy (VMAT). Int J Radiat Oncol Biol Phys. 2009;73(2):537–45.
15. Pasler M, Wirtz H, Lutterbach J. Impact of gantry rotation time on plan quality and dosimetric verification — volumetric modulated arc therapy (VMAT) vs. intensity modulated radiotherapy (IMRT). Strahlenther Onkol. 2011;187(12):812–19.
16. Nicolini G, Clivio A, Cozzi L, Fogliata A, Vanetti E. On the impact of dose rate variation upon RapidArc implementation of volumetric modulated arc therapy. Med Phys. 2011;38(1):264–71.
17. Dearnaley D, Syndikus I, Sumo G, et al. Conventional versus hypofractionated high-dose intensity-modulated radiotherapy for prostate cancer: preliminary safety results from the CHHiP randomised controlled trial. Lancet Oncol. 2012;13(1):43–54.
18. Bedford JL, Lee YK, Wai P, South CP, Warrington AP. Evaluation of the Delta4 phantom for IMRT and VMAT verification. Phys Med Biol. 2009;54(9):N167–N176.
19. Baker SJ, Budgell GJ, MacKay RI. Use of an amorphous silicon electronic portal imaging device for multileaf collimator quality control and calibration. Phys Med Biol. 2005;50(7):1377–92.
20. Budgell GJ and Clarke MF. Analysis of the measurement precision of an amorphous silicon EPID used for MLC leaf position quality control and the long-term calibration stability of an optically controlled MLC. Phys Med Biol. 2008;53(15):N297–N306.
21. Fredh A, Korreman S, Rosenschold PM. Automated analysis of images acquired with electronic portal imaging device during delivery of quality assurance plans for inversely optimized arc therapy. Radiother Oncol. 2010;94(2):195–98.
22. James HV, Atherton S, Budgell GJ, Kirby MC, Williams PC. Verification of dynamic multileaf collimation using an electronic portal imaging device. Phys Med Biol. 2000;45(2):495–509.
23. Boylan CJ, Rowbottom CG, Mackay RI. The use of a realistic VMAT delivery emulator to optimize dynamic machine parameters for improved treatment efficiency. Phys Med Biol. 2011;56(13):4119–33.
24. Nicolini G, Ghosh-Laskar S, Shrivastava SK, et al. volumetric modulation arc radiotherapy with flattening filter-free beams compared with static gantry IMRT and 3D conformal radiotherapy for advanced esophageal cancer: a feasibility study. Int J Radiat Oncol Biol Phys. 2012;84(2):553–60.
25. Zhang P, Happersett L, Yang Y, Yamada Y, Mageras G, Hunt M. Optimization of collimator trajectory in volumetric modulated arc therapy: development and evaluation for paraspinal SBRT. Int J Radiat Oncol Biol Phys. 2010;77(2):591–99.
26. Lee YK, Brooks CJ, Bedford JL, Warrington AP, Saran FH. Development and evaluation of multiple isocentric volumetric modulated arc therapy technique for craniospinal axis radiotherapy planning. Int J Radiat Oncol Biol Phys. 2012;82(2):1006–12.

2.5. Publication 5

Pre-treatment independent plan verification for VMAT using a treatment delivery emulator and Monte Carlo dose model

Accepted (in a shortened form) by Radiotherapy and Oncology, September 2013

Authors:

CJ Boylan

AH Aitkenhead

CG Rowbottom

RI Mackay

Author Contributions

Hypothesis:

I proposed the development of an independent plan verification system for VMAT, which uses Monte Carlo calculations. I generated the hypothesis that the inclusion of realistic linac motion would improve the accuracy of such a system.

Methodology:

I developed the Monte Carlo model and performed the validation measurements. I designed and performed the experiments. The GATE/GEANT4 computing infrastructure was set up by myself and AA. The gamma analysis software was written by AA, and both myself and AA developed the automated verification system.

Analysis:

I performed the data analysis and wrote the manuscript.

26 pages

Abstract

Purpose: A Monte Carlo model for Elekta VMAT delivery is presented, and incorporated into a pre-treatment verification system. The model simulates the dynamic delivery of VMAT though the inclusion of a realistic linac emulator. Within this study, the model is validated against measurements, and compared to simulations without linac motion.

Methods: A beam model was produced using the GATE platform for GEANT4 Monte Carlo calculations. Initially, validation was performed against water tank measurements for depth-dose curves, MLC-defined profiles, output factors and an MLC bar test. The model was then integrated with a VMAT delivery emulator, which reads plan files and generates a set of dynamic delivery instructions analogous to the linac control system (i.e. choice of dose rate, gantry speed, and MLC motion between each control point). The emulator then simulates delivery through the application of parameters such as gantry inertia, and MLC speed variability with respect to gravity. The beam model was validated through comparison to measurements of 10 patient plans, comprising 5 single arc prostate plans and 5 dual-arc head and neck plans. Prostate plans were delivered to a cylindrical dosimetric phantom (Delta^4) while head and neck plans were delivered to a heterogeneous anatomical phantom (MARVIN). Gamma evaluation was performed between phantom measurements and two Monte Carlo models – one which simulates only fixed control points and one simulating continuous motion utilising the emulator. For routine clinical use, the model was incorporated into a fully automated pre-treatment verification system.

Results: Comparisons between the model and water tank measurements showed agreement at a range of depths for static test fields. The VMAT simulations also showed agreement with measurements: mean gamma pass ($\Gamma < 1$) over 5 prostate plans was 100.0% at 3%/3mm and 97.4% at 2%/2mm when compared to the Delta^4. Equivalent gamma analysis without the simulation of linac motion gave mean passes of 98.6% and 91.6% respectively. For the head and neck plans delivered to the

anatomical phantom, gamma passes were 99.4% at 4%/4mm and 94.94% at 3%/3mm. The same gamma analysis gave 98.8% and 92.8% respectively without the inclusion of linac motion. Within an automated verification system, the Monte Carlo model required 400-600 CPU hours to ensure a median calculation uncertainty of <2% within the 5% isodose on the patient CT volume. For a prostate and head and neck plan, gamma passes were observed which are within our centre's tolerance for pre-treatment plan QA.

Conclusions: This system demonstrates that routine VMAT plan QA can be performed using a GEANT4-based Monte Carlo solution. Through comparison to phantom measurements, it was found that the incorporation of a realistic linac motion emulator improves the accuracy of the model compared to the simulation of fixed control points. The ability to accurately calculate dose as a second check of the planning system, and determine realistic delivery characteristics, may allow for the reduction of machine-based pre-treatment plan QA for VMAT.

1. Introduction

A critical component of a safe radiotherapy service is the provision for pre-treatment quality assurance of individual patient plans [1]. This can be achieved in a number of ways, including independent second dose calculations, or by delivering the plan to a dosimetric phantom on the linear accelerator (linac) [2, 3]. Between centres there are a wide range of protocols concerning pre-treatment plan QA, but in general more simple plans (i.e. conventional or conformal techniques) tend only to require an independent monitor unit check to identify errors in the planning process [4]. Conversely, plans that involve a higher degree of complexity, such as intensity modulated radiotherapy (IMRT) or volumetric modulated arc therapy (VMAT), may not be suited to simple monitor unit calculation and require direct measurements on the linac itself [5]. In both cases, some method of checking the file transfer between the planning system and the linac is also essential [6].

The delivery of radiotherapy with VMAT has become increasingly commonplace, as various studies have demonstrated the ability to produce highly modulated dose distributions in a significantly shorter treatment time that fixed-field IMRT [7]. Several dosimetry systems exist to perform pre-treatment QA for VMAT, some of which involve the delivery of the plan to arrays of detectors arranged in a cylindrical geometry [8-10]. Gamma evaluation is then used to determine any differences between the measurement and the treatment planning system (TPS) dose. Direct measurement on the treatment machine is an important check of the TPS's dose calculation, particularly for elongated or unusual field shapes, as is commonly seen with VMAT plans [11].

For departments with large numbers of IMRT or VMAT patients, time constraints often mean that it is not feasible or desirable to perform linac-based QA on every plan. It may be instead appropriate to take measurements on a small, randomly-selected sample of plans, while running the remainder through a secondary, independent monitor unit calculator. There are several software solutions for performing monitor unit calculations [12, 13], some of which have been expanded to

work with IMRT and VMAT. Such monitor unit calculators utilize simplified geometric dose calculations for speed, and as such the complexities of calculating dose through small or complex multi-leaf collimator (MLC) defined fields may not be fully taken into account [14, 15]. Furthermore, accurate VMAT dosimetry is heavily dependant on the linac deliverability – that is, the ability to modulate gantry speed, dose rate and leaf motion over the arc [16]. Independent monitor unit checkers offer only a confirmation of the treatment planning system dose calculation, and hence on-linac measurements are also required to provide dosimetric confidence for VMAT pre-treatment checks. For departments seeking a workflow benefit with VMAT (which has been reported to offer a >50% decrease in delivery time [17, 18]), this may be offset by the requirement for increased plan verification time on the linac. An independent software solution capable of accurately modelling VMAT dose delivery would therefore be of benefit. Such a system could then allow more targeted plan verifications, thus reducing the amount of QA time required on the linac.

Monte Carlo dose calculation methods have been used widely in radiotherapy for many years [19, 20]. Various radiation transport codes have been shown to produce highly accurate simulations of dose deposition at the range of energies used for radiotherapy [21, 22]. The use of Monte Carlo has also been demonstrated for treatment plan evaluation [14, 23-25] and for rotational radiotherapy [26-28]. Furthermore, attempts have been made to incorporate the continuous dose delivery of VMAT, either by reconstructing the linac position from delivery log files [29, 30] or by linearly interpolating gantry and MLC positions between control points [29, 31].

The purpose of this paper is to introduce and validate a novel Monte Carlo plan verification system which is able to accurately simulate Elekta VMAT dose delivery (Elekta, Crawley, UK), such that machine-based pre-treatment quality assurance can be reduced. Utilizing the GATE platform for GEANT4 calculations [32], a beam model has been developed and integrated with a VMAT delivery emulator [33]. The

emulator replicates a linac control system's handling of a treatment plan (i.e. choice of dose rate, gantry speed and MLC motion over the arc) and then realistically simulates the delivery by incorporating the effects of gantry inertia and MLC speed with respect to gravity. A 'one-click' automated verification system has been developed around this beam model, whereby plans exported from a TPS can be sent for independent dose calculation and the results of 3D gamma evaluation between the TPS and Monte Carlo can be returned to the user. Within this study, the beam model is validated through comparison to water tank and dosimetric phantom measurements. For a number of VMAT plans, the accuracy of the Monte Carlo calculations is assessed both with and without the simulation of linac motion. Finally, the automated verification system is demonstrated for prostate and head and neck VMAT cases.

2. Materials and Methods

2.1. Monte Carlo model

A Monte Carlo linear accelerator model was produced using the open source toolkit GATE 6.1, which is an incorporation of the GEANT4 transport code within a platform specific for medical applications [32]. Grevillot *et al* [34] have demonstrated the use of GATE to model the output of a conventional linac, and showed good agreement with water tank measurements for a range of profiles and depth-dose curves. In this study, a model was created of a 6MV Elekta Synergy linac with the MLCi2 treatment head. Initially, a full model of the head was created from the target to the MLCs and jaws, using the manufacturer's specifications as a reference (Figure 1). To accurately model the photon beam energy, simulations were set up on a homogenous water phantom to acquire percentage depth dose (PDD) measurements and beam profiles at a range of field sizes (from 4x4cm to 20x20cm) and depths (1.6cm to 30cm). These simulations were compared to real ionization chamber measurements on the linac taken in a plotting tank. A process of electron beam 'tuning' was undertaken (as described by Grevillot [34] and Verhaegen [20]), whereby the electron energy and spot size on the target was adjusted until the photon PDD curves and profile penumbrae matched the measurements adequately.

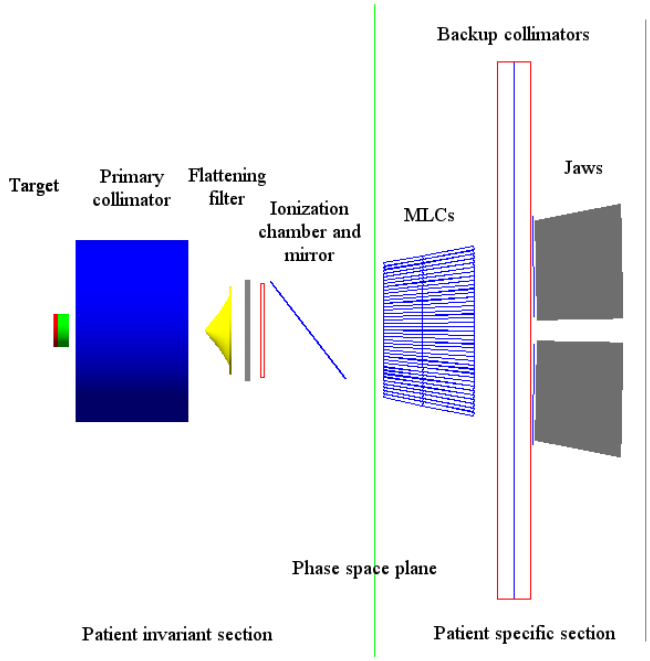

Figure 1. Schematic (generated in GATE) of the Monte Carlo linac head model, identifying the major components. The phase space plane is situated 10mm upstream of the MLC bank in order to model only the patient invariant part of the head.

Once the electron beam was tuned, further measurements were taken to ensure that the model was adequate for the simulation of intensity-modulated beams. Measurements of output factors were made, measuring the dose at 10 cm deep in water at 90 cm source-surface distance (SSD) for a range of field sizes. The same number of particles was simulated for each field size, and measurements were normalized to the dose recorded for the 10x10cm field size. The resulting output factors were compared to those determined by measurement on the linac itself.

The MLCi2 leaf bank was also modelled within GATE according to the manufacturer's specifications. Because of the complex geometry of the leaves (e.g. the rounded leaf tips, and pitched arrangement within the leaf bank), further tests were carried out to ensure the model was accurate. MLC-defined profiles were taken using an ionization chamber in a plotting tank at 4 x 4 cm to 20 x 20 cm. A 'bar-test' was also performed, whereby a y-axis (gun-target) profile was taken with sets of two leaves alternately open and closed within the field. The bar test checked the inter-leaf leakage and also the relative positioning of the leaves within the leaf

bank. Simulations were compared to measurements at 10 cm deep, 90 cm SSD. All comparisons between Monte Carlo and plotting tank measurements were made using gamma analysis [27, 34].

For patient simulations, the part of the linac head above the MLCs and jaws (as indicated in Figure 1) is invariant. As such, a phase space plane was recorded at this point and used for all subsequent simulations. Phase space files are used frequently in radiotherapy Monte Carlo simulations [19], as they improve the efficiency of the calculation by storing the energy and direction of simulated photons from the invariant part of the linac.

2.2. Integration of delivery emulator

A delivery emulator for the Elekta VMAT system has previously been developed which simulates the linac control system and delivery [33]. The software reads in DICOM-RT plan files and initially calculates the required gantry speed, dose rate and MLC motion for each control point. The choice of these parameters is determined by the number of monitor units to be delivered in the given control point, and the amount of time required for the MLCs to reach their new desired position. Under the Elekta Integrity control system, the linac will preferentially select the highest dose rate achievable, but will step down the dose rate and gantry speed through knowledge of the nominal leaf speed. Once the desired parameters have been determined, the software realistically emulates VMAT delivery by incorporating the effects of gantry and leaf acceleration and deceleration, along with the variable leaf speed with respect to gravity. As described previously [33], the emulator uses dynamic parameters derived from measurements, and has been shown to accurately predict realistic VMAT deliveries. The outputs of the emulator are gantry position, MLC positions, jaw/collimator positions, and dose rate over time.

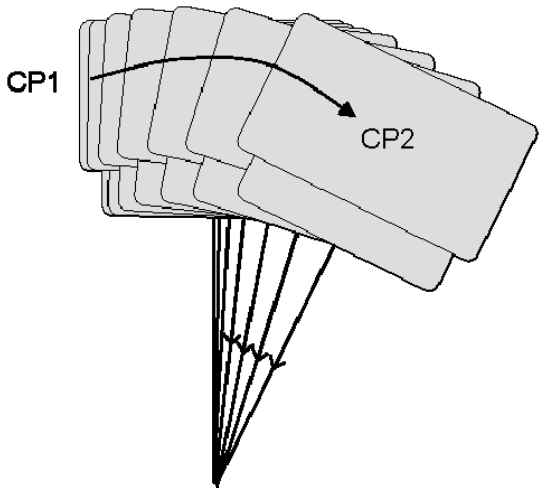

Figure 2. An exaggerated demonstration of how the delivery emulator distributes monitor units between control points (CP1 – CP2). Where the linac gantry must accelerate, the monitor units will not be evenly distributed over the sector. Integrating knowledge of the head acceleration into the simulation allows the particles to be distributed more realistically.

In order to integrate the emulator with the VMAT Monte Carlo model, two assumptions were made: that dose rate switching is instantaneous, and that it remains constant for each control point. These assumptions then allow the monitor units of each control point (and hence the number of particles in the Monte Carlo simulation) to be divided into arbitrarily small but equal sizes. Thus, a series of static linac head positions can be simulated, approximating continuous VMAT delivery. This is shown schematically in Figure 2. In this study, the level of interpolation applied was 20, such that, in a situation where the gantry speed is constant between control points separated by 4°, then the Monte Carlo simulation would resolve the VMAT dose calculation down to 0.2°.

Once a dose calculation has been performed (on a CT data set representing either the patient anatomy or a dosimetry phantom, as described below), a conversion is required to determine the absolute dose in Gy for each voxel of the dose array. At our centre, linacs are calibrated such that 100 MU gives 100 cGy at d_{max} in water for a 10x10cm, 100cm SSD field. As such, the following calibration was performed on each calculated dose voxel *i*:

$$D_i = M_i \times \frac{MU_e}{D_{cal} \times \left(\frac{N_e}{N_{cal}} \right)} \times F \quad (1)$$

where D_i is the dose in cGy, M_i is the calculated value from the Monte Carlo system, MU_e is the number of monitor units in the given plan for F number of fractions, N_e is the number of particles simulated in the experiment. D_{cal} is the value measured at d_{max} for a Monte Carlo simulation (with N_{cal} particles) of a 10x10cm field incident at 100cm SSD on a water phantom.

2.3. Validation measurements

To test the ability of the model to accurately simulate VMAT treatments, a number of plans were computed with the Monte Carlo system and compared to measurements on the linac. 10 VMAT plans in total were investigated, comprising 5 prostate patients and 5 head and neck patients, all of which were randomly selected and had previously been treated with VMAT in our department. Plans were created with the Pinnacle SmartArc module (Philips Medical Systems, Madison, USA). The prostate plans consisted of a single 6 MV VMAT arc travelling from a gantry angle of 181° to 180°, with a control point separation of 4° and a static collimator twist of 45°. A three dose level protocol was employed, with a prescription dose of 57 Gy in 19 fractions to the prostate, and lower doses to surrounding at-risk target volumes. The mean number of monitor units was 445.8 MU. Of the 5 head and neck patients, 3 had primary disease of the oropharynx, 1 in the hypopharynx, and 1 in the supraglottis. Three dose levels were prescribed for all sites: 66 Gy to PTV1, 60 Gy to PTV2 and 54 Gy to PTV3 using a simultaneous integrated boost (SIB) technique, in 30 fractions. All head and neck plans employed two counter-rotating VMAT arcs, with a control point separation of 4° and a collimator rotation of 10°. The mean monitor units for the head and neck plans was 534.6 MU.

All 10 plans were exported in DICOM-RT format both to the linac and the Monte Carlo system. For the prostates, dosimetric measurements were taken using the

Delta^4 phantom (Scandidos, Uppsala, Sweden). For the head and neck plans, a heterogeneous anthropomorphic phantom was used [35]. The MARVIN phantom has an anatomical design incorporating density heterogeneities in the mandible and nasal cavity. For this study, Gafchromic EBT2 film (ISP Corp. New Jersey, USA) was positioned in the mid-sagittal plane within the neck module of the MARVIN phantom. Each VMAT plan was delivered three times to the phantom to ensure adequate darkening of the EBT2 film, and then scanned on an Epson 10000 LX flatbed scanner. Scans were analysed using the red and green colour channels, before being converted to dose using a prior calibration.

For the Monte Carlo calculations, two strategies were compared – firstly, a fixed control point arrangement, analogous to the treatment planning system, whereby only the individual apertures (separated by 4°) were simulated. Secondly, the linac emulator was used to generate gantry and MLC positions between control points and approximate continuous delivery. Absorbed dose was calculated within Monte Carlo representations of the Delta^4 and MARVIN phantoms with a grid resolution of 2 x 2 x 2 mm. In order to determine the required number of particles to simulate, test runs were performed. The measurement uncertainty within the irradiated volume was estimated using the methodology described by Chetty *et al* [36] and reproduced below:

$$S_{d_K} = \sqrt{\frac{1}{N-1}\left(\frac{\sum_{i=1}^{N} d_{k,i}^{\,2}}{N} - \left(\frac{\sum_{i=1}^{N} d_{k,i}}{N}\right)^2\right)} \qquad (2)$$

where S_{dk} is the estimate of the error in the mean dose of voxel k, $d_{k,i}$ is the dose deposited in voxel k by the particle history i, and N is the total number of histories. It was found that, in order to ensure < 2 % uncertainty within the irradiated area, 20 billion photons were required for simulation. Dosimetric comparisons were then made between the Monte Carlo simulations (converted to absolute dose using equation 1) and the linac measurements. For the 10 VMAT plans, analysis was

performed at various gamma levels. Comparison between the fixed control point and the emulator simulations was made using a non-parametric Wilcoxon signed-rank test, where significance was demonstrated when $p < 0.05$.

2.4. Automated plan QA system

For practical implementation of the beam model into routine use, a 'one-click' verification system was developed, shown schematically in Figure 3. From the TPS the radiotherapy plan, CT images, structures and calculated dose are exported in DICOM-RT format to a host PC. Upon receipt of the DICOM files, the PC automatically anonymizes and packages the data for transfer to a Monte Carlo computing cluster. A system on the cluster then prepares the plan for dose calculation. At this stage, the system is able to override the densities of certain volumes - for example, to exclude the CT couch from the dose calculation the volume outside the body can be overridden to a density of air. Once the plan is ready for calculation, it is split into several 'jobs' and submitted to a cluster scheduler. For this study, the cluster consisted of 11 nodes each with a quad-core CPU (Intel i5-2500 @ 3.3GHz), thus allowing Monte Carlo runs to be divided into 44 simultaneous calculations.

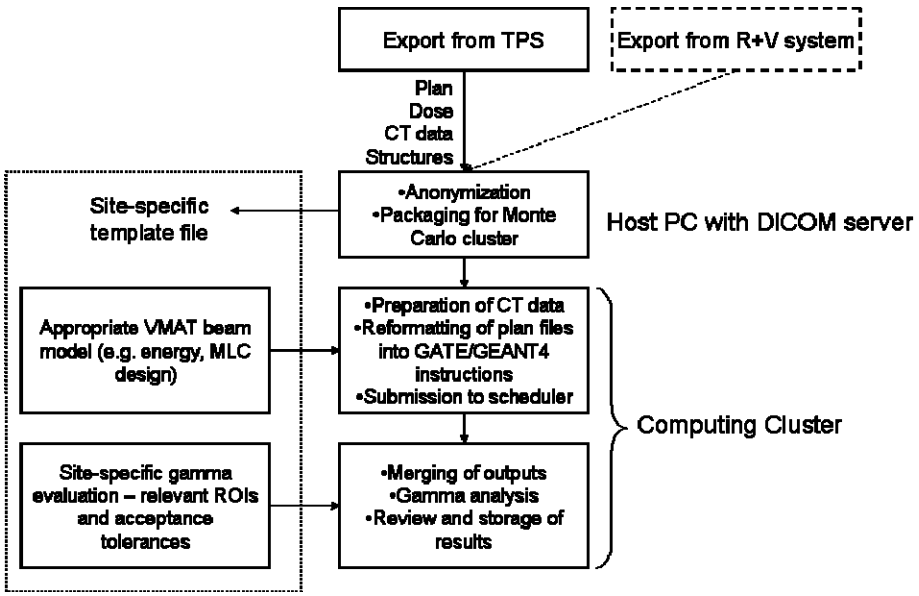

Figure 3. Flowchart detailing the process of the automated Monte Carlo plan verification system.

Following the calculation, the outputs are automatically merged into a single file containing the dose distribution. The system then performs a 3D gamma evaluation between the Monte Carlo dose and the TPS planned dose [37]. The software allows a wide range of configuration options to be set automatically as defined by a clinical site-specific configuration file. In the case of our test examples, the configuration settings for head and neck plans differed from prostate plans in the dose-difference (DD) and distance-to-agreement (DTA) criteria applied and in the ROIs selected for analysis.

Since the DICOM-RT structure geometries are also given as an input to the gamma analysis software, gamma results can be reported separately for selected organs and ROIs. This is a key advantage of performing the verification calculation on the patient CT dataset, as the location in the patient of any discrepancies can be identified and the potential clinical impact assessed. The software presents results in the form of ROI-specific gamma volume histograms [38], in addition to a summary reporting the percentage volume of each ROI having a gamma index <= 1.

For the purposes of demonstration, one prostate and one head and neck VMAT plan were verified with the automated QA system. Gamma evaluation was performed, along with the gamma statistics for various regions of interest, in order to examine the effectiveness and potential of the QA system.

3. Results

3.1. Monte Carlo model tuning

Within the full linac head model, an incident electron energy of 6.7 MeV and a Gaussian spot size of 3 mm full width at half-maximum (FWHM) was found to best match the depth dose curves and profiles of the real linac. Using the recorded phase space file, depth dose curves showed agreement compared to water tank measurements at field sizes of 4x4 cm, 10x10 cm and 20x20 cm. Figure 4a shows a comparison between plotting tank measurements and the Monte Carlo simulation.

Estimated uncertainty (calculated using equation 2) was below 2% within the 5% isodose line. From d_{max} to 30 cm deep in water, > 95% of the Monte Carlo calculation points passed a 2% / 2mm gamma evaluation at all field sizes (mean 99.1%). At 1% / 1 mm, > 90% of measurements point passed the gamma analysis (mean 90.8%).

Figure 4b shows comparisons between the Monte Carlo and measured MLC-defined profiles for 4x4 cm, 10x10 cm and 20x20 cm at 90 cm SSD. Gamma analysis between Monte Carlo and water tank measurements gave >90% points passing at the 2%/2mm level (mean 95.7%), and >95% at 3%/3mm (mean 96.5%).

Output factors (Figure 4c) were determined from field sizes of 2x2cm up to 40x40cm at 90cm SSD. The Monte Carlo model and water tank measurements were within 2% across the range of field sizes, indicating that phantom and head scatter is being modelled adequately. The average difference between the Monte Carlo calculated and measured output factors was −0.1% (st. dev. 0.9%).

Results of the MLC bar test, designed to confirm the modelling of the MLC leaves and leaf bank arrangement, are shown in Figure 4d. At 90cm SSD, 10cm deep in water, the Monte Carlo calculation had 91.4% of points passing a 2%/2mm gamma analysis compared to the plotting tank measurements, and 98.6% passing within 3%/3mm.

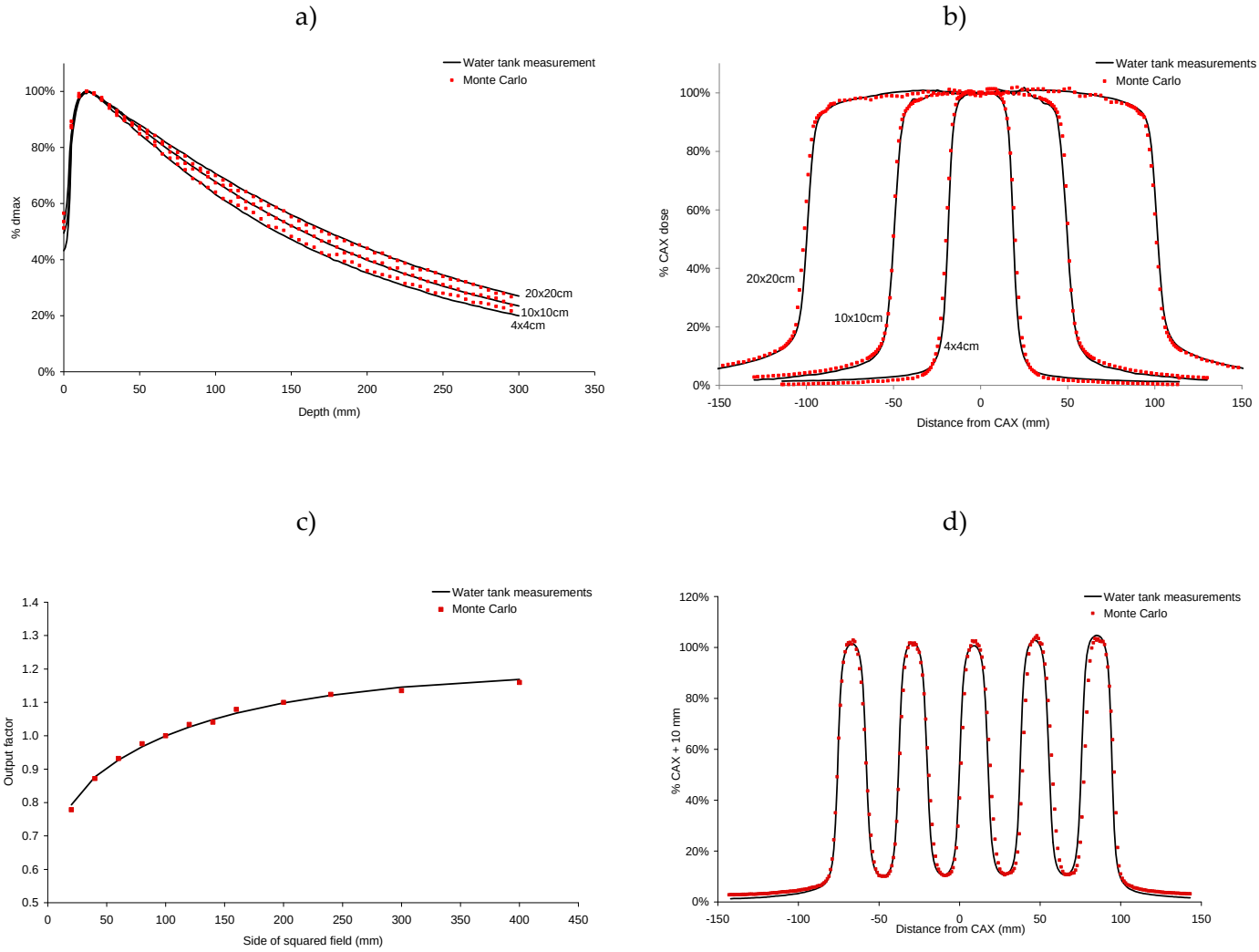

Figure 4. Result of the Monte Carlo head modelling, comparing calculated and water tank measurements for (a) depth dose curves at 100cm SSD, (b) MLC-defined profiles at 90cm SSD, 10cm depth, (c) output factors taken at 90cm SSD, 10cm depth, normalized to 10x10cm field size, (d) bar test taken at 90cm SSD, 10cm depth.

3.2. Comparison to phantom measurements

Gamma evaluations between the Monte Carlo-simulated and Delta^4-measured prostate plans are shown in Table 1. For all plans, gamma analysis was performed at a range of gamma levels within the 5% isodose. For the fixed control point simulation strategy, the mean gamma pass rates for 1%/1mm, 2%/2mm, and 3%/3mm were calculated as 73.7 (±1.1) %, 91.6 (±1.3) % and 98.6 (±0.9) % respectively. Modelling the linac positions with the emulator, the same gamma values were calculated as 77.0 (±1.5) %, 97.4 (±0.5) % and 100.0 (±0.0) %, which

showed significant improvement ($p < 0.01$ for all gamma levels) over the fixed control points.

	Fixed control points			Emulator		
Patient	1%/1mm	2%/2mm	3%/3mm	1%/1mm	2%/2mm	3%/3mm
1	74.17	91.77	97.54	77.58	97.82	100.00
2	75.02	93.50	97.54	75.31	98.02	100.00
3	74.01	91.43	99.44	78.99	97.28	100.00
4	72.41	91.09	99.15	77.36	96.70	100.00
5	72.87	90.00	99.15	75.92	97.17	100.00
Mean	**73.70**	**91.56**	**98.56**	**77.03**	**97.40**	**100.00**
St. dev.	**1.05**	**1.27**	**0.94**	**1.45**	**0.53**	**0.00**

Table 1. Gamma analysis results (% pixels with gamma < 1 within the 5% isodose) for the five prostate VMAT patients. Results are shown for both the fixed control point and the emulator Monte Carlo models.

For the dual-arc head and neck plans the gamma index was calculated by comparing the Monte Carlo measurement to Gafchromic film within the Marvin phantom (example shown in Figure 5). Results are given in Table 2. Over 5 patients, the mean gamma passes at the 2%/2mm, 3%/3mm and 4%/4mm were 73.7 (±3.7) %, 92.8 (±2.0) % and 98.8 (±0.7) % using the fixed control point simulation. Incorporating the emulator into the simulation, the same gamma analyses were calculated as 76.6 (±1.6) %, 93.8 (±3.2) % and 99.1 (±1.8) %. Statistical significance was only observed at the 2%/2mm level ($p < 0.01$), with $p > 0.1$ for the 3%/3mm and 4%/4mm analyses.

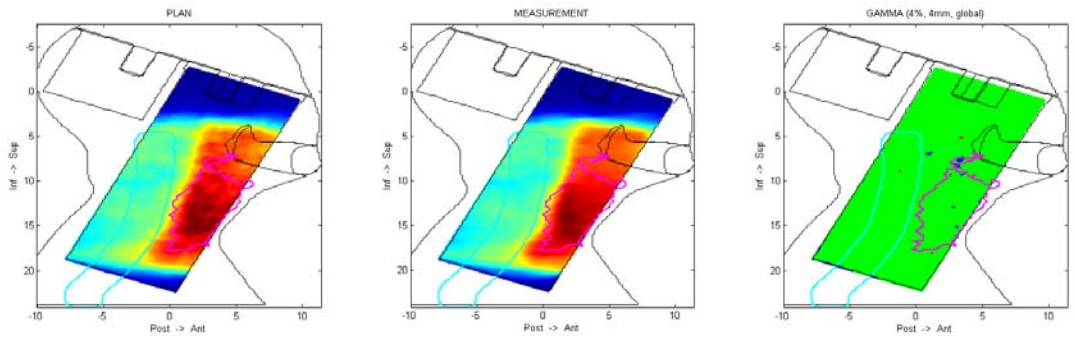

Figure 5. Gamma analysis (far right) between Monte Carlo calculation (left) and Gafchromic film (middle) within the MARVIN phantom for one of the head and neck patients. Green

indicates a gamma pass, blue and red are gamma failures (under- and over-dose respectively).

	Fixed control points			Emulator		
Patient	2%/2mm	3%/3mm	4%/4mm	2%/2mm	3%/3mm	4%/4mm
1	77.60	93.99	99.22	79.41	96.35	99.93
2	73.80	94.73	99.73	78.15	94.37	99.36
3	67.55	89.72	97.85	72.24	92.12	98.21
4	74.40	92.00	98.70	74.40	92.00	98.70
5	75.01	93.48	98.67	78.99	93.90	99.40
Mean	**73.67**	**92.78**	**98.83**	**76.64**	**93.75**	**99.12**
St. dev.	**3.72**	**1.98**	**0.70**	**1.59**	**3.16**	**1.79**

Table 2. Gamma analysis results (% pixels with gamma < 1 within the 5% isodose) for the five head and neck VMAT patients. Results are shown for both the fixed control point and the emulator Monte Carlo models.

3.3. Automated TPS verification on patient geometry

A prostate VMAT patient was exported from Pinnacle to the automated QA system for analysis. Results of the gamma evaluation (Monte Carlo versus TPS) are shown in Figure 6. The gamma pass at 3%/3mm within the body volume was 99.82%. This is in line with our centre's tolerance for prostate VMAT verification. As an example, gamma passes for various ROIs have also been reported in Figure 6, with all PTVs passing > 95%, and the rectum volume passing at 100%. It is possible to compare the dose-volume histograms (DVHs) from both the TPS dose grid and the dose calculated with the Monte Carlo system. In this instance, the target coverage (PTV1, PTV2 and PTV3) was found to be poorer than the Pinnacle-planned values. DVHs for the rectum and bladder were broadly similar, although a larger volume of low dose was observed with the Monte Carlo calculation. Median uncertainty of this measurement was estimated at 1.85% within the 5% isodose line.

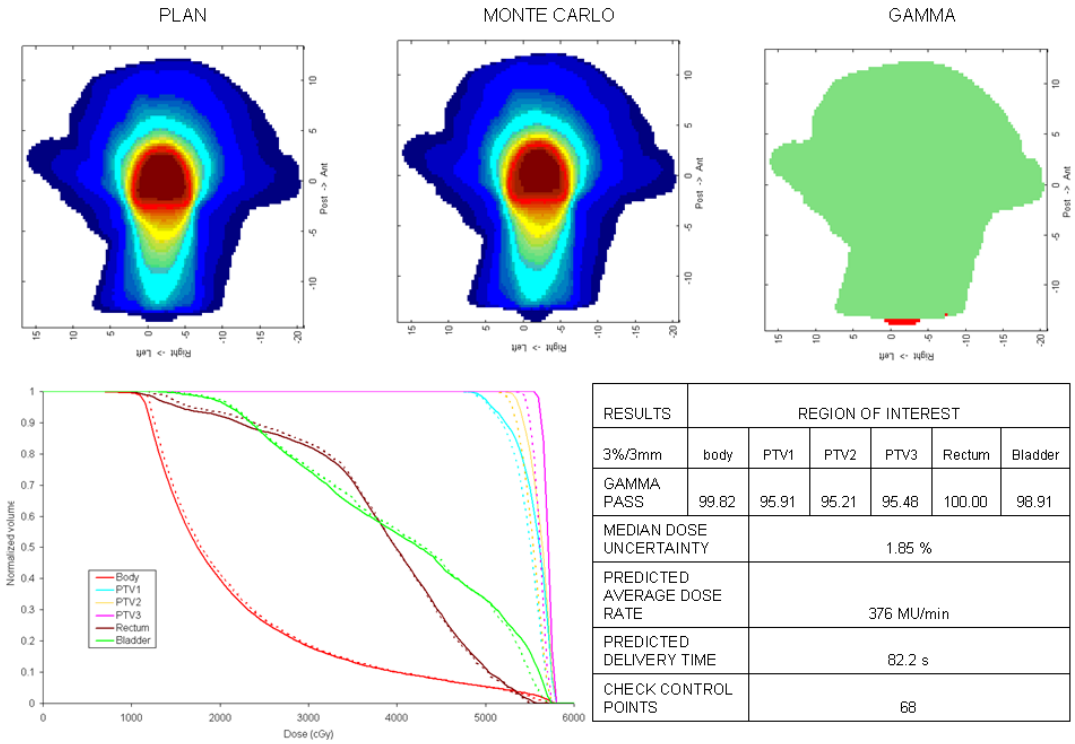

RESULTS	REGION OF INTEREST					
3%/3mm	body	PTV1	PTV2	PTV3	Rectum	Bladder
GAMMA PASS	99.82	95.91	95.21	95.48	100.00	98.91
MEDIAN DOSE UNCERTAINTY	1.85 %					
PREDICTED AVERAGE DOSE RATE	376 MU/min					
PREDICTED DELIVERY TIME	82.2 s					
CHECK CONTROL POINTS	68					

Figure 6. Results of the automated verification of a prostate VMAT patient. For the DVH, dashed lines represent the Monte Carlo doses, while solid lines are from the planning system.

Figure 6 also shows various outputs from the delivery emulator, including the predicted delivery time (82.2 s) and average dose rate (376 MU/min) over the arc. Following the methodology reported previously [33], the emulator also determines potentially problematic control points. These were defined as situations were one or more MLC leaves are >1 mm from their intended position at the end of a control point. In the example prostate patient, one control point (no. 68) was flagged for closer examination.

The results of a head and neck VMAT verification are shown in Figure 7. Following this centre's gamma analysis criteria for head and neck plan QA, it was found, for the target volumes, brainstem and spinal cord, that > 95 % pixels had a gamma < 1 at 4%/4mm. Within the 'body' outline, the gamma pass was 98.4%, in which the failing pixels were mainly confined to areas of air within the oral cavity and trachea. The Monte Carlo dose in these regions was very low due to the absence of tissue, whereas Pinnacle's dose calculation was higher. Extracting the dose-volume histograms for the target volumes and nearby organs at risk, the Monte Carlo-

calculated and Pinnacle-calculated distributions were similar over a range of doses. Median uncertainty of the calculation was 1.77% within the body volume. Again, aspects of the delivery were reported with a predicted average dose rate of 231 MU/min, and a total delivery time of 164.2 seconds. No potential leaf positioning errors were found by the emulator.

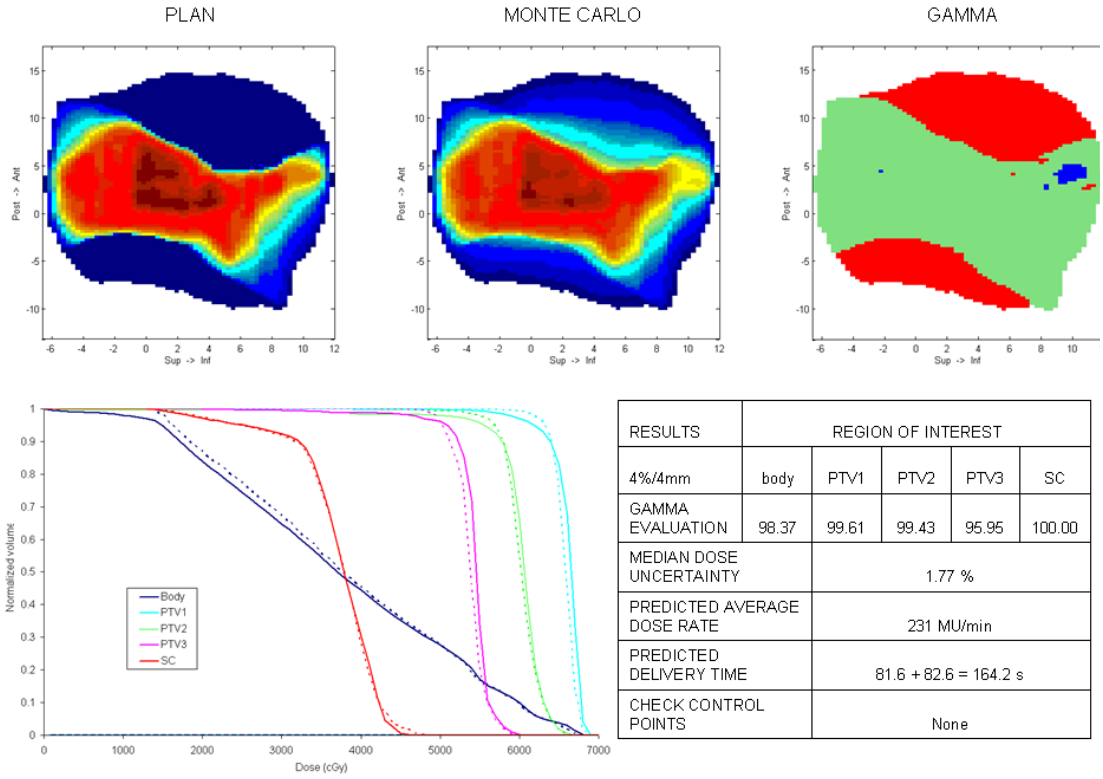

RESULTS	REGION OF INTEREST				
4%/4mm	body	PTV1	PTV2	PTV3	SC
GAMMA EVALUATION	98.37	99.61	99.43	95.95	100.00
MEDIAN DOSE UNCERTAINTY	1.77 %				
PREDICTED AVERAGE DOSE RATE	231 MU/min				
PREDICTED DELIVERY TIME	81.6 + 82.6 = 164.2 s				
CHECK CONTROL POINTS	None				

Figure 7. Results of the automated verification of a head and neck VMAT patient. For the DVH, dashed lines represent the Monte Carlo doses, while solid lines are from the planning system.

For comparison, the same head and neck plan was simulated again but with the linac delivery parameters adjusted. Whereas the results above were generated assuming the linac is capable of continuously-variable dose rate (CVDR, used within the Elekta Integrity system), the plan was repeated only allowing the older binned dose rate delivery (BDR, having only 5 fixed dose rate bins). For complex plans requiring large amounts of modulation, this makes a 'smooth' delivery more difficult. As would be expected, the emulator predicts a longer delivery time with BDR (total 250.9 s) and a lower average dose rate (143 MU/min). Lower gamma pass rates were observed for the analysed ROIs (PTV1: 97.96%, PTV2: 97.90, PTV3:

88.55%, spinal cord: 99.82%) at 4%/4mm within the 5% isodose line, compared to the CVDR simulation.

4. Discussion

The use of VMAT has gained widespread interest due to the ability to produce IMRT-equivalent dose distributions, which are deliverable in a significantly shorter treatment time. The widely-reported delivery efficiency of VMAT has allowed many centres to improve workflow, and hence increase the provision of intensity modulated delivery for a given linear accelerator [39, 40]. With IMRT there are well-established secondary dose calculations (monitor unit checkers) providing a layer of dosimetric confidence between the planning system and the linear accelerator. Such secondary dose checks are usually accompanied by pre-treatment verification measurements on a subset of patient plans. With VMAT, however, such a strategy is problematic. VMAT plans are heavily dependent on the ability of the linac to reliably modulate gantry speed, dose rate and MLC motion over an arc. These deliverability characteristics are not available in conventional treatment planning systems or secondary dose calculations. As such, the potential workflow benefits of VMAT are currently counteracted by the requirement for additional routine pre-treatment verification on the linac. Presented here is a software solution to reduce the number of these linac measurements, using Monte Carlo dose calculations to provide an independent check of the TPS. Realistic linac motion is accounted for within the model, such that a verification of both the planning system calculation and the linac deliverability can be determined.

The linac model was developed using GATE, which has previously been demonstrated as feasible for radiotherapy applications, and static modelling results agree with those presented by Grevillot *et al* [34] for a similar linear accelerator. The use of GEANT4-based Monte Carlo for radiotherapy has previously been primarily confined to research topics, and so the introduction of GATE – an open-source interface specifically designed for medical physics and radiotherapy applications –

is attractive for more clinically-focussed projects. The GEANT4 code itself has been validated for a large range of photon energies and also for hadron interactions, such that in the future GATE/GEANT4 may provide useful single platform for comparisons between photon and proton radiotherapy treatment plans [41]. We intend to also integrate a clinical proton beam model into the automated QA system presented here.

Measurements in the Delta^4 and MARVIN phantoms indicated that the Monte Carlo beam model was capable of accurate VMAT simulations. All gamma evaluations for prostate and head and neck deliveries were within this centre's tolerance for pre-treatment verification: i.e. that >95% of pixels should pass a 3%/3mm gamma evaluation for prostates, and 4%/4mm for head and neck patients. Tables 1 and 2 show that simulation of linac motion between control points (using the emulator) gave results which were closer to the phantom measurements compared to the simulation of fixed control points. For the prostate plans, statistical significance in favour of the delivery emulator was observed at all gamma levels (1%/1mm to 3%/3mm). For the head and neck plans, significance was only observed at 2%/2mm, indicating that the static and dynamic models were equivalent at 3%/3mm and 4%/4mm. The Monte Carlo model, through integration of the VMAT delivery emulator, thus provides a level of accuracy comparable with the dosimetric phantoms for the purposes of pre-treatment verification.

Previous VMAT Monte Carlo models have either simulated static control points, or used linear interpolation of the dose, gantry and MLC positions between the control points, and similar accuracy has been observed for both techniques [23]. However, linear interpolation may over-simplify VMAT delivery, particularly by assuming that gantry speed is constant between each control point. VMAT delivery can include scenarios where large changes are required in gantry speed [19]. In such situations, due to the finite gantry acceleration/deceleration time, MLCs may reach their next intended positions before gantry does, or (conversely) all MUs may have been delivered before gantry reaches intended position. In this study, the emulator

is capable of accounting for these scenarios, which may explain for the improvement observed when compared to the fixed simulations. As shown in the head and neck example, the same plan has an improved pass rates with CVDR delivery compared to binned dose rates – the only difference between the two simulations being the characteristically 'smoother' switching between dose rates and gantry speeds with CVDR [13].

Verification examples were provided here for prostate and head and neck patients, allowing a gamma comparison to be made between the TPS and Monte Carlo for various regions of interest. These results could be useful in determining systematic differences between planned and measured dose-volume histograms. Having gamma pass rates for individual ROIs may also be useful, as it is an indication of the quality of the plan in clinically relevant structures. It should be noted that some of the available dosimetric devices for IMRT and VMAT QA (such as the Delta^4, ArcCheck and Octavius phantoms), now provide some form of measured DVH analysis – similar to that presented for the Monte Carlo system. However, these tools require some conversion from the geometry of the detector system to the geometry of the patient, and it is not clear to what extent these tools have been validated.

The automated verification system (Figure 3) has been developed in order to easily integrate the Monte Carlo model into routine use. By automatically setting up and scheduling the calculations from a single-click TPS export, all VMAT patients can be sent for independent verification as part of routine planning and checking. Work is now underway to determine acceptable tolerances for the verification and to identify problematic or complex VMAT plans. For the practical implementation of this system, it is intended that a reduced programme of pre-treatment linac verification will remain. The Monte Carlo system will thus allow more targeted linac verifications – i.e. concentrating on plans which drop below a certain gamma tolerance, or (as in the example prostate plan in this study) contain potentially problematic control points.

Computing hardware has a significant impact on the speed of Monte Carlo calculations. The patient calculations presented here required approximately 400-600 CPU hours to achieve a calculated uncertainty within the 5 % isodose of < 2%. For the 44 core cluster used in this study, this translated to a mean calculation time of ~10-12 hours running on all cores. The cluster, therefore, does not presently offer the level of practicality required for integration into the clinical workflow. While the cluster is capable of expansion, it will be of interest to deploy the verification system on different computing architectures, such as a grid [42] or Condor pool (HTCondor, University of Madison, WI, USA) [43]. Test runs on the University of Manchester Condor system have yielded equivalent uncertainty simulations in less than one hour, due to the access to several hundred nodes. Alternatively the use of programmable graphics processing units (GPUs) for Monte Carlo is gaining increasing attention [44]. Generally, the trend towards faster hardware and more optimized algorithms indicates that the routine clinical use of Monte Carlo (for both planning and QA) is becoming achievable.

The movement to software-based plan verification means that routine linac quality assurance (and preventative maintenance) is of paramount importance. A number of authors have discussed quality control tests specific to VMAT and suggested the frequency of such tests [45, 46]. Furthermore, plan verification on the linac would normally provide a check of the file transfer between the TPS and the record-and-verify (R&V) system. Presently at our centre, transfer checks for IMRT are performed either by linac-based verification, or through manual inspection of the segment shapes and MUs. For VMAT the latter strategy becomes unfeasible, as there can be large numbers of control points (e.g. 180 for the head and neck plans in this study). To account for this, the verification system presented here is capable of reading plans exported from R&V systems as well, thus providing a check of plan file transfers prior to treatment. It may also be of interest to verify the VMAT plans retrospectively from linac delivery log files, as has been demonstrated previously [29, 47]. While the present system here is focussed on pre-treatment verification

without the need for machine access, a complete verification system incorporating both planned and delivered dosimetric analysis would be of additional value.

5. Conclusions

This study has introduced and validated a plan verification system for VMAT radiotherapy, utilizing a GATE/GEANT4 Monte Carlo model. Through comparison to phantom measurements, it was found that the incorporation of a realistic linac motion emulator improves the accuracy of the model compared to the simulation of fixed control points. The model has been integrated into an automated verification system which prepares, schedules and distributes the calculations on a computing cluster. Work is now being done to determine acceptable tolerances for the calculations, which will allow for more targeted machine verifications and hence a reduction in the amount of required linac measurement time. Further development of the computing architecture is also underway to meet clinical workload demands.

Acknowledgements and Conflict of Interest Statement

The authors would like to thank the OpenGate community for their support, the University of Manchester's Condor computing team, and Elekta for providing modelling details. CB's post is partly funded by an Elekta research grant**.**

References

1. Fraass, B., et al., *American Association of Physicists in Medicine Radiation Therapy Committee Task Group 53: quality assurance for clinical radiotherapy treatment planning.* Med Phys, 1998. **25**(10): p. 1773-829.
2. IMRT-CWG, *Intensity-modulated radiotherapy: current status and issues of interest.* Int J Radiat Oncol Biol Phys, 2001. **51**(4): p. 880-914.
3. James, H.E., *Guidance for the Clinical Implementation of Intensity Modulated Radiation Therapy*. 2008: Institute of Physics and Engineering in Medicine.
4. Ayyangar, K.M., et al., *Independent calculations to validate monitor units from ADAC treatment planning system.* Med Dosim, 2003. **28**(2): p. 79-83.
5. Ma, C.M., et al., *A quality assurance phantom for IMRT dose verification.* Phys Med Biol, 2003. **48**(5): p. 561-72.

6. Moran, J.M., et al., *Safety considerations for IMRT: executive summary.* Med Phys, 2011. **38**(9): p. 5067-72.
7. Yu, C.X. and G. Tang, *Intensity-modulated arc therapy: principles, technologies and clinical implementation.* Phys Med Biol, 2011. **56**(5): p. R31-54.
8. Bedford, J.L., et al., *Evaluation of the Delta4 phantom for IMRT and VMAT verification.* Phys Med Biol, 2009. **54**(9): p. N167-76.
9. Van Esch, A., et al., *On-line quality assurance of rotational radiotherapy treatment delivery by means of a 2D ion chamber array and the Octavius phantom.* Med Phys, 2007. **34**(10): p. 3825-37.
10. Yan, G., et al., *Calibration of a novel four-dimensional diode array.* Med Phys, 2010. **37**(1): p. 108-15.
11. Pasler, M., H. Wirtz, and J. Lutterbach, *Impact of gantry rotation time on plan quality and dosimetric verification--volumetric modulated arc therapy (VMAT) vs. intensity modulated radiotherapy (IMRT).* Strahlenther Onkol, 2011. **187**(12): p. 812-9.
12. Kung, J.H., G.T. Chen, and F.K. Kuchnir, *A monitor unit verification calculation in intensity modulated radiotherapy as a dosimetry quality assurance.* Med Phys, 2000. **27**(10): p. 2226-30.
13. Iftimia, I., et al., *Quality assurance methodology for Varian RapidArc treatment plans.* J Appl Clin Med Phys, 2010. **11**(4): p. 3164.
14. Ma, C.M., et al., *Monitor unit calculation for Monte Carlo treatment planning.* Phys Med Biol, 2004. **49**(9): p. 1671-87.
15. Yang, Y., et al., *Independent dosimetric calculation with inclusion of head scatter and MLC transmission for IMRT.* Med Phys, 2003. **30**(11): p. 2937-47.
16. Bertelsen, A., E.L. Lorenzen, and C. Brink, *Validation of a new control system for Elekta accelerators facilitating continuously variable dose rate.* Med Phys, 2011. **38**(8): p. 4802-10.
17. Matuszak, M.M., et al., *Clinical applications of volumetric modulated arc therapy.* Int J Radiat Oncol Biol Phys, 2010. **77**(2): p. 608-16.
18. Verbakel, W.F., et al., *Rapid delivery of stereotactic radiotherapy for peripheral lung tumors using volumetric intensity-modulated arcs.* Radiother Oncol, 2009. **93**(1): p. 122-4.
19. Chetty, I.J., et al., *Report of the AAPM Task Group No. 105: Issues associated with clinical implementation of Monte Carlo-based photon and electron external beam treatment planning.* Med Phys, 2007. **34**(12): p. 4818-53.
20. Verhaegen, F. and J. Seuntjens, *Monte Carlo modelling of external radiotherapy photon beams.* Phys Med Biol, 2003. **48**(21): p. R107-64.
21. Fix, M.K., et al., *A multiple source model for 6 MV photon beam dose calculations using Monte Carlo.* Phys Med Biol, 2001. **46**(5): p. 1407-27.
22. Reynaert, N., et al., *MCDE: a new Monte Carlo dose engine for IMRT.* Phys Med Biol, 2004. **49**(14): p. N235-41.
23. Spezi, E. and G. Lewis, *An overview of Monte Carlo treatment planning for radiotherapy.* Radiat Prot Dosimetry, 2008. **131**(1): p. 123-9.
24. Spezi, E., D.G. Lewis, and C.W. Smith, *A DICOM-RT-based toolbox for the evaluation and verification of radiotherapy plans.* Phys Med Biol, 2002. **47**(23): p. 4223-32.

25. Pisaturo, O., et al., *A Monte Carlo-based procedure for independent monitor unit calculation in IMRT treatment plans.* Phys Med Biol, 2009. **54**(13): p. 4299-310.
26. Lobo, J. and I.A. Popescu, *Two new DOSXYZnrc sources for 4D Monte Carlo simulations of continuously variable beam configurations, with applications to RapidArc, VMAT, TomoTherapy and CyberKnife.* Phys Med Biol, 2010. **55**(16): p. 4431-43.
27. Belec, J., et al., *Position-probability-sampled Monte Carlo calculation of VMAT, 3DCRT, step-shoot IMRT, and helical tomotherapy dose distributions using BEAMnrc/DOSXYZnrc.* Med Phys, 2011. **38**(2): p. 948-60.
28. Bush, K., et al., *Monte Carlo evaluation of RapidArc oropharynx treatment planning strategies for sparing of midline structures.* Phys Med Biol, 2010. **55**(16): p. 4465-79.
29. Teke, T., et al., *Monte Carlo based, patient-specific RapidArc QA using Linac log files.* Med Phys, 2010. **37**(1): p. 116-23.
30. Fleckenstein, J., et al., *Development of a Geant4 based Monte Carlo Algorithm to evaluate the MONACO VMAT treatment accuracy.* Z Med Phys, 2012.
31. Bush, K., R. Townson, and S. Zavgorodni, *Monte Carlo simulation of RapidArc radiotherapy delivery.* Phys Med Biol, 2008. **53**(19): p. N359-70.
32. Jan, S., et al., *GATE V6: a major enhancement of the GATE simulation platform enabling modelling of CT and radiotherapy.* Phys Med Biol, 2011. **56**(4): p. 881-901.
33. Boylan, C.J., C.G. Rowbottom, and R.I. Mackay, *The use of a realistic VMAT delivery emulator to optimize dynamic machine parameters for improved treatment efficiency.* Phys Med Biol, 2011. **56**(13): p. 4119-33.
34. Grevillot, L., et al., *Simulation of a 6 MV Elekta Precise Linac photon beam using GATE/GEANT4.* Phys Med Biol, 2011. **56**(4): p. 903-18.
35. Mackay, R.I., A.H. Aitkenhead, and C.G. Rowbottom, *EP-1331 Experience using an anatomical head and neck phantom for verification and audit of complex radiotherapy.* Radiotherapy and Oncology, 2012. **103, Supplement 1**(0): p. S506.
36. Chetty, I.J., et al., *Reporting and analyzing statistical uncertainties in Monte Carlo-based treatment planning.* Int J Radiat Oncol Biol Phys, 2006. **65**(4): p. 1249-59.
37. Low, D.A., et al., *A technique for the quantitative evaluation of dose distributions.* Med Phys, 1998. **25**(5): p. 656-61.
38. Spezi, E. and D.G. Lewis, *Gamma histograms for radiotherapy plan evaluation.* Radiother Oncol, 2006. **79**(2): p. 224-30.
39. Fogarty, G.B., et al., *Volumetric modulated arc therapy is superior to conventional intensity modulated radiotherapy--a comparison among prostate cancer patients treated in an Australian centre.* Radiat Oncol, 2011. **6**: p. 108.
40. Studenski, M.T., et al., *Clinical experience transitioning from IMRT to VMAT for head and neck cancer.* Med Dosim, 2012.
41. Grevillot, L., et al., *GATE as a GEANT4-based Monte Carlo platform for the evaluation of proton pencil beam scanning treatment plans.* Phys Med Biol, 2012. **57**(13): p. 4223-44.
42. Thiam, C.O., et al., *Validation of a dose deposited by low-energy photons using GATE/GEANT4.* Phys Med Biol, 2008. **53**(11): p. 3039-55.

43. Baum, K.G. and M. Helguera, *Execution of the SimSET Monte Carlo PET/SPECT simulator in the condor distributed computing environment.* J Digit Imaging, 2007. **20 Suppl 1**: p. 72-82.
44. Jahnke, L., et al., *GMC: a GPU implementation of a Monte Carlo dose calculation based on Geant4.* Phys Med Biol, 2012. **57**(5): p. 1217-29.
45. Ling, C.C., et al., *Commissioning and quality assurance of RapidArc radiotherapy delivery system.* Int J Radiat Oncol Biol Phys, 2008. **72**(2): p. 575-81.
46. Bedford, J.L. and A.P. Warrington, *Commissioning of volumetric modulated arc therapy (VMAT).* Int J Radiat Oncol Biol Phys, 2009. **73**(2): p. 537-45.
47. Qian, J., et al., *Dose reconstruction for volumetric modulated arc therapy (VMAT) using cone-beam CT and dynamic log files.* Phys Med Biol, 2010. **55**(13): p. 3597-610.

(page intentionally blank)

2.6. Publication 6

A megavoltage scatter correction technique for cone-beam CT images acquired during VMAT delivery

Published in Physics in Medicine and Biology, 2012, vol. 57, pp. 3727-3739

Authors:

CJ Boylan
TE Marchant
J Stratford
J Malik
A Choudhury
R Shrimali
J Rogers
CG Rowbottom

Author Contributions

Hypothesis:

I hypothesised that scatter corrected simultaneous CBCTs taken during VMAT delivery could provide sufficient image quality for IGRT. I proposed the technique whereby a separate set of 'scatter' acquisitions are used to correct the simultaneous acquisitions.

Methodology:

The technique to allow the reconstruction of CBCTs from fluoroscopic kV images was developed by myself and TEM. I developed the scatter correction techniques, and wrote the software. The CBCT scoring technique was originally produced by RS and then refined by JR. The clinical staff (JS, JM, AC and JR) scored the patient images.

Analysis:

I performed the analysis of the phantom and patient measurements, evaluated the scatter correction methods, and wrote the manuscript.

13 pages

Phys. Med. Biol. **57** (2012) 3727–3739 doi:10.1088/0031-9155/57/12/3727

A megavoltage scatter correction technique for cone-beam CT images acquired during VMAT delivery

C J Boylan[1,2], T E Marchant[1,2], J Stratford[3], J Malik[4], A Choudhury[4], R Shrimali[4], J Rodgers[3] and C G Rowbottom[1,2]

[1] Christie Medical Physics and Engineering (CMPE), The Christie NHS Foundation Trust, Wilmslow Road, Manchester M20 4BX, UK
[2] Manchester Academic Health Science Centre (MAHSC), Faculty of Medical and Human Sciences, University of Manchester, Manchester M13 9PL, UK
[3] Wade Centre for Radiotherapy Research, The Christie NHS Foundation Trust, Wilmslow Road, Manchester M20 4BX, UK
[4] Department of Radiation Oncology, The Christie NHS Foundation Trust, Wilmslow Road, Manchester M20 4BX, UK

E-mail: christopher.boylan@christie.nhs.uk

Received 24 February 2012, in final form 30 March 2012
Published 23 May 2012
Online at stacks.iop.org/PMB/57/3727

Abstract

Kilovoltage cone-beam CT (kV CBCT) can be acquired during the delivery of volumetric modulated arc therapy (VMAT), in order to obtain an image of the patient during treatment. However, the quality of such CBCTs is degraded by megavoltage (MV) scatter from the treatment beam onto the imaging panel. The objective of this paper is to introduce a novel MV scatter correction method for simultaneous CBCT during VMAT, and to investigate its effectiveness when compared to other techniques. The correction requires the acquisition of a separate set of images taken during VMAT delivery, while the kV beam is off. These images—which contain only the MV scatter contribution on the imaging panel—are then used to correct the corresponding kV/MV projections. To test this method, CBCTs were taken of an image quality phantom during VMAT delivery and measurements of contrast to noise ratio were made. Additionally, the correction was applied to the datasets of three VMAT prostate patients, who also received simultaneous CBCTs. The clinical image quality was assessed using a validated scoring system, comparing standard CBCTs to the uncorrected simultaneous CBCTs and a variety of correction methods. Results show that the correction is able to recover some of the low and high-contrast signal to noise ratio lost due to MV scatter. From the patient study, the corrected CBCT scored significantly higher than the uncorrected images in terms of the ability to identify the boundary between the prostate and surrounding soft tissue. In summary, a simple MV scatter correction method has been developed and,

using both phantom and patient data, is shown to improve the image quality of simultaneous CBCTs taken during VMAT delivery.

(Some figures may appear in colour only in the online journal)

1. Introduction

Volumetric modulated arc therapy (VMAT) is now established as an effective technique for delivering intensity modulated dose distributions comparable to fixed-beam IMRT (Yu and Tang 2011). Crucially, VMAT offers a significant delivery time advantage due to the simultaneous rotation of the linear accelerator gantry, movement of the multi-leaf collimators (MLCs) and modulation of the dose rate (Otto 2008, Cao *et al* 2009, Zhang *et al* 2010). The rotational geometry of VMAT delivery has more recently been exploited to acquire kilovoltage cone-beam computed tomography (kV CBCT) images concurrently during treatment, with the linac delivering the megavoltage (MV) treatment beam and a kV imaging beam orthogonally (Nakagawa *et al* 2009a, 2011).

There are a number of advantages in acquiring kV cone-beam images during treatment delivery. With the aim of treatment to deliver radiation doses safely but effectively, there is the increasing use of image-guided radiotherapy (IGRT) to ensure that the therapeutic ratio is optimized (Verellen *et al* 2008). Simultaneous cone-beam imaging during VMAT allows IGRT to be performed with images of patient anatomy *in vivo* rather than before or after treatment. Studies investigating intrafractional changes in patient position suggest there is an advantage to be gained from knowledge of internal anatomy during treatment (Nakagawa *et al* 2009b). Such knowledge could influence the choice of treatment margins and/or prescription dose, particularly for stereotactic patients, for whom accurate positioning is paramount (Sonke *et al* 2009). Simultaneous cone-beam imaging during VMAT also reduces the amount of in-room time for the patient, providing an advantage for department throughput.

While simultaneous cone-beam imaging is desirable, its quality is significantly degraded by MV x-ray scatter from the linac head, patient and support structures onto the kV imager (Williams *et al* 2004). The effect of this scatter is to introduce significant noise into the images, reducing the visibility of low contrast soft tissue boundaries and therefore making it difficult to perform soft tissue registration. Furthermore, any potential adaptive replanning strategy using simultaneous CBCTs is likely to be complicated by the difficulty in reliably outlining the target volume and organs at risk.

A number of solutions have been proposed to recover image quality, either by predicting the MV scatter contribution from the plan (Hugo *et al* 2008), through direct measurement of the scatter concurrently during delivery (van Herk *et al* 2011), or by avoiding MV scatter altogether by dividing the treatment arc into interlaced sectors for treatment and imaging (Ling *et al* 2011). Each of these methods have potential limitations. Prediction of the scatter using the treatment plan requires detailed knowledge of the linac motion and assumes that the scatter is uniform in the plane of the detector. The method proposed by van Herk *et al* (2011) notes that measurement of the scatter using alternate kV-on and kV-off frames halves the total number of projections for reconstruction, which may not cause major problems for slow treatments (i.e. stereotactic), but will reduce the quality of images taken during shorter delivery times. Furthermore, periodic interruption of the treatment beam for imaging, as described by Ling *et al* (2011), is appropriate only if plan quality is retained and delivery duration is not significantly increased. A direct measurement of MV scatter, which does not reduce the number of imaging frames or require the interruption of the treatment arc, is therefore desirable.

Table 1. Reference cone-beam imaging protocol for prostate patients.

Tube potential	120 kV
Nominal mAs per frame	40 mAs
Collimation	Medium field of view (MFOV)
Imaging dose	7.9 mGy
Pulse length	16 ms
Approx. number of frames	∼650

The purpose of this paper is to investigate the effectiveness of a novel MV scatter correction technique. In contrast to other proposed methods, the correction utilizes a direct measurement of MV scatter such that it is patient and plan specific. Different variants of this method were first assessed through quantitative measurements of image quality on a phantom. The correction was then applied to three sets of simultaneous CBCT images from VMAT prostate treatments. A comparison of clinical image quality was then made, using an objective, validated scoring system for prostate CBCT images.

2. Method

2.1. Phantom study

The image quality phantom used was the CATPhan 600 (Phantom Laboratory, Salem, USA), which was surrounded by additional scatter material to mimic the size and shape of the pelvis (figure 1(a)). The phantom was set up at the isocentre of an Elekta linear accelerator fitted with the Synergy CBCT system version 4.2 (Elekta, Crawley, UK). Reference cone-beam images were taken (without MV delivery), using the standard prostate imaging protocol from this centre (parameters in table 1).

CBCT acquisitions were then taken concurrently during three different VMAT deliveries. The deliveries were all previously treated VMAT prostate plans, typical of the current treatments at this centre, where the prescription is 57 Gy in 19# to the mean of the prostate. The plans were created using Pinnacle v.9.0 (Philips Medical Systems, Madison, USA) and consisted of a single 8 MV arc, 4 degree control point spacing and a mean of 488 monitor units. In order to perform the scatter correction, the individual frames of the acquisition were retrieved for processing prior to back projection.

2.2. Scatter correction methodology

2.2.1. 2D scatter map from patient during treatment. A direct measurement of the scatter contribution was made by allowing the kV imager to acquire frames during VMAT treatment, but without a kV imaging beam. These scatter images are a series of 1024×1024 acquisitions taken at a constant frame rate over the treatment. The signal from these images is due only to the MV scatter received by panel, and therefore fluctuates over the course of the VMAT arc. For the CATPhan, the scatter images were taken immediately after the corresponding simultaneous MV/kV acquisition. As described later, the patient scatter images were acquired on a non-imaging treatment fraction.

Both the simultaneous CBCT frames, and the scatter images contain interference artefacts from the pulsing of the treatment beam, in the form of vertical lines. These artefacts were suppressed by identifying the position of the peaks and smoothing them. The scatter images also required further processing, such as the application of a 'bad pixel' mask and a median filter to remove excessive high frequency noise.

(a)

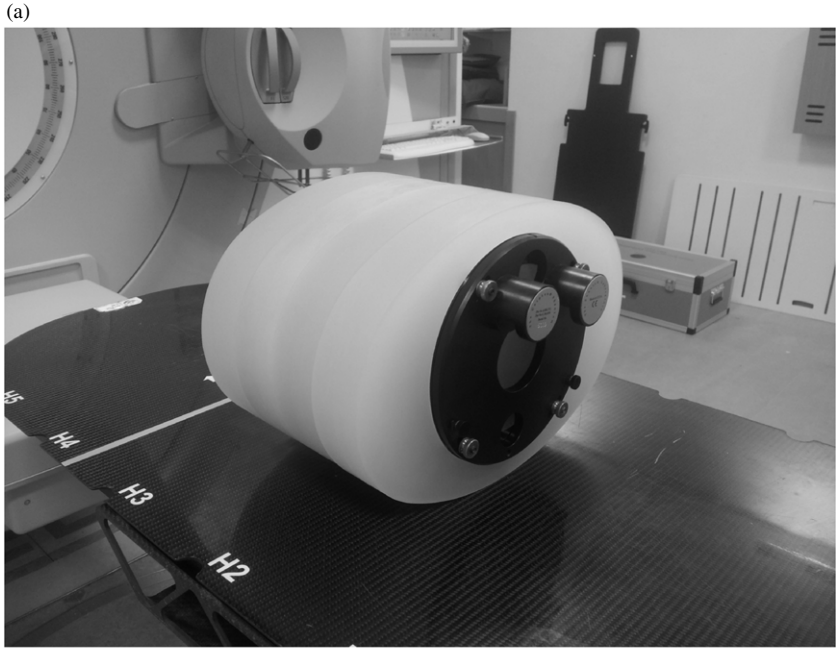

(b)

Figure 1. (a) The CATPhan image quality phantom for kV CBCT, within additional scatter material, (b) the RANDO anatomical phantom (torso only).

For all projections acquired using the Synergy system, the associated linac gantry angle is recorded. In order to carry out the scatter correction, software was written which cycled through the simultaneous CBCT images and found the closest scatter image based on the

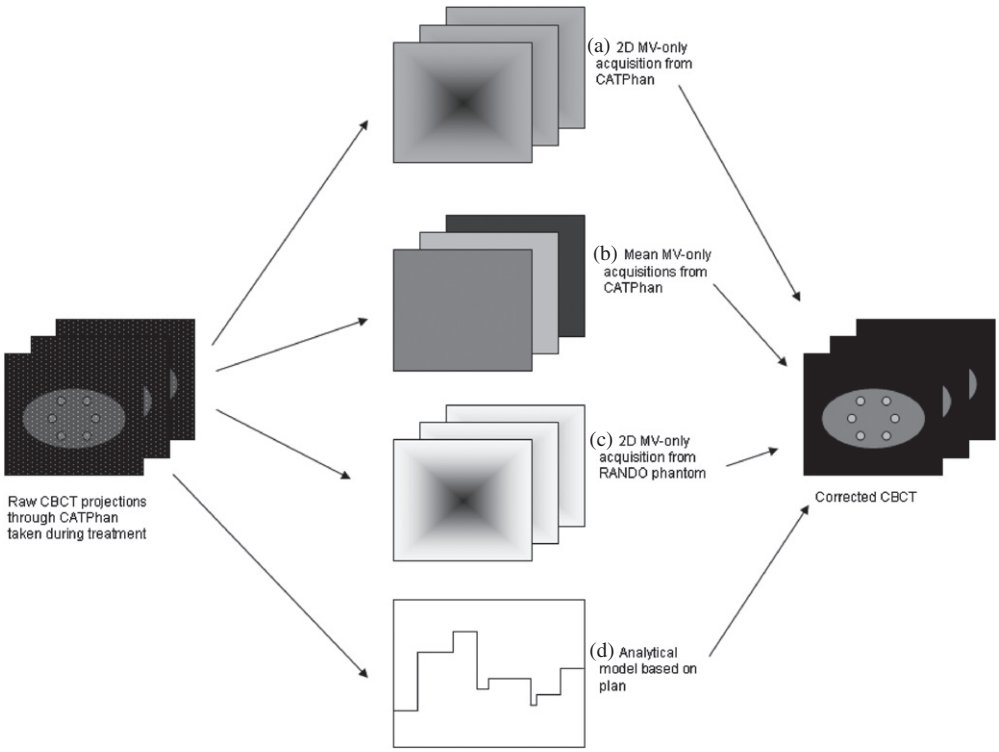

Figure 2. Schematic showing the correction strategies employed for the phantom imaging study.

gantry angle. A subtraction of the scatter image was then made. Details are given below of the other variants investigated for this study, and are shown schematically in figure 2.

2.2.2. 1D uniform scatter map. The method described above uses a 2D image of the MV scatter for correction. However, it is apparent that there is no distinct structure or shape visible in the scatter images—instead they consist of a coarse 'glow' of higher signal intensity in the centre dropping slowly to the edges of the imager (figure 3). Therefore, the scatter correction was also tested by subtracting the mean signal of each scatter image from the corresponding simultaneous image.

2.2.3. 2D scatter map from different scattering material. Methods (a) and (b) both utilize the MV scatter-only images taken during the CATPhan 'treatments'. In order to investigate the sensitivity of the MV scatter to patient size and shape, scatter images were also acquired using a different phantom. Delivering the same plans to the RANDO phantom (Phantom Laboratory, Salem, USA), pictured in figure 1(b), the scatter images were acquired again and scatter correction was applied as described in (a) on the simultaneous CATPhan projections.

2.2.4. Analytical correction. Hugo *et al* (2008) suggests that the MV scatter at a given gantry angle can be estimated with the product of the dose rate and the field size at that point. In order to compare this analytical model to direct measurement of scatter, each treatment plan was run through a VMAT delivery emulator (Boylan *et al* 2011) to predict the dose rate over the arc. The exposed field area was also calculated for each gantry angle. An estimate

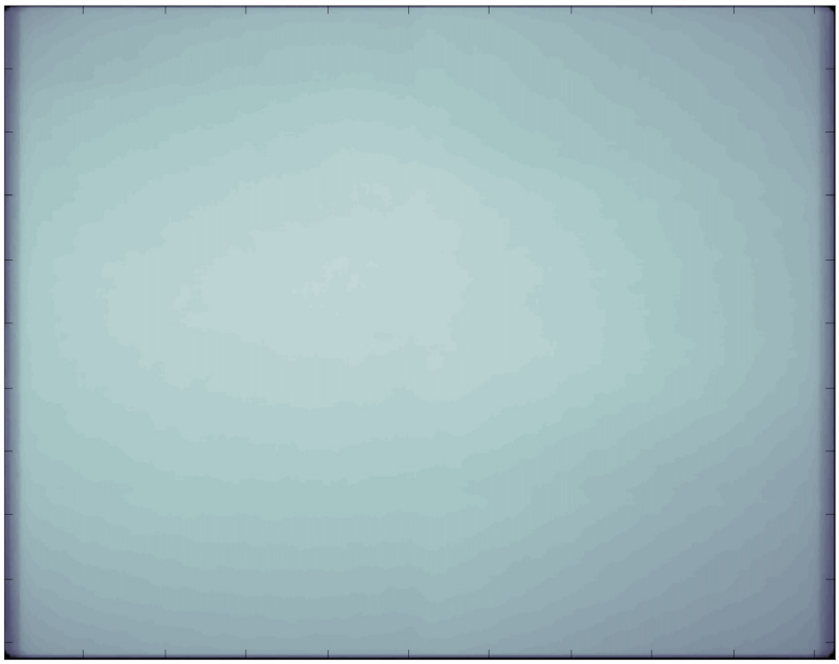

Figure 3. One of the MV scatter-only frames taken during VMAT delivery. Scatter correction method (a) utilizes the full 2D data from these frames, whereas method (b) takes the mean signal.

of MV scatter was made by multiplying these values and applying a single empirical scaling factor based on experiment. For each simultaneous MV/kV projection, the estimated scatter was then subtracted prior to reconstruction.

For methods (a)–(d), the corrected projections were reconstructed using the same algorithm as the standard prostate kV-only CBCTs. Using the CTP404 test module within the CATPhan, low and high-contrast signal to noise ratios (SNR) were measured for the standard CBCTs, the uncorrected simultaneous CBCTs, and the four scatter corrected CBCTs (a)–(d). The low-contrast SNR was calculated as

$$\mathrm{SNR}_{\mathrm{low}} = \frac{\bar{x}_{\mathrm{LDPE}} - \bar{x}_{\mathrm{PMP}}}{\sigma_{\mathrm{centre}}},$$

where $\bar{x}_{\mathrm{LDPE}}$ is the mean signal in the LDPE (low-density polyethylene) insert, $\bar{x}_{\mathrm{PMP}}$ is the mean signal in the PMP (polymethylpentene) insert, and σ_{centre} is the standard deviation of the signal in the centre of the CATPhan. The high-contrast SNR was calculated similarly but using the signals from the Delrin® insert (which has a similar density to cortical bone) and PMP.

2.3. Patient study

A study is ongoing in this centre investigating the clinical value of CBCT images acquired simultaneously with VMAT delivery. The Simultaneous Cone-beam during Arc Therapy (SCART) study is a non-randomized phase 1 trial in which standard VMAT prostate patients (57 Gy in 19) receive four simultaneous CBCTs over the course of their treatment. The usual imaging protocol at this centre is to take a minimum of 6 CBCT during treatment, on fractions

Table 2. Prostate CBCT image quality scoring scale.

Score	Description
1	Able to define all interfaces between the prostate and peri-prostatic tissues. Appropriate for clinical decision making.
2	Able to identify the soft tissue interface between the prostate and the anterior rectum, *and* the prostate and the posterior-superior bladder. Appropriate for clinical decision making.
3	Able to identify the soft tissue interface between the prostate and the anterior rectum only. Appropriate for clinical decision making.
4	Difficult to define the interface between the prostate and the rectum/bladder, however, able to identify anterior rectal wall and thus infer the position of the posterior prostate border. Appropriate for clinical decision making.
5	Low quality image. Prostate, rectum and bladder appear as a homogenous mass with soft tissue delineation planes difficult to visualise, or too many artefacts to be able to infer the position of the prostate. Inappropriate for clinical decision making.

1, 2, 3, 6, 11 and 16. In addition to this, the SCART patients receive simultaneous CBCTs on fractions 2, 6, 11 and 16. By comparing the simultaneous CBCTs to the standard CBCTs taken on the same fraction, the ultimate aim of the SCART study is to assess whether these images are appropriate for clinical decision-making—i.e. the ability to perform soft tissue registration to reliably assess the coverage of the target volume and avoidance of organs at risk.

For the present study, the sixth fraction images from the first three SCART patients were retrieved. For each patient, a standard CBCT (parameters as in table 1) and a simultaneous CBCT were acquired on this fraction. The MV scatter images, required for correction, were acquired as described in section 2.2 during a non-imaging fraction of the patient's treatment. For example, the scatter images for patient 1 were taken during fraction 10 of 19.

Clinical image quality was assessed using a validated scoring system developed for the SCART trial, which is specific to prostate cone-beam imaging. The scoring system (shown in table 2), consists of a five tiered scale where 1 is a high quality image in which the soft tissue boundary of the prostate is clearly visible, and 5 is a clinically inadequate CBCT with which IGRT cannot be reliably carried out.

For the three patients, the clinical image quality scores were compared between the standard CBCT, the uncorrected simultaneous CBCT, and the 2D scatter corrected images as described in (a). In addition, to determine the effectiveness of simplified scatter models, the uniform scatter corrected images (b) and the analytical (predicted) scatter corrected images (d) were also included. Therefore, 15 separate CBCTs were scored. Four observers (two clinicians and two treatment radiographers) assessed the anonymized CBCTs independently. The order of the CBCTs was randomized for each observer and six repeat images were inserted in order to monitor intra-observer consistency. The average score for each CBCT was then calculated and compared.

3. Results

3.1. Phantom study

Figure 4(a) shows how the mean signal from each projection varies over the arc. In comparison to a standard CBCT, the simultaneous projections consist of large peaks corresponding to

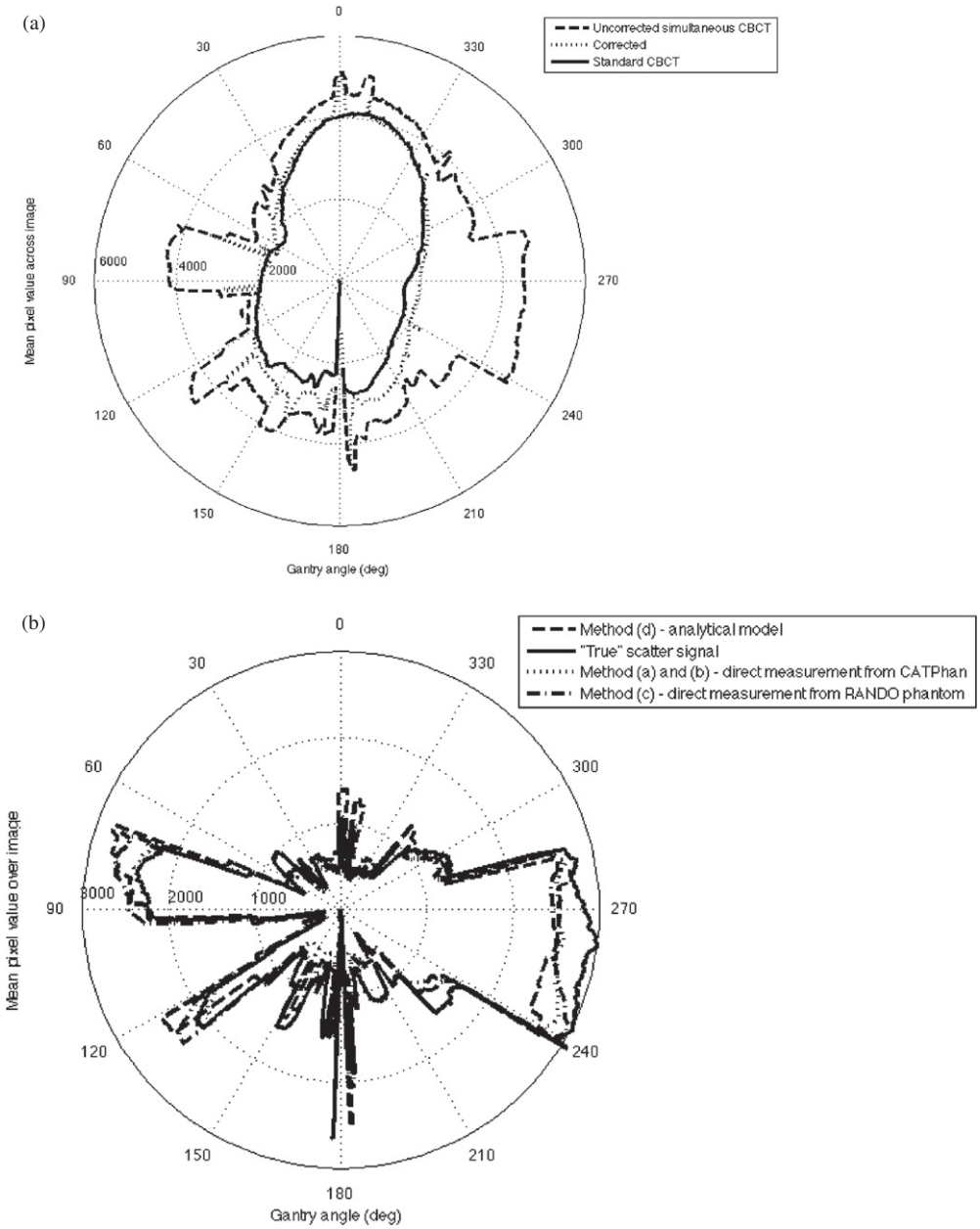

Figure 4. (a) Mean image signal over a treatment arc for the CATPhan, (b) comparison of the scatter signals over the treatment arc for each correction method.

sectors of the arc in which MV scatter is the highest. The effect of the correction is to reduce the excess scatter signal from these frames. The spikes in the corrected projections are due to small angular mismatches between the scatter images and the simultaneous projections. The effect of these spikes was mitigated through the application of a median filter prior to CBCT reconstruction.

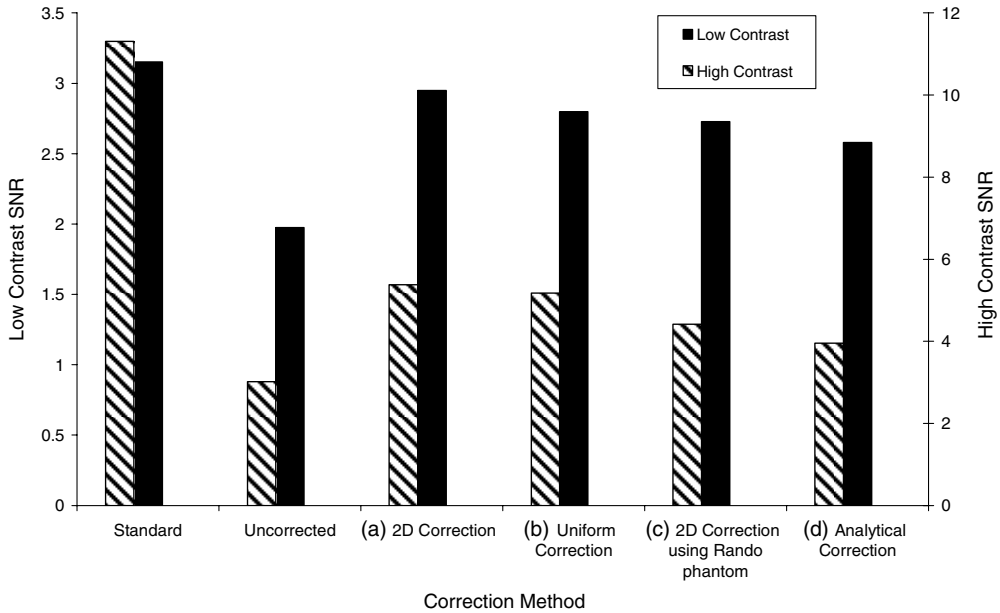

Figure 5. Comparison of low- and high-contrast SNR utilizing the different scatter correction techniques (a)–(d).

Figure 4(b) shows the mean MV scatter signal from each of the correction methods over a delivery arc. The 'true' scatter signal (solid line) was determined by subtracting the standard (kV-only) projections from the simultaneous (kV/MV) projections. The signal from methods (a) and (b) is due only to the MV scatter contribution with the CATPhan on the treatment couch and has a correlation coefficient of 0.91 when compared to the 'true' scatter signal. The signal from method (c), which has the RANDO phantom on the couch, offers an approximation of the CATPhan scatter, and a correlation coefficient of 0.89. Method (d), which only uses the plan data, differs in magnitude from the other measurements, and has a correlation coefficient of 0.78.

The effect of the MV scatter reduces the low-contrast SNR from 3.2 (standard CBCT) to 2.0 (simultaneous CBCT) and the high-contrast SNR from 11.3 to 3.0. The four different scatter correction methods (a)–(d) improve the SNRs by different amounts, as shown in figure 5. Method (a), employing the full 2D scatter images, shows the largest recovery of SNR. The analytical correction (d) showed the smallest increase in SNR compared to the uncorrected images.

3.2. Patient study

The inter-observer variation for the scoring was low, with 19/21 CBCTs graded within 1 point of each other. Each of the four observers also viewed six repeated CBCTs to monitor consistency. One of these repeat observations differed (by 1 point) from the observer's original scoring, which was considered an acceptable level of intra-observer variation. The average scores are shown in table 3, and an example of the reconstructed CBCTs are shown in figure 6.

The score for the uncorrected CBCTs was significantly worse than for the kV-only CBCTs—an average increase of 1.4 points on the scoring scale ($p = 0.01$). In all patients

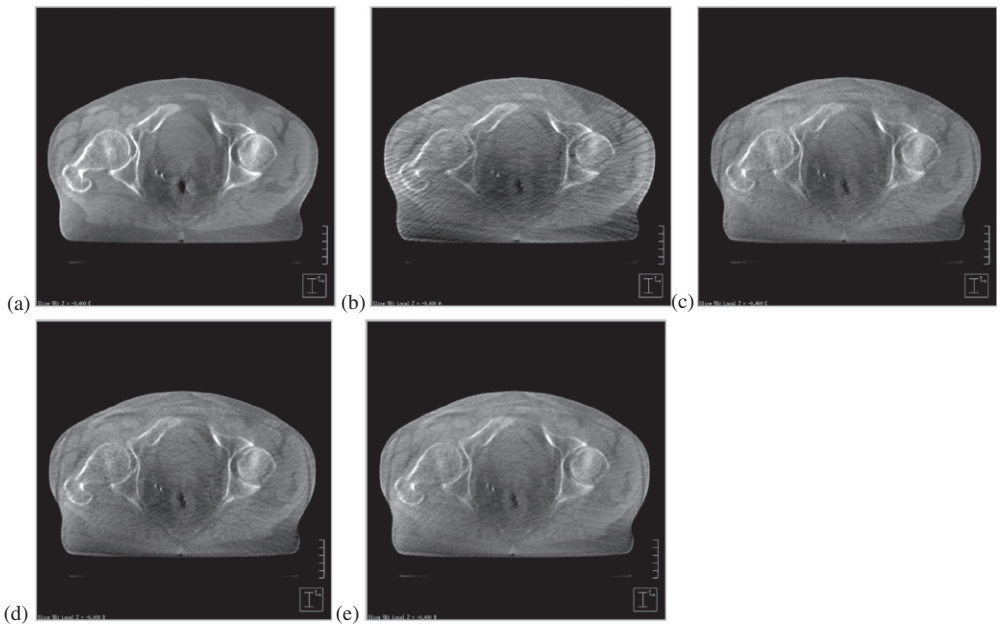

Figure 6. Single CBCT slice from patient 1. (a) Standard CBCT taken prior to treatment, (b) uncorrected CBCT taken during VMAT delivery, (c) 2D correction (method (a)), (d) uniform correction (method (b)), (e) analytical correction (method (d)).

Table 3. Averaged quality scores for the three sets of patient images.

	Patient 1	Patient 2	Patient 3
Standard CBCT	1.7	1.7	2.0
Uncorrected simultaneous CBCT	3.0	2.3	4.3
Method (a) corrected	2.3	2.3	3.3
Method (b) corrected	2.0	2.0	3.7
Method (d) corrected	2.5	2.0	3.7

the corrected images (using methods (a), (b) and (d)) scored better than the uncorrected images. Comparing the effectiveness of each method, the 2D scatter correction (a) resulted in the largest improvement, improving the quality score on average by 0.67 compared to the uncorrected CBCT ($p = 0.04$). The 1D (uniform) correction, on average, improved the score by 0.54 points, but without significance over three patients ($p = 0.1$), and the analytical correction improved the average score by 0.5 points ($p = 0.03$).

4. Discussion

Simultaneous cone-beam imaging during VMAT is a potentially useful technique which could influence the quality and efficiency of IGRT. It is anticipated that the ongoing SCART study will answer questions about the clinical value of such images, allowing for a safe change in imaging protocol in the future. Initial experiences of the acquisition and reconstruction of simultaneous images has been broadly positive at this centre, although the MV scatter remains a problem.

The effect of MV scatter is clear from both the phantom and patient studies. Low-contrast SNR was significantly decreased for the uncorrected images, which is an important parameter when attempting to discriminate between soft tissue interfaces. These results were supported by the patient images—the average image quality score was reduced by 1.4 for the uncorrected CBCTs. The observers noted that some of these images were inappropriate for IGRT, due to problems identifying any soft tissue boundary in the prostate region.

Four correction techniques were compared for the phantom study. Methods (a)–(c) utilized scatter images acquired during a VMAT delivery, while (d) used an analytical model derived from the treatment plan. The 2D correction (a) outperforms the uniform correction method (b), implying that the shape of the MV scatter image (figure 3) is important for correction. Furthermore, comparing methods (a) and (c), which used a different phantom, it is apparent that the MV scatter contribution is somewhat dependent on the patient geometry (this is discussed further below). The clinical image scoring results support the phantom results, with the full 2D correction outperforming the uniform correction and the analytical method.

Of the options assessed in this study, a full 2D correction using scatter images acquired from the patient provides the biggest increase in image quality. However, the practicality of when to acquire these projections may be problematic. For the patients considered in this study, undergoing a standard offline imaging protocol, a pre-treatment CBCT to verify set-up will still be required on the first fraction. In this case, the scatter projections could be taken on fraction 1, and then used to correct simultaneous CBCTs from fractions 2, 3, 6, 11 and 16. However, for other fractionation schemes (such as stereotactic treatments), some alternate method of acquiring the scatter images will be needed.

It was observed that method (c), utilizing a different scattering phantom, was able to recover some of the low and high-contrast SNR for the CATPhan images—although not as much as method (a), which used the CATPhan itself as the scattering volume. Potentially, scatter images from a phantom could be taken prior to a patient's first fraction on the treatment machine, and then used to correct the subsequent patient CBCTs. Work is underway to establish whether delivery to a pre-treatment dosimetric verification phantom can provide viable scatter images. It should be noted that the results presented here do not show a strong dependency on patient geometry, which may be due to the fact that the CATPhan and RANDO phantoms are not significantly different in terms of size and shape. Further work will be required to determine whether method (c) is still effective if there is a large disparity between the patient and the phantom shape.

The scatter correction method described here differs from previously reported methods. The technique proposed by van Herk *et al* (2011) interlaces kV imaging frames with MV scatter acquisitions, such that the correction can —in principle—be performed 'on the fly'. This method has clear benefits in that it does not require the acquisition of a separate scatter acquisition. However, due to the halving of the number of kV projections, the authors note that soft tissue contrast may be compromised for fast VMAT treatments. As there is a trend towards shorter VMAT treatment durations for standard fractionation regimes, the reduction in the number of frames becomes less desirable (although, reconstruction algorithms have been proposed for sparse projections (Choi *et al* 2010)). Conversely, for stereotactic radiotherapy treatments, the method proposed by van Herk *et al* (2011) becomes more useful, as the number of frames is large enough to produce clinically acceptable reconstructions.

The technique proposed by Ling *et al* (2011) effectively removes the problem of MV scatter by dividing the VMAT arc into sectors for imaging and treatment. Signal to noise ratio is retained, as only the scatter-free projections are selected for reconstruction. The authors anticipate that further engineering efforts are required to co-ordinate the switching between MV and kV delivery before it can be implemented widely. However, the periodic interruption

of the treatment beam leads to an increase in treatment time, which may be at odds with the trend towards shorter VMAT deliveries. It is also not clear what effect the interruption has on the plan or dosimetric quality. In comparison, the scatter correction presented in this study has no impact on the treatment duration, and allows the imager to acquire the standard number of projections for an acceptable CBCT.

The use of the analytical model—method (d)—did not perform as well as the direct measurements of MV scatter, but figure 5 and table 3 indicate that this technique did recover some image quality. Such a model would be beneficial as there would be no requirement for measurements on the linac prior to patient treatment. However, figure 4(b) indicates that the model may require some refinement to more accurately approximate the scatter signal. In particular, it will be of interest to determine whether geometric characteristics of the patient (e.g. effective thickness at each gantry angle) could be included to improve the analytical model.

This study has shown that the application of a novel scatter correction method leads to an improved low and high-contrast SNR on phantom CBCTs. Through the scoring of patient CBCTs, the corrected images were also observed to be of higher clinical quality. The results also suggest that a patient-specific direct measurement of scatter, rather than an analytical model-based approach, is required to best recover image quality.

Acknowledgments

The authors would like to thank the Wade Centre for Radiotherapy Research for their assistance with the clinical aspects of this study. The lead author's work is partially funded by an Elekta research grant.

References

Boylan C J, Rowbottom C G and Mackay R I 2011 The use of a realistic VMAT delivery emulator to optimize dynamic machine parameters for improved treatment efficiency *Phys. Med. Biol.* **56** 4119–33

Cao D, Afghan M K, Ye J, Chen F and Shepard D M 2009 A generalized inverse planning tool for volumetric-modulated arc therapy *Phys. Med. Biol.* **54** 6725–38

Choi K, Wang J, Zhu L, Suh T S, Boyd S and Xing L 2010 Compressed sensing based cone-beam computed tomography reconstruction with a first-order method *Med. Phys.* **37** 5113–25

Hugo G, Matuszak M M, Campbell J and Yan D 2008 Cone beam CT acquisition during volumetric arc radiotherapy delivery: correction for induced artifacts *Med. Phys.* **35** 2892

Ling C, Zhang P, Etmektzoglou T, Star-Lack J, Sun M, Shapiro E and Hunt M 2011 Acquisition of MV-scatter-free kilovoltage CBCT images during RapidArc or VMAT *Radiother. Oncol.* **100** 145–9

Nakagawa K *et al* 2009a First clinical cone-beam CT imaging during volumetric modulated arc therapy *Radiother. Oncol.* **90** 422–3

Nakagawa K, Kida S, Haga A, Masutani Y, Yamashita H, Imae T, Tanaka K, Ohtomo K, Iwai Y and Yoda K 2011 Cone beam computed tomography data acquisition during VMAT delivery with subsequent respiratory phase sorting based on projection image cross-correlation *J. Radiat. Res. (Tokyo)* **52** 112–3

Nakagawa K, Shiraishi K, Kida S, Haga A, Yamamoto K, Saegusa S, Terahara A, Itoh S, Ohtomo K and Yoda K 2009b First report on prostate displacements immediately before and after treatment relative to the position during VMAT delivery *Acta Oncol.* **48** 1206–8

Otto K 2008 Volumetric modulated arc therapy: IMRT in a single gantry arc *Med. Phys.* **35** 310–7

Sonke J J, Rossi M, Wolthaus J, van Herk M, Damen E and Belderbos J 2009 Frameless stereotactic body radiotherapy for lung cancer using four-dimensional cone beam CT guidance *Int. J. Radiat. Oncol. Biol. Phys* **74** 567–74

van Herk M, Ploeger L and Sonke J J 2011 A novel method for megavoltage scatter correction in cone-beam CT acquired concurrent with rotational irradiation *Radiother. Oncol.* **100** 365–9

Verellen D, De Ridder M and Storme G 2008 A (short) history of image-guided radiotherapy *Radiother. Oncol.* **86** 4–13

Williams P, Sykes J and Moore C 2004 The effects of radiation scatter from simultaneous MV irradiation on kV fluoroscopic and x-ray volume imaging with the Elekta synergy system *Radiother. Oncol.* **73** S229–30

Yu C X and Tang G 2011 Intensity-modulated arc therapy: principles, technologies and clinical implementation *Phys. Med. Biol.* **56** R31–54

Zhang P, Happersett L, Hunt M, Jackson A, Zelefsky M and Mageras G 2010 Volumetric modulated arc therapy: planning and evaluation for prostate cancer cases *Int. J. Radiat. Oncol. Biol. Phys.* **76** 1456–62

3. DISCUSSION AND FURTHER WORK

The aim of this thesis was to investigate whether VMAT offers any advantages over fixed-field IMRT for the delivery of radical radiotherapy. IMRT has been shown previously to represent a 'gold standard' treatment technique, in which the therapeutic ratio can be optimised by allowing for in-plane modulation of radiation fluence. Various studies have demonstrated the ability of IMRT to reduce normal tissue toxicity while maintaining an adequate level of tumour control. For this reason, national and international guidance have recommended increasing the provision of IMRT in the clinic. The delivery of IMRT using arcs, potentially improving treatment workflow, is presently of interest to achieve this increase in provision. However, in order to be considered a viable alternative to IMRT, VMAT must demonstrate high plan quality, stable and efficient delivery, along with a positive impact on workflow.

In this thesis, projects were undertaken in the areas of treatment planning, delivery and imaging to fully characterise VMAT as a technique. In this section the outcomes of each of the publications are discussed in the context of the above aims and motivation. The impact of each project is also considered, along with suggestions for further work in these areas.

3.1. VMAT plan creation from static IMRT segments

Publication 1 detailed the development of a novel treatment planning solution for VMAT. By expanding on the principle that dynamic VMAT delivery can be approximated by a series of static control points [56], it was demonstrated that plans could be created using a commercial IMRT direct-aperture optimisation technique. Comparing this technique to 5-field IMRT for prostate patients indicated that dose distributions were similar, but treatment time was significantly shorter (from an average 6 minutes to 2.5 minutes with VMAT). It was also found that the VMAT deliveries were robust in terms of their repeatability and resilience to communication

errors. The efficient delivery is attributable to the intelligent sequencing of the MLC control points, such that smooth transitions between different shapes are achieved.

The development of this planning technique shows that, in practice, VMAT does not require any simultaneous optimisation of all MLC positions around the arc. Only a coarse representation of static control points (15 equi-spaced beams) was required for re-sequencing into an arc, producing the desired dose distribution. Crucially, Publication 1 uses DAO to produce control points which are *a priori* deliverable. This represents an alternative to the two- or three-step planning techniques demonstrated previously for VMAT (described in section 1.4.1).

Prior to the release of a commercial planning solution for the Elekta VMAT system, this in-house method was implemented clinically at The Christie hospital, with 10 prostate patients treated in 2009. This represented the first clinical use of Elekta VMAT to treat multiple dose-level prostate patients. The following iteration of the Pinnacle software (v.9.0) introduced the SmartArc algorithm for VMAT planning. SmartArc [104] uses a similar principle, beginning with DAO-IMRT optimisation, and then intelligently sequencing the control points based on knowledge of the linac characteristics. Most treatment planning systems now utilise direct aperture optimisation for the production of VMAT plans, acknowledging the importance of including dynamic linac capabilities within the planning process.

3.2. Automated plan comparison study

Using the SmartArc planning system, Publication 2 performed an automated plan comparison study between IMRT and VMAT for nasopharynx patients. This publication demonstrated that it is possible to use a planner-free technique for the production of inverse-optimised radiotherapy plans. The advantage of this is that the user dependence on plan quality can be reduced, so as to allow a fairer comparison between treatment techniques. For the planning strategies investigated, VMAT and IMRT gave similar results for routine plan creation and dose escalation. However, an

advantage was observed with VMAT for the parotid sparing strategy, leading to a reduction in mean parotid dose of 2.5 Gy compared to IMRT. Publication 2 therefore shows that - if the delivery efficiency of VMAT is neglected - then there is a potential plan quality improvement compared to IMRT. To the authors' best knowledge, this project represents the first use of a planner-free technique to objectively compare two radiotherapy delivery methods.

The automated technique described in Publication 2 has since been developed further for other projects. Stanford *et al* [105] have shown that the system can be configured to produce clinically-acceptable prostate IMRT plans unsupervised by any planner. This could potentially allow for more routine clinical application of the automated technique. Hamlett *et al* have also used this system to find the maximum achievable prescription dose for isotoxic lung treatments [106]. Using a set of strict normal tissue tolerances (for example, maximum volume of lung receiving 20 Gy or more) the automated system was configured to produce IMRT plans with increasing target dose prescriptions until the tolerances are met.

In the future, the automated technique could be further optimised to allow for more routine use – in particular, it will be of interest to determine whether providing the system with an initial 'rough' class solution can help to generate clinically acceptable plans in a faster time. A three-way study could then be performed, comparing the clinical quality of a) manually produced plans, b) standard class solution only, and c) class solution plus the automated planning technique. Combined with recent advances in automated segmentation of regions of interest [107], such a technique could provide a useful 'first-pass' production of IMRT or VMAT plans, potentially allowing workflow to be optimised.

One of the observations from Publication 2 was that neither IMRT or VMAT was superior for the escalation of dose to the main PTV. Within the text it was suggested that one reason for this could be that the differences in individual patient geometry (and the geometry of the target volumes) may be larger than the difference between

IMRT and VMAT as a delivery technique. This may warrant further investigation - particularly in light of the trend towards more individualised cancer treatments [108]. As there now exist a number of different radiotherapy treatment options (e.g. IMRT, VMAT, and protons), it may be possible to predict which technique would be beneficial for an individual patient based on knowledge of patient geometry (e.g. target shape, and proximity to nearby OARs). Such 'expert systems' have been demonstrated previously in oncology [109, 110]. The automated planning technique could be integrated into such an expert system to aid the individualisation of patient treatment strategies.

3.3. VMAT delivery emulator

Through the use of a software emulator, Publication 3 assessed the impact of various dynamic linac components on the efficiency of VMAT plan delivery. One of the main conclusions from this publication was that MLC speed represents a significant limiting factor for treatment efficiency. Even a modest increase in the allowable leaf speed to 3.0 cm/s improved the average dose rate and treatment time significantly (+19% and -22%, respectively, when compared to 2.0 cm/s). Furthermore, reformulating the emulator to determine the ideal linac parameters required for an efficient delivery within 60 s, it was found that the leaf speed must be at least 2.8cm/s with a maximum continuously variable dose rate of 1400 MU/min.

This emulator study demonstrates the importance of the linac delivery characteristics for arc therapy, and shows how the quality and complexity of a VMAT treatment is ultimately limited by the achievable leaf speed and dose rate. This trade-off between complexity and treatment efficiency has been previously seen as the limiting factor of the VMAT technique [55]. In Publication 3, however, it is shown that three changes are required to achieve both high modulation and high efficiency: increased leaf speed, continuously variable dose rate, and a maximum dose rate >1000 MU/min.

Subsequent to this publication, Elekta introduced the Integrity delivery upgrade, allowing for CVDR-VMAT. More recently, a new MLC design ('Agility') has been commercially released, which allows for leaf speeds of up to 6.5 cm/s [111]. Investigations have also been made into the delivery of VMAT plans using flattening filter-free linacs [112], approaching the > 1000 MU/min proposed by the emulator study, resulting in a highly-efficient delivery system. As such, the complexity-efficiency trade off may not present such a limiting factor in the context of more modern linear accelerator design.

3.4. Investigation into CVDR delivery

Following the commercial availability of Elekta Integrity, it was of interest to perform a comparison between the previous binned-dose rate system and CVDR delivery (Publication 4). The main conclusions from this study were that a) both BDR and CVDR VMAT provide adequate dosimetric agreement for a range of plans, b) MLC positioning accuracy was poorer with the faster CVDR deliveries, and c) beam flatness and stability was improved with CVDR. The results from this publication agree with the emulator results, in that the measured delivery times with CVDR were very similar to those predicted. Furthermore, this study confirms for the first time that the higher average dose rate achieved with CVDR has a benefit in terms of beam stability over the arc.

Publication 4 demonstrates practically that VMAT can be a stable, fast and efficient method for the delivery of complex radiotherapy. Conclusions about the dosimetric quality of CVDR delivery have been reported previously [84], but by taking additional MLC tracking and beam stability measurements during treatment, this study further characterises the technique. It will be of future interest to determine whether CVDR is extendable to high maximum dose rates, such as those achieved by flattening filter-free delivery. It was shown in the emulator study that the 255 dose rate bins available with Integrity does not approximate well to a continuous variable when the maximum dose rate is ~1400 MU/min. Instead, it was proposed that 1023

dose rate bins would be required to achieve constant maximum gantry speed for an idealised VMAT delivery. With the recent availability of commercial flattening-filter-free systems, this will require further investigation.

It is of interest to note that MLC positioning accuracy was slightly poorer with CVDR compared to BDR. A similar result was obtained previously by Pasler *et al* [113], albeit only comparing 'fast' and 'slow' gantry speed BDR VMAT deliveries. Pasler suggests that a faster gantry rotation results in more MLCs not reaching their intended position at the end of each control point, and this may also be the case for CVDR delivery. Wijesooriya *et al* [114] reported a similar effect for RapidArc deliveries. In Appendix 1 (page 75), further work has been undertaken to develop a 'rotational synchronicity' test for VMAT. Using a standard dosimetry phantom (the Delta^4), a test was designed which compared the dose distribution from a rotating but fixed MLC field with that delivered by rotating and moving field. Using different dose prescriptions it was possible to force the linac into selecting different combinations of dose rate and gantry speed. As shown in Appendix 1, the deliveries with a faster gantry speed (requiring a faster MLC speed) resulted in lower gamma pass rates when compared to the static field. This further supports the tracking results from Publication 4, which found that CVDR deliveries increased the mean MLC positioning errors. With the availability of modern MLC designs, it will be of interest to investigate whether this effect remains observable for faster leaf speeds.

3.5. Monte Carlo VMAT verification system

Publication 5, which detailed the development of a Monte Carlo model for VMAT, showed that machine measurements may not be necessarily required for pre-treatment plan QC. Instead, this publication presented a software solution which can automatically set up and perform independent dose calculations, allowing a comparison to the treatment planning system dose. An important conclusion from this work was that knowledge of dynamic linac motion was required for the most accurate dosimetry.

The ability to perform measurement-free plan QA is of particular use for VMAT. Whereas fixed-field IMRT tends to be well-characterised within the treatment planning system (i.e. static beam angles, constant dose rate, fixed aperture shapes for step-and-shoot delivery), VMAT is a more complex technique requiring the simultaneous modulation of gantry speed, dose rate and MLC motion. As a result, the clinical implementation of VMAT has been accompanied by a programme of routine pre-treatment verification, which may counteract the workflow benefit of VMAT as originally desired. Publication 5 demonstrates that an accurate software-based verification is achievable, through the use of a Monte Carlo model alongside a realistic delivery emulator. As such, this system could allow a reduced verification regime similar to those used for IMRT, whereby pre-treatment measurements are more targeted, and routine comprehensive QC tests are relied upon to monitor the delivery system.

The issue of what additional QC is required for VMAT remains a source of debate within the literature, although it is commonly recognised that some attempt should be made to check the interdependency and synchronisation of the MLC positioning, gantry speed and modulation of dose rate. As a simple, routine method for checking the VMAT system, a rotational synchronicity test such as that proposed in Appendix 1 could prove to be useful. However, further work would be required to determine the sensitivity of this type of test to realistic errors.

As the VMAT beam model in Publication 5 allows for approximately continuous calculation of dose around the arc, future work will consider the effects of rotational delivery on patient dosimetry. Figure 13 shows the same VMAT plan, calculated using the Monte Carlo model, using a) 90 static control points and b) 'continuous' delivery. The absolute dose difference between the two is also shown, where differences of up to +3.1 Gy were observed on this transverse slice, albeit in areas far from the target volume. Gamma analysis between the two dose distributions indicates that, while there is strong agreement between the distributions within the

high dose areas (> 99% pixels passing 3%/3mm within the 20% isodose line), the gamma pass rate drops to 95.9% when the whole body is included in the analysis. This is a result of the under-sampling phenomenon described in section 1.4.1 - dose calculations close to the rotational axis of the arc are accurate from fixed fluences, but at large distances they poorly approximate the continuous delivery of VMAT.

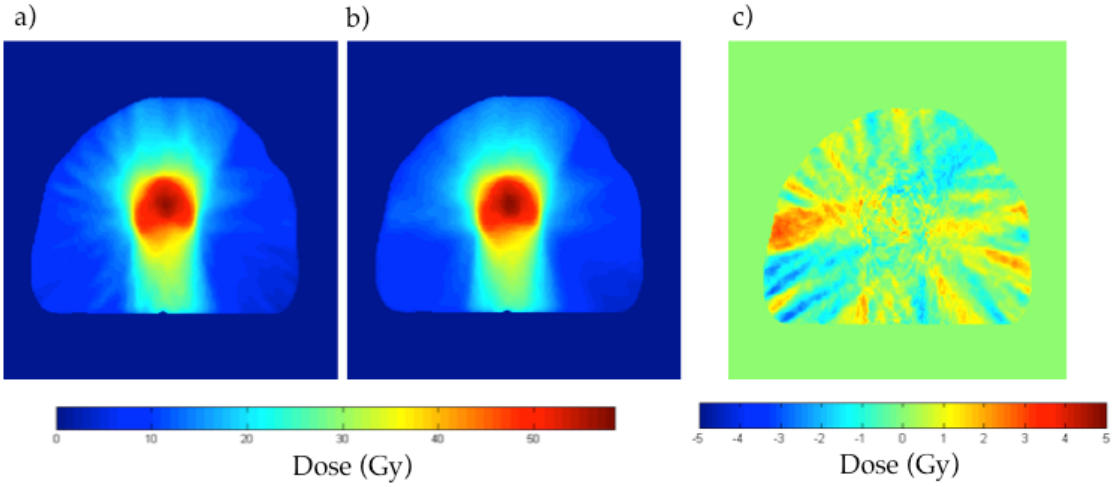

Figure 13. Monte Carlo simulation of a prostate VMAT plan using a) 90 fixed control points and b) continuous delivery. The absolute dose difference (b) – (a) is shown in c).

It is difficult to assess the clinical significance of the increased volume of low dose due to rotational delivery. In the above prostate patient, the effect is relatively small, and detailed analysis is limited in part due to the large number of particles that need to be simulated with Monte Carlo to achieve reasonable uncertainties in these low dose areas. Following the move from conformal therapy to IMRT, there was concern expressed about the potential for induced secondary malignancies due to the increased leakage and scatter, which led to a higher volume of the patient receiving low doses [74, 75, 115-117]. When moving to the continuous rotational delivery of VMAT, this low dose volume may be greater than from IMRT [73], and within this thesis, it was observed that VMAT prostate patients (in Publication 1) receive a higher volume of low dose than the IMRT technique. It will be of future interest to fully characterise the low dose effects of VMAT, and to potentially develop a method for quantifying the risk of VMAT as opposed to IMRT in respect to secondary cancer induction. The Monte Carlo model presented here could be a useful tool for such a

study, potentially combined with software models of standard humans (such as the ICRP phantoms).

3.6. Investigation into simultaneous cone beam imaging during VMAT

Publication 6 showed that it is possible to reconstruct cone beam CT scans from kV projections taken during VMAT delivery. As these images are adversely affected by MV scatter onto the imaging panel, techniques for scatter correction were compared. All of the correction techniques recovered image quality, with the largest recovery achieved when using the acquisition of a separate MV-only scatter map. This scatter correction technique differs from those proposed previously [100, 101], in that it utilises the entire set of acquisitions over a continuously-delivered treatment beam.

The outcome of this study indicates that VMAT may offer a benefit over IMRT, in that it is possible to perform image-guided radiotherapy using on-treatment patient imaging. Such CBCTs may provide an advantage, as they provide information about patient position during the treatment delivery, rather than before or after. Simultaneous VMAT-CBCTs also allow the in-room time for the patient to be further reduced, requiring only one rotation of the linac gantry for treatment and imaging.

This project was performed as the precursor to a local clinical study to investigate the value of CBCTs acquired during VMAT delivery. The aim of the Simultaneous Cone-beam during Arc Radiation Therapy (SCART) study was to determine whether these images provide sufficient information to perform routine IGRT, when compared to standard CBCTs. 50 prostate VMAT patients were recruited into the SCART study during 2012, with the final patient finishing treatment in early 2013. The study was designed such that each patient received four simultaneous CBCTs over their course of treatment - these were taken on days when the patient also received standard CBCT imaging. The simultaneous CBCTs were corrected using the method described in Publication 6, which has since been modified to allow for batch corrections, and runs alongside the Elekta XVI database. The scoring system for the CBCTs has been

further developed [118], aiming to provide an objective, clinically-relevant method of determining the image quality (Table 1). At the time of submission this clinical image scoring study is still underway.

The SCART images are also being used for further work. In particular Mayes [119] has investigated the differences between the prostate, rectum and bladder positions before treatment (using the standard CBCTs) and during treatment (using the scatter corrected simultaneous CBCTs). A preliminary study, using 5 SCART patients, found mean centroid shifts of 0.53 cm, 0.52 cm and 0.59 cm for the bladder, prostate and rectum respectively. As this was a small data set, it is anticipated that this work will continue on the remaining SCART CBCTs, in order to characterise any differences in off-line and on-line imaging for a population of prostate patients. In the future it may also be of interest to investigate the use the simultaneous CBCTs for adaptive replanning, which will require assessing the accuracy of CT numbers, allowing for a comparison of dose delivered to the on-treatment geometry compared to the planned distribution. There remains no routine clinical implementation of simultaneous CBCT, but a forthcoming commercial release (of the Elekta XVI software) does include some provision for this technique. Results of the SCART study will further confirm whether it will be an effective method for IGRT.

Score	Definition	Description
1	The prostate cannot be distinguished from surrounding structures.	The position of prostate cannot be identified with confidence and the scan could not be used to make a clinical decision.
2	Loss of image quality means that soft tissue boundaries are not clearly defined. Despite this, the borders of the prostate can still be identified, or inferred from the position of surrounding structures such as the anterior rectal wall.	The position of prostate can be identified with sufficient confidence that the scan could be used for clinical decision making.
3	The boundaries between the prostate and peri-prostatic tissues can be clearly defined on most slices. The position of the seminal vesicles can be identified.	The position of prostate and seminal vesicles can be identified with confidence and the scan could be used for clinical decision making.

Table 1. The revised SCART image quality scoring system. From Dickinson [118].

4. CONCLUSION

Taken together, these projects indicate that the delivery of intensity modulated radiotherapy using arcs rather than static beams offers a number of advantages without a reduction in treatment effectiveness. Foremost among these advantages is the much-reduced treatment time, although a potentially improved plan quality has also been demonstrated. Furthermore, the use of on-treatment imaging offers positional verification which is of increased clinical relevance, and may also offer a further improvement in treatment workflow.

A previous concern about VMAT has been the perceived trade-off between the amount of modulation required for an effective treatment, and the ability of the linac to deliver the plan efficiently and accurately. This is both a planning issue (in that knowledge of the dynamic machine limitations need to be integral to the plan creation) and a delivery issue. The simultaneous motion of the linac gantry, modulation of dose rate, and movement of leaves is still a relatively novel method for the delivery of radiotherapy. While the retrospective installation of VMAT on existing linear accelerator technology has been demonstrated as robust, the results presented here suggest that more modern linac components are essential to gain the most effective use of arc therapy. In particular, advances in MLC speed along with high, continuously variable dose rates have allowed for much greater delivery efficiency, particularly for plans requiring a large degree of modulation.

If the provision of intensity modulated treatments is to be increased, allowing more patients access to a technique which can offer an increase in the therapeutic ratio between tumour control and normal tissue sparing, then the work undertaken as part of this thesis indicates that VMAT would be an effective candidate to achieve this aim.

REFERENCES

1. G. Delaney, S. Jacob, C. Featherstone, et al. The role of radiotherapy in cancer treatment: estimating optimal utilization from a review of evidence-based clinical guidelines. Cancer 2005; 104(6):1129-37.
2. M. V. Williams, E. T. Summers, K. Drinkwater, et al. Radiotherapy dose fractionation, access and waiting times in the countries of the UK in 2005. Clin Oncol (R Coll Radiol) 2007; 19(5):273-86.
3. M. B. Barton, V. Gebski, C. Manderson, et al. Radiation therapy: are we getting value for money? Clin Oncol (R Coll Radiol) 1995; 7(5):287-92.
4. P. P. Connell, S. Hellman. Advances in radiotherapy and implications for the next century: A historical perspective. Canc Res 2009; 69(2):383–392.
5. Radiobiological Modelling in Radiation Oncology, ed. R.G. Dale and B. Jones. 2007: British Institute of Radiology.
6. G. Bauman, R. B. Rumble, J. Chen, et al. Intensity-modulated radiotherapy in the treatment of prostate cancer. Clin Oncol (R Coll Radiol) 2012; 24(7):461-73.
7. S. Webb and A. E. Nahum. A model for calculating tumour control probability in radiotherapy including the effects of inhomogeneous distributions of dose and clonogenic cell density. Phys Med Biol 1993; 38(6):653-66.
8. ICRU Report 62: Prescribing, recording and reporting photon beam therapy (supplement to ICRU report 50). 1999: Bethesda: International Commission on Radiation Units and Measurements.
9. S. Webb. Intensity Modulated Radiation Therapy. 2001: Institute of Physics Publishing, Bristol.
10. D. J. Brenner, R. E. Curtis, E. J. Hall, et al. Second malignancies in prostate carcinoma patients after radiotherapy compared with surgery. Cancer 2000; 88(2):398-406.
11. J. Staffurth and Radiotherapy Development Board. A review of the clinical evidence for intensity-modulated radiotherapy. Clin Oncol (R Coll Radiol) 2010; 22(8):643-57.
12. A. B. Miah, S. A. Bhide, M. T. Guerrero-Urbano, et al. Dose-escalated intensity-modulated radiotherapy is feasible and may improve locoregional control and laryngeal preservation in laryngo-hypopharyngeal cancers. Int J Radiat Oncol Biol Phys 2012; 82(2):539-47.
13. C. M. Nutting, J. P. Morden, K. J. Harrington, et al. Parotid-sparing intensity modulated versus conventional radiotherapy in head and neck cancer (PARSPORT): a phase 3 multicentre randomised controlled trial. Lancet Oncol 2011; 12(2):127-36.
14. F. C. Wong, A. W. Ng, V. H. Lee, et al. Whole-field simultaneous integrated-boost intensity-modulated radiotherapy for patients with nasopharyngeal carcinoma. Int J Radiat Oncol Biol Phys 2010; 76(1):138-45.
15. S. Webb. The physical basis of IMRT and inverse planning. Br J Radiol 2003; 76(910):678-89.
16. L. J. Verhey. Issues in optimization for planning of intensity-modulated radiation therapy. Semin Radiat Oncol 2002; 12(3):210-8.

17. X. Zhang, H. Liu, X. Wang, et al. Speed and convergence properties of gradient algorithms for optimization of IMRT. Med Phys 2004; 31(5):1141-52.
18. Intensity Modulated Radiation Therapy Collaborative Working Group. Intensity-modulated radiotherapy: current status and issues of interest. Int J Radiat Oncol Biol Phys 2001; 51(4):880-914.
19. D. M. Shepard, M. A. Earl, X. A. Li, et al. Direct aperture optimization: a turnkey solution for step-and-shoot IMRT. Med Phys 2002; 29(6):1007-18.
20. A. C. Hartford, J. M. Galvin, D. C. Beyer, et al. American College of Radiology (ACR) and American Society for Radiation Oncology (ASTRO) Practice Guideline for Intensity-modulated Radiation Therapy (IMRT). Am J Clin Oncol 2012; 35(6):612-7.
21. E. Schreibmann and L. Xing. Feasibility study of beam orientation class-solutions for prostate IMRT. Med Phys 2004; 31(10):2863-70.
22. B. Vanderstraeten, W. Duthoy, W. De Gersem, et al. [18F]fluoro-deoxy-glucose positron emission tomography ([18F]FDG-PET) voxel intensity-based intensity-modulated radiation therapy (IMRT) for head and neck cancer. Radiother Oncol 2006; 79(3):249-58.
23. D. Verellen, M. De Ridder, and G. Storme. A (short) history of image-guided radiotherapy. Radiother Oncol 2008; 86(1):4-13.
24. M. B. Sharpe, D. J. Moseley, T. G. Purdie, et al. The stability of mechanical calibration for a kV cone beam computed tomography system integrated with linear accelerator. Med Phys 2006; 33(1):136-44.
25. J. L. Bedford, P. J. Childs, V. Nordmark Hansen, et al. Commissioning and quality assurance of the Pinnacle(3) radiotherapy treatment planning system for external beam photons. Br J Radiol 2003; 76(903):163-76.
26. M. B. Sharpe, B. M. Miller, D. Yan, et al. Monitor unit settings for intensity modulated beams delivered using a step-and-shoot approach. Med Phys 2000; 27(12):2719-25.
27. E. Spezi, A. L. Angelini, F. Romani, et al. Characterization of a 2D ion chamber array for the verification of radiotherapy treatments. Phys Med Biol 2005; 50(14):3361-73.
28. D. Létourneau, M. Gulam, D. Yan, et al. Evaluation of a 2D diode array for IMRT quality assurance. Radiother Oncol 2004; 70(2):199-206.
29. J. H. Kung, G. T. Chen, and F. K. Kuchnir. A monitor unit verification calculation in intensity modulated radiotherapy as a dosimetry quality assurance. Med Phys 2000; 27(10):2226-30.
30. I. Iftimia, E. T. Cirino, L. Xiong, et al. Quality assurance methodology for Varian RapidArc treatment plans. J Appl Clin Med Phys 2010; 11(4):3164.
31. M. T. Guerrero Urbano and C. M. Nutting. Clinical use of intensity-modulated radiotherapy: part II. Br J Radiol 2004; 77(915):177-82.
32. V. Khoo. Radiotherapy of prostate cancer. Eur J Cancer 2011; 47(S3):S298-301.
33. D. A. Kuban and L. Dong. High-dose intensity modulated radiation therapy for prostate cancer. Curr Urol Rep 2004; 5(3):197-202.
34. D. Thomson, S. Merrick, R. Swindell, et al. Dose-escalated hypofractionated intensity-modulated radiotherapy in high-risk carcinoma of the prostate: outcome and late toxicity. Prostate Cancer 2012; 2012:1-10.

35. M. J. Zelefsky, Z. Fuks, and S. A. Leibel. Intensity modulated radiation therapy for prostate cancer. Semin Radiat Oncol 2002; 12(3):229-37.
36. M. J. Zelefsky, E. J. Levin, M. Hunt, et al. Incidence of late rectal and urinary toxicities after three-dimensional conformal radiotherapy and intensity-modulated radiotherapy for localized prostate cancer. Int J Radiat Oncol Biol Phys 2008; 70(4):1124-9.
37. S. Jefferies, A. Taylor, R. Reznek, et al. Results of a national survey of radiotherapy planning and delivery in the UK in 2007. Clin Oncol (R Coll Radiol) 2009; 21(3):204-17.
38. W. P. Mayles and Radiotherapy Development Board. Survey of the availability and use of advanced radiotherapy technology in the UK. Clin Oncol (R Coll Radiol) 2010; 22(8):636-42.
39. B. O'Sullivan, R. B. Rumble, P. Warde, et al. Intensity-modulated radiotherapy in the treatment of head and neck cancer. Clin Oncol (R Coll Radiol) 2012; 24(7):474-87.
40. M. K. Kam, S. F. Leung, B. Zee, et al. Prospective randomized study of intensity-modulated radiotherapy on salivary gland function in early-stage nasopharyngeal carcinoma patients. J Clin Oncol 2007; 25(31):4873-9.
41. Radiotherapy Services in England 2012. 2012, Department of Health: London.
42. S. R. Hummel, M. D. Stevenson, E. L. Simpson, et al. A model of the cost-effectiveness of intensity-modulated radiotherapy in comparison with three-dimensional conformal radiotherapy for the treatment of localised prostate cancer. Clin Oncol (R Coll Radiol) 2012; 24(10):e159-67.
43. C. X. Yu and G. Tang. Intensity-modulated arc therapy: principles, technologies and clinical implementation. Phys Med Biol 2011; 56(5):R31-54.
44. A. Bertelsen, C. R. Hansen, J. Johansen, et al. Single Arc Volumetric Modulated Arc Therapy of head and neck cancer. Radiother Oncol 2010; 95(2):142-8.
45. S. Takahashi. Conformation radiotherapy. Rotation techniques as applied to radiography and radiotherapy of cancer. Acta Radiol Diagn (Stockh) 1965:Suppl 242:1+.
46. A. Brahme, J. E. Roos, and I. Lax. Solution of an integral equation encountered in rotation therapy. Physics in Medicine and Biology 1982; 27(10):1221-9.
47. T. R. Mackie, T. Holmes, S. Swerdloff, et al. Tomotherapy: a new concept for the delivery of dynamic conformal radiotherapy. Med Phys 1993; 20(6):1709-19.
48. C. X. Yu. Intensity-modulated arc therapy with dynamic multileaf collimation: an alternative to tomotherapy. Phys Med Biol 1995; 40(9):1435-49.
49. W. Duthoy, W. De Gersem, K. Vergote, et al. Whole abdominopelvic radiotherapy (WAPRT) using intensity-modulated arc therapy (IMAT): first clinical experience. Int J Radiat Oncol Biol Phys 2003; 57(4):1019-32.
50. W. Duthoy, W. De Gersem, K. Vergote, et al. Clinical implementation of intensity-modulated arc therapy (IMAT) for rectal cancer. Int J Radiat Oncol Biol Phys 2004; 60(3):794-806.
51. A. M. Chen, R. L. Jennelle, R. Sreeraman, et al. Initial clinical experience with helical tomotherapy for head and neck cancer. Head Neck 2009; 31(12):1571-8.

52. D. Cao, M. K. Afghan, J. Ye, et al. A generalized inverse planning tool for volumetric-modulated arc therapy. Phys Med Biol 2009; 54(21):6725-38.
53. J. Pardo-Montero and J. D. Fenwick. An approach to multiobjective optimization of rotational therapy. Med Phys 2009; 36(7):3292-303.
54. T. Bortfeld. The number of beams in IMRT--theoretical investigations and implications for single-arc IMRT. Phys Med Biol 2010; 55(1):83-97.
55. T. Bortfeld and S. Webb. Single-Arc IMRT? Phys Med Biol 2009; 54(1):N9-20.
56. S. Webb and D. McQuaid. Some considerations concerning volume-modulated arc therapy: a stepping stone towards a general theory. Phys Med Biol 2009; 54(14):4345-60.
57. K. Yang, D. Yan, and N. Tyagi. Sensitivity analysis of physics and planning SmartArc parameters for single and partial arc VMAT planning. J Appl Clin Med Phys 2012; 13(6):3760.
58. K. Otto. Volumetric modulated arc therapy: IMRT in a single gantry arc. Med Phys 2008; 35(1):310-7.
59. J. L. Bedford. Treatment planning for volumetric modulated arc therapy. Med Phys 2009; 36(11):5128-38.
60. M. Rao, D. Cao, F. Chen, et al. Comparison of anatomy-based, fluence-based and aperture-based treatment planning approaches for VMAT. Phys Med Biol 2010; 55(21):6475-90.
61. X. Zhu, D. Thongphiew, R. McMahon, et al. Arc-modulated radiation therapy based on linear models. Phys Med Biol 2010; 55(13):3873-83.
62. P. Zhang, L. Happersett, M. Hunt, et al. Volumetric modulated arc therapy: planning and evaluation for prostate cancer cases. Int J Radiat Oncol Biol Phys 2010; 76(5):1456-62.
63. D. Palma, E. Vollans, K. James, et al. Volumetric modulated arc therapy for delivery of prostate radiotherapy: comparison with intensity-modulated radiotherapy and three-dimensional conformal radiotherapy. Int J Radiat Oncol Biol Phys 2008; 72(4):996-1001.
64. D. Wolff, F. Stieler, G. Welzel, et al. Volumetric modulated arc therapy (VMAT) vs. serial tomotherapy, step-and-shoot IMRT and 3D-conformal RT for treatment of prostate cancer. Radiother Oncol 2009; 93(2):226-33.
65. S. Yoo, Q. J. Wu, W. R. Lee, et al. Radiotherapy treatment plans with RapidArc for prostate cancer involving seminal vesicles and lymph nodes. Int J Radiat Oncol Biol Phys 2010; 76(3):935-42.
66. R. Shaffer, W. J. Morris, V. Moiseenko, et al. Volumetric modulated Arc therapy and conventional intensity-modulated radiotherapy for simultaneous maximal intraprostatic boost: a planning comparison study. Clin Oncol (R Coll Radiol) 2009; 21(5):401-7.
67. P. Ost, B. Speleers, G. De Meerleer, et al. Volumetric Arc therapy and Intensity-Modulated Radiotherapy for Primary Prostate Radiotherapy With Simultaneous Integrated Boost to Intraprostatic Lesion With 6 and 18 MV: A Planning Comparison Study. Int J Radiat Oncol Biol Phys 2011; 79(3):920-926.
68. M. Guckenberger, A. Richter, T. Krieger, et al. Is a single arc sufficient in volumetric-modulated arc therapy (VMAT) for complex-shaped target volumes? Radiother Oncol 2009; 93(2):259-65.

69. C. S. Mayo, L. Ding, A. Addesa, et al. Initial Experience with Volumetric IMRT (RapidArc) for Intracranial Stereotactic Radiosurgery. Int J Radiat Oncol Biol Phys 2010; 78(5):1457-66.
70. R. A. Popple, J. B. Fiveash, I. A. Brezovich, et al. RapidArc radiation therapy: first year experience at the University of Alabama at Birmingham. Int J Radiat Oncol Biol Phys 2010; 77(3):932-41.
71. M. Scorsetti, A. Fogliata, S. Castiglioni, et al. Early clinical experience with Volumetric Modulated Arc Therapy in head and neck cancer patients. Radiat Oncol 2010; 5(1):93.
72. M. T. Studenski, V. Bar-Ad, J. Siglin, et al. Clinical experience transitioning from IMRT to VMAT for head and neck cancer. Med Dosim 2012; 38(2):171-5.
73. N. P. Brodin, P. Munck Af Rosenschöld, M. C. Aznar, et al. Radiobiological risk estimates of adverse events and secondary cancer for proton and photon radiation therapy of pediatric medulloblastoma. Acta Oncol 2011; 50(6):806-16.
74. A. Dasu, I. Toma-Dasu, J. Olofsson, et al. The use of risk estimation models for the induction of secondary cancers following radiotherapy. Acta Oncol 2005; 44(4):339-47.
75. S. F. Kry, M. Salehpour, D. S. Followill, et al. The calculated risk of fatal secondary malignancies from intensity-modulated radiation therapy. Int J Radiat Oncol Biol Phys 2005; 62(4):1195-203.
76. M. M. Matuszak, D. Yan, I. Grills, et al. Clinical applications of volumetric modulated arc therapy. Int J Radiat Oncol Biol Phys 2010; 77(2):608-16.
77. S. D. McGrath, M. M. Matuszak, D. Yan, et al. Volumetric modulated arc therapy for delivery of hypofractionated stereotactic lung radiotherapy: A dosimetric and treatment efficiency analysis. Radiother Oncol 2010; 95(2):153-7.
78. C. Ong, W. F. Verbakel, J. P. Cuijpers, et al. Dosimetric impact of interplay effect on RapidArc lung stereotactic treatment delivery. Int J Radiat Oncol Biol Phys 2011; 79(1):305-311.
79. W. F. Verbakel, S. Senan, J. P. Cuijpers, et al. Rapid delivery of stereotactic radiotherapy for peripheral lung tumors using volumetric intensity-modulated arcs. Radiother Oncol 2009; 93(1):122-4.
80. E. Vanetti, A. Clivio, G. Nicolini, et al. Volumetric modulated arc radiotherapy for carcinomas of the oro-pharynx, hypo-pharynx and larynx: a treatment planning comparison with fixed field IMRT. Radiother Oncol 2009; 92(1):111-7.
81. D. Rangaraj, S. Oddiraju, B. Sun, et al. Fundamental properties of the delivery of volumetric modulated arc therapy (VMAT) to static patient anatomy. Med Phys 2010; 37(8):4056-67.
82. J. L. Bedford and A. P. Warrington. Commissioning of volumetric modulated arc therapy (VMAT). Int J Radiat Oncol Biol Phys 2009; 73(2):537-45.
83. D. G. Kaurin, L. E. Sweeney, E. I. Marshall, et al. VMAT testing for an Elekta accelerator. J Appl Clin Med Phys 2012; 13(2):3725.
84. A. Bertelsen, E. L. Lorenzen, and C. Brink. Validation of a new control system for Elekta accelerators facilitating continuously variable dose rate. Med Phys 2011; 38(8):4802-10.

85. M. S. Bhagwat, Z. Han, S. K. Ng, et al. An oscillating sweeping gap test for VMAT quality assurance. Physics in Medicine and Biology 2010; 55(17):5029-44.
86. C. C. Ling, P. Zhang, Y. Archambault, et al. Commissioning and quality assurance of RapidArc radiotherapy delivery system. Int J Radiat Oncol Biol Phys 2008; 72(2):575-81.
87. Guidance for the Clinical Implementation of Intensity Modulated Radiation Therapy, ed. H. James. 2008: Institute of Physics and Engineering in Medicine.
88. A. Serna, F. Mata, and V. Puchades. Establishing an optimized patient-specific verification program for volumetric modulated arc therapy. Med Dosim 2013; 38(3):274-9.
89. A. Mans, P. Remeijer, I. Olaciregui-Ruiz, et al. 3D Dosimetric verification of volumetric-modulated arc therapy by portal dosimetry. Radiother Oncol 2010; 94(2):181-7.
90. A. Van Esch, C. Clermont, M. Devillers, et al. On-line quality assurance of rotational radiotherapy treatment delivery by means of a 2D ion chamber array and the Octavius phantom. Med Phys 2007; 34(10):3825-37.
91. M. J. Zelefsky, M. Kollmeier, B. Cox, et al. Improved clinical outcomes with high-dose image guided radiotherapy compared with non-IGRT for the treatment of clinically localized prostate cancer. Int J Radiat Oncol Biol Phys 2012; 84(1):125-9.
92. K. Nakagawa, K. Shiraishi, S. Kida, et al. First report on prostate displacements immediately before and after treatment relative to the position during VMAT delivery. Acta Oncol 2009; 48(8):1206-8.
93. J. Boda-Heggemann, F. Lohr, F. Wenz, et al. kV cone-beam CT-based IGRT: a clinical review. Strahlenther Onkol 2011; 187(5):284-91.
94. P. R. Poulsen, B. Cho, and P. J. Keall. A method to estimate mean position, motion magnitude, motion correlation, and trajectory of a tumor from cone-beam CT projections for image-guided radiotherapy. Int J Radiat Oncol Biol Phys 2008; 72(5):1587-96.
95. W. Fu, Y. Yang, N. J. Yue, et al. A cone beam CT-guided online plan modification technique to correct interfractional anatomic changes for prostate cancer IMRT treatment. Phys Med Biol 2009; 54(6):1691-703.
96. K. Nakagawa, H. Yamashita, K. Shiraishi, et al. Verification of in-treatment tumor position using kilovoltage cone-beam computed tomography: a preliminary study. Int J Radiat Oncol Biol Phys 2007; 69(4):970-3.
97. J. A. Ng, J. T. Booth, P. R. Poulsen, et al. Kilovoltage intrafraction monitoring for prostate intensity modulated arc therapy: first clinical results. Int J Radiat Oncol Biol Phys 2012; 84(5):e655-61.
98. L. A. Dawson and M. B. Sharpe. Image-guided radiotherapy: rationale, benefits, and limitations. Lancet Oncol 2006; 7(10):848-58.
99. P. Williams, J. Sykes, and C. Moore. The effects of radiation scatter from simultaneous MV irradiation on kV fluoroscopic and X-ray volume imaging with the Elekta Synergy system (Abstract). Radiother Oncol 2004; 73(S1):S229-230.

100. M. van Herk, L. Ploeger, and J. J. Sonke. A novel method for megavoltage scatter correction in cone-beam CT acquired concurrent with rotational irradiation. Radiother Oncol 2011; 100(3):365-9.
101. C. Ling, P. Zhang, T. Etmektzoglou, et al. Acquisition of MV-scatter-free kilovoltage CBCT images during RapidArc or VMAT. Radiother Oncol 2011; 100(1):145-9.
102. K. Bush, R. Townson, and S. Zavgorodni. Monte Carlo simulation of RapidArc radiotherapy delivery. Phys Med Biol 2008; 53(19):N359-70.
103. T. Teke, A. M. Bergman, W. Kwa, et al. Monte Carlo based, patient-specific RapidArc QA using Linac log files. Med Phys 2010; 37(1):116-23.
104. K. Bzdusek, H. Friberger, K. Eriksson, et al. Development and evaluation of an efficient approach to volumetric arc therapy planning. Med Phys 2009; 36(6):2328-39.
105. C. Stanford, C. Boylan, and C. Rowbottom. OC-0549: Is it possible to produce acceptable imrt plans free from planner bias using an automated planning technique? Radiotherapy and Oncology 2012; 103(S1):S219.
106. L. Hamlett, C. Boylan, and C. Rowbottom. PO-0832: Is an automated planning technique a useful tool for use in isotoxic lung planning? Radiotherapy and Oncology 2013; 106(S2):S1.
107. M. La Macchia, F. Fellin, M. Amichetti, et al. Systematic evaluation of three different commercial software solutions for automatic segmentation for adaptive therapy in head-and-neck, prostate and pleural cancer. Radiat Oncol 2012; 7:160-176.
108. J. Heukelom, O. Hamming, H. Bartelink, et al. Adaptive and innovative Radiation Treatment FOR improving Cancer treatment outcomE (ARTFORCE); a randomized controlled phase II trial for individualized treatment of head and neck cancer. BMC Cancer 2013; 13:84-91.
109. D. M. Wells and J. Niederer. A medical expert system approach using artificial neural networks for standardized treatment planning. Int J Radiat Oncol Biol Phys 1998; 41(1):173-82.
110. D. M. Wells, D. Walrath, and P. S. Craighead. Improvement in tangential breast planning efficiency using a knowledge-based expert system. Med Dosim 2000; 25(3):133-8.
111. J. L. Bedford, M. D. Thomas, and G. Smyth. Beam modeling and VMAT performance with the Agility 160-leaf multileaf collimator. J Appl Clin Med Phys 2013; 14(2):4136.
112. M. Zhuang, T. Zhang, Z. Chen, et al. Volumetric modulation arc radiotherapy with flattening filter-free beams compared with conventional beams for nasopharyngeal carcinoma: a feasibility study. Chin J Cancer 2012; 32(7):397-402.
113. M. Pasler, H. Wirtz, and J. Lutterbach. Impact of gantry rotation time on plan quality and dosimetric verification--volumetric modulated arc therapy (VMAT) vs. intensity modulated radiotherapy (IMRT). Strahlenther Onkol 2011; 187(12):812-9.
114. K. Wijesooriya, E. Aliotta, S. Benedict, et al. RapidArc patient specific mechanical delivery accuracy under extreme mechanical limits using linac log files. Med Phys 2012; 39(4):1846-53.

115. E. J. Hall and C. S. Wuu. Radiation-induced second cancers: the impact of 3D-CRT and IMRT. Int J Radiat Oncol Biol Phys 2003; 56(1):83-8.
116. X. G. Xu, B. Bednarz, and H. Paganetti. A review of dosimetry studies on external-beam radiation treatment with respect to second cancer induction. Phys Med Biol 2008; 53(13):R193-241.
117. J. A. Purdy. Dose to normal tissues outside the radiation therapy patient's treated volume: a review of different radiation therapy techniques. Health Phys 2008; 95(5):666-76.
118. P. Dickinson, J. Stratford, C. Boylan, et al. EP-1087: The clinical usefulness of simultaneous cone beam CT scans captured during prostate radiotherapy. Radiotherapy and Oncology 2013; 106(S2):S1.
119. S. Mayes, L. Hamlett, J. Stratford, et al. PO-0724: Comparison of volume delineation on simultaneous and standard cone beam CT images during arc radiotherapy (SCART). Radiotherapy and Oncology 2013; 106(S2):S1.

(page intentionally blank)

APPENDIX 1

A routine rotational synchronicity test for VMAT: feasibility study

CJ Boylan

W Beasley

Contributions:

I developed the hypothesis and the experimental strategy. WB and I took the measurements and performed the data analysis.

Introduction

Quality control regimes for fixed-field IMRT are well-established [1], and there have been a number of published guidelines for the types of tests to perform and their frequency [2, 3]. More recently, the question of what additional routine quality control measures are required for VMAT have been discussed by a number of authors [4-6].

Generally, these studies suggest that three specific aspects of VMAT delivery need to be routinely checked: the dynamic MLC motion accuracy, gantry positioning, and dose rate modulation. While each of these can be analysed independently, in order to test the complete VMAT system it is important to verify the inter-dependency of these dynamic components. For example, Ling *et al* propose the delivery of a series of fields onto film with different combinations of dose rate and gantry speed. The uniformity between these fields can then be assessed to determine the effects of different dynamic parameters [4]. Furthermore, Bedford and Warrington suggest a test whereby an MLC-defined sweeping field is delivered to film placed inside a cylindrical phantom [5]. The phantom is offset laterally on the couch such that, when the gantry rotates, the swept field remains centred on the same part of the film. The intention of this test is to check the synchronisation of the MLC and gantry motion. A similar test was also proposed by Bhagwat *et al* [6].

The proposed QC regimes above involve a number of separate tests designed to confirm the accuracy of VMAT delivery. Many of the tests are also resource intensive – for example, with the use of dosimetry film, requiring subsequent development and scanning prior to analysis. It is desirable, therefore, to develop a routine quality control test for VMAT, which can check the interdependency of various dynamic delivery components, shows sensitivity to realistic errors and is quick to perform and analyse.

Methods

Measurements were taken at 6MV on an Elekta Synergy linac, which utilised the RTD version 6.0 control software. As such, the 'binned dose rate' VMAT delivery method was used. All dosimetric measurements were taken using the Delta^4 phantom (Figure 1), which is a verification device for VMAT and IMRT plans, consisting of two diode arrays in a cylindrical PMMA phantom (Scandidos, Uppsala, Sweden).

Figure 1. The Delta^4 dosimetric phantom positioned on a linac couchtop

The proposed QC test is adapted from the rotational test described by Bedford and Warrington, and is shown schematically in Figure 2. First, a plan consisting of a static MLC-defined field of 2 cm x 20 cm was delivered in an arc around the Delta^4. The delivered dose distribution (nominally a cylindrical distribution of dose in the long

axis of the Delta^4) was recorded. Secondly, the Delta^4 was offset by 7cm from the central axis (Figure 2b). A plan was then delivered which consisted of a dynamic 2 cm x 20 cm aperture, which swept across the field as the gantry rotates, remaining centred on the Delta^4. Ideally, the two dose distributions should be identical.

a) Static b) Dynamic

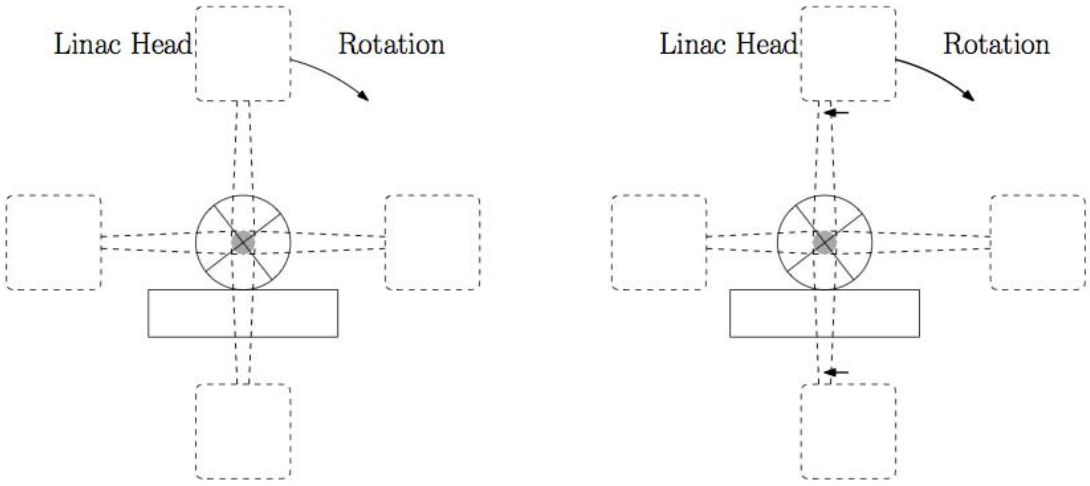

Figure 2. Schematic of the a) static MLC delivery around the arc, and b) dynamic delivery, whereby the MLCs sweep across the field, but remain centrered on the Delta^4 which is offset by 7cm from the central axis.

These fields were delivered with different prescribed monitor units: 600, 300 and 150 MU. This ensured that different dose rates and gantry speeds would be selected by the linac, and remain constant over the arc. It was then possible to compare the static and dynamic deliveries by means of gamma analysis within the Delta^4 software [7]. Using the static delivery as the 'reference' measurement, the results then determine the effect of gantry speed on the synchronisation of the MLC motion.

To check the dependency of dose rate, further deliveries were made. By delivering the 300MU plan twice without stopping the Delta^4 measurement, it was possible to compare this acquisition via gamma analysis to the single 600MU delivery. Thus, a comparison between deliveries with different dose rates could be made. This was then repeated by delivering the 150MU plan twice and comparing to the 300MU acquisition.

Finally, a series of intentional errors were produced in the dynamic plans. By shifting the entire VMAT plans around the gantry by 1 deg and 2 deg, it was possible to simulate a loss of synchronous motion between the leaves and the gantry. Whereas the original plan rotated from 182° to 178°, the introduction of an error led to a rotation of 183° to 179°. The resulting dose distributions were recorded and compared to the 'correct' deliveries to investigate the sensitivity of the test.

Results and Discussion

The test plans showed good repeatability, with comparisons between repeated consecutive deliveries passing a 1%/1mm gamma analysis at 100% for all detectors. Table 1 shows the gamma comparisons between the static and dynamic MLC deliveries for different MU prescriptions. The higher MU prescriptions are associated with a higher dose rate and gantry speed, whereas the lower MU prescriptions are delivered in a lower dose rate bin and a slower gantry speed. Figure 3 shows the dose distributions in the axial plane between a static and dynamic delivery.

			Comparison between static and dynamic deliveries % Detectors with $\Gamma < 1$		
Prescribed MU	**Gantry speed (°/s)**	**Dose rate (MU/min)**	**3%/3mm**	**2%/2mm**	**1%/1mm**
600	5.14	520	99.6	98.8	88.8
300	4.94	250	100.0	99.7	97.3
150	4.94	125	100.0	100.0	100.0

Table 1. Gamma pass rates between the static and dynamic MLC deliveries for the different dose prescriptions, gantry speeds and dose rates

a) Static b) Dynamic

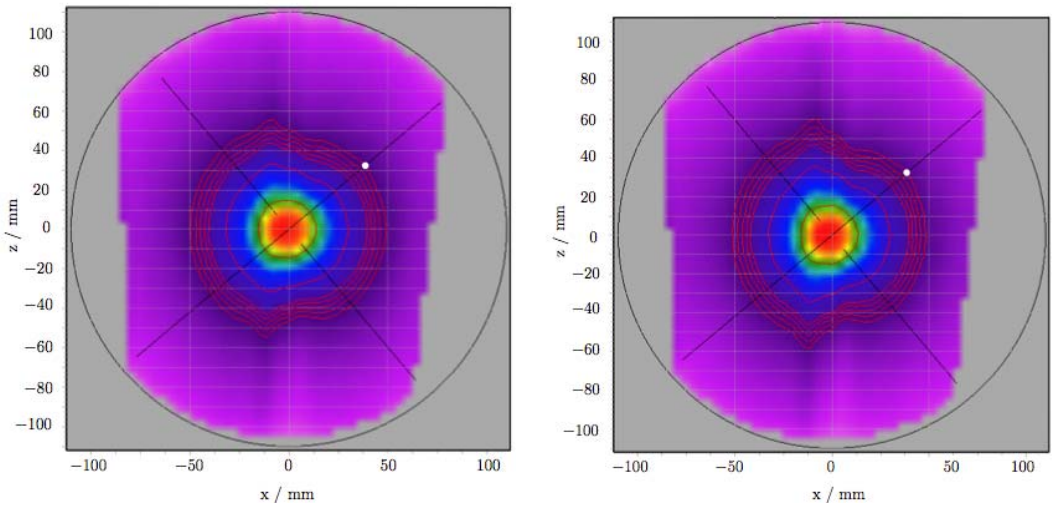

Figure 3. Dose distributions in the axial plane for the a) static delivery and b) dynamic.

While the 3%/3mm gamma evaluations show good agreement, there are more pronounced differences between the static and dynamic deliveries at tighter gamma tolerances. In particular, at 1%/1mm there is a notable reduction in the number of detectors passing the gamma analysis for the faster (600 MU) delivery. Noting that the dose rate and gantry speeds are identical for both the static and dynamic deliveries, it is apparent that the requirement for faster gantry speed in the 600 MU delivery is leading to poorer dosimetry – an effect from either the increased requirement for MLC speed and/or a lack of synchronicity with the rotation of the gantry. It should be noted also that the dynamic tolerance for the leaf positions during VMAT delivery is 4 mm.

Comparison of the 2 x 300MU versus 600MU deliveries, and the 2 x 150MU versus 300MU deliveries showed good agreement at tight gamma tolerances (98.6% and 100.0% of detectors having $\Gamma < 1$ at 1%/1mm, respectively). This indicates that the linac is able to consistently deliver dose at different dose rates.

	Comparison between static and dynamic deliveries % Detectors with Γ < 1		
	3%/3mm	**2%/2mm**	**1%/1mm**
Standard delivery	99.3	97.3	82.8
1° error	99.3	91.8	61.4
2° error	95.3	95.2	39.4

Table 2. Gamma analysis between the 'standard' delivery and intentional gantry offsets of 1° and 2°.

The introduction of gantry errors (simulating a lack of synchronisation between MLC position and gantry position) produced the results shown in Table 2. Results show the gamma pass rates between the plans delivered with deliberate errors and a 'correct' delivery. At gamma levels of 2%/2mm and 1%/1mm there is a noticeable drop in the number of detectors with $\Gamma < 1$ for the plans with errors. Taking into account also the results from Table 1, a gamma analysis at 2%/2mm appears to be the most appropriate choice to provide sensitivity to problems in MLC, dose rate and gantry synchronisation.

Conclusion and Further Work

This report has demonstrated the feasibility of a rotational synchronicity test which checks the ability of the linac to synchronise gantry and MLC motion, as well as the ability to deliver at different dose rates. The use the Delta[4] and the ability to perform gamma evaluation immediately means that this test can be performed routinely without the requirement for significant additional resources.

There remains further work required to develop this QC process. In the above study, 6 deliveries were required (3 static and 3 dynamic) in order to perform all of the evaluations. It will be of interest to investigate whether this number of deliveries can be reduced by modulating the dose rate in different parts of an arc. This is shown schematically in Figure 4. A plan could be created such that the dose is delivered in four distinct sectors (gantry angles -180 to -90, -90 to 0, 0 to 90 and 90 to 180), each with a different dose rate and gantry speed. This is first done without leaf motion (i.e.

with the Delta^4 at the isocentre), and then with the sweeping field (with the Delta^4 offset by 7cm). Gamma analysis could then be performed between these two deliveries. Ideally, each of the abutting sections of the cylinder will have received the same dose distribution, albeit with different combinations of gantry speed, leaf speed and dose rate.

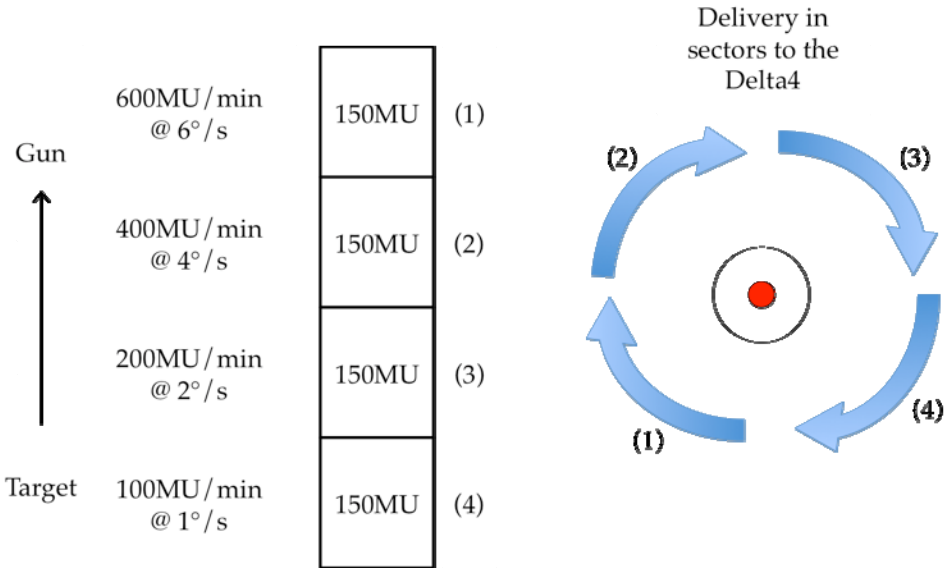

Figure 4. Schematic of the proposed QC test. A series of abutting MLC-defined fields are delivered in 90° sectors to the Delta^4. The fields have the same dose but are delivered in different combinations of dose rate and gantry speed. Comparison will be made between a static MLC to the dynamic sweeping MLC delivery. For the dynamic delivery, reversing the order of the dose rate / gantry speed combinations will also allow a comparison to be made.

It was observed in the above work that a gantry error of 1 deg could be detected – however, further work will be required to determine the sensitivity to more clinically realistic errors. For example, it will be useful to introduce deliberate random and systematic MLC positioning errors and investigate the effect on gamma values. Furthermore, in the context of continuously-variable dose rate (CVDR) it will be necessary to further expand the range dose rates and gantry speeds investigated. It is suggested that such a test – monitoring the inter-dependence of various dynamic VMAT components – could form part of a routine quality control regime for VMAT, alongside the static, IMRT-based assessments of MLC positioning accuracy, beam flatness and symmetry at gantry angle, and output stability over a range of dose rates.

References

1. S. Webb. Intensity Modulated Radiation Therapy. 2001: Institute of Physics Publishing, Bristol.
2. G. A. Ezzell, J. W. Burmeister, N. Dogan, et al. IMRT commissioning: multiple institution planning and dosimetry comparisons, a report from AAPM Task Group 119. Med Phys 2009; 36(11):5359-73.
3. Intensity Modulated Radiation Therapy Collaborative Working Group. Intensity-modulated radiotherapy: current status and issues of interest. Int J Radiat Oncol Biol Phys 2001; 51(4):880-914.
4. C. C. Ling, P. Zhang, Y. Archambault, et al. Commissioning and quality assurance of RapidArc radiotherapy delivery system. Int J Radiat Oncol Biol Phys 2008; 72(2):575-81.
5. J. L. Bedford and A. P. Warrington. Commissioning of volumetric modulated arc therapy (VMAT). Int J Radiat Oncol Biol Phys 2009; 73(2):537-45.
6. M. S. Bhagwat, Z. Han, S. K. Ng, et al. An oscillating sweeping gap test for VMAT quality assurance. Physics in Medicine and Biology 2010; 55(17):5029-44.
7. D. A. Low, W. B. Harms, S. Mutic, et al. A technique for the quantitative evaluation of dose distributions. Med Phys 1998; 25(5):656-61.